STRUCTURED EPIDEMIOLOGICAL MODELS WITH APPLICATIONS TO COVID-19, EBOLA, AND CHILDHOOD-DISEASES

A Dissertation

Submitted to the Faculty

of

Purdue University

by

Joan Ponce

In Partial Fulfillment of the

Requirements for the Degree

of

Doctor of Philosophy

December 2020

Purdue University

West Lafayette, Indiana

THE PURDUE UNIVERSITY GRADUATE SCHOOL
STATEMENT OF DISSERTATION APPROVAL

Prof. Zhilan Feng, Chair

Department of Mathematics

Prof. Guang Lin

Department of Mathematics

Prof. Nung K. Yip

Department of Mathematics

Dr. John Glasser

Centers for Disease Control and Prevention

Approved by:

Prof. Plamen Stefanov

Associate Head for Graduate Studies, Department of Mathematics

To Maria Teresa Viteri

ACKNOWLEDGMENTS

Firstly, I would like to express my gratitude to my advisor, Professor Zhilan Feng, for her continued support throughout my Ph.D. Her outstanding mentorship, patience, and motivation has been pivotal in my development as a researcher. I would also like to sincerely thank my co-advisor, Professor Guang Lin, for his encouragement and guidance in my thesis and other research projects. Working with him has been an inspiring and enriching experience. I want to thank the National Science Foundation for funding my graduate studies through two grants: DGE-1333468 and DMS-1814545. During my doctorate, I had the opportunity to travel to several conferences and workshops. None of it would have been possible without the financial support of the Department of Mathematics.

I would like to thank Dr. John Glasser at the CDC for taking the time to review my presentations and drafts. His helpful suggestions helped my professional growth considerably, and I have learned much from him. I would also like to gratefully acknowledge Professor Aaron Nung Kwan Yip for so many insightful discussions; his door was always open to me whenever I needed some help.

I want to express special thanks to my wonderful collaborators I had the opportunity to meet and work with on the 2019 Collaborative Workshop for Women in Mathematical Biology: Professors Folashade Agusto, Suzanne Sindi, Omayra Ortega, Sally Blower, and Sofya Zaytseva. Their kindness, expertise, and perspective have helped my growth as a researcher and a person.

Having supportive mentors to give me academic advice has allowed me to make informed decisions about my career. Professor Edray Goins has been the best mentor anyone could ask for since my first day at Purdue. He has helped me make valuable professional connections, invited me to give talks, and always lent a helping hand whenever I needed it. Professor Goldberg and Professor Bañuelos have been incredibly

supportive in mentoring me about career choices, and I am very grateful for all their advice. I cordially thank Dr. Castillo-Chavez for all the support and encouragement he has provided throughout my career.

My friends have been a great support system since I started my Ph. D. . Big thanks to my academic brother, Kyle Dahlin, who was happy to lend me a helping hand anytime I needed. Frankie Chan merits a special mention for his immense support, emotional and academic, as well as encouragement that made graduate school an incredible time in my life. Xin Ye, Wei Deng, Xiaodong Wang, Jingshuang Chen, and Jiahao Zhang made days spent at the office productive and fun. Sheng Zhang deserves special mention for being a valuable collaborator and friend. Dr. Pedro Merino has been a great friend, and I am very grateful for all the support he has given me in my research's computational aspects. I am also thankful to Dr. Oscar Jarrin for his friendship and kindness.

Lastly, but most importantly, I would like to thank my parents and my siblings for everything I have achieved. The education, values, and immense support they have given me every step of the way have made anything possible.

TABLE OF CONTENTS

Page

LIST OF TABLES

LIST OF FIGURES

ABSTRACT

Ponce, Joan Ph.D., Purdue University, December 2020. Structured Epidemiological Models with Applications to COVID-19, Ebola, and Childhood-Diseases. Major Professor: Zhilan Feng.

Public health policies increasingly rely on complex models that need to approximate epidemics realistically and be consistent with the available data. Choosing appropriate simplifying assumptions is one of the critical challenges in disease modeling. In this thesis, we focus on some of these assumptions to show how they impact model outcomes. In this thesis, an ODE model with a gamma-distributed infectious period is studied and compared with an exponentially distributed infectious period. We show that, for childhood diseases, isolating infected children is a possible mechanism causing oscillatory behavior in incidence. This is shown analytically by identifying a Hopf bifurcation with the isolation period as the bifurcation parameter. The threshold value for isolation to generate sustained oscillations from the model with gamma-distributed isolation period is much more realistic than the exponentially distributed model.

The consequences of not modeling the spectrum of clinical symptoms of the 2014 Ebola outbreak in Liberia include overestimating the basic reproduction number and effectiveness of control measures. The outcome of this model is compared with those of models with typical symptoms, excluding moderate ones. Our model captures the dynamics of the recent outbreak of Ebola in Liberia better, and the basic reproduction number is more consistent with the WHO response team's estimate. Additionally, the model with only typical symptoms overestimates the basic reproduction number and effectiveness of control measures and exaggerates changes in peak size attributable to interventions' timing.

1. INTRODUCTION

The COVID-19 pandemic has brought the prediction and control of infectious diseases to the forefront. However, modeling an ongoing outbreak presents a host of challenges, including limited access to reliable data and a lack of thorough understanding of the disease's biology. An essential requisite for a model to provide valid predictions is that the assumptions made correspond to reality as much as possible, given that every model is a simplified representation of reality. Therefore, making realistic model assumptions is crucial to evaluate control measures properly and design effective health policies.

The classic SIR (susceptible-infected-recovered) ordinary differential equations (ODEs) model proposed by Kermack and McKendrick has commonly been used to model epidemics [1]. The SIR model consists of three compartments that divide the total population (N) based on their epidemiological status. The susceptible class ($S(t)$: number of susceptible individuals at time t) consists of individuals who can contract the disease when they come into contact with an infected individual in the infective class ($I(t)$: number of infectious individuals at time t). $R(t)$ denotes the number of removed individuals from the interactions by either recovery or death. The SIR model takes the following form:

$$\begin{aligned} \frac{dS}{dt} &= -\beta SI, \\ \frac{dI}{dt} &= \beta SI - \gamma I, \\ \frac{dR}{dt} &= \gamma I. \end{aligned} \tag{1.1}$$

The transmission rate of the disease from an infected individual is β, and infected individuals recover at a rate of γ. This model is the basis for all the models considered in this dissertation. However, this simple model cannot account for all the factors

contributing to the spread of infectious diseases or include all the details necessary to model every outbreak. For example, certain diseases, such as smallpox, have very long latent periods, implying that individuals have been infected but are not yet contagious. Other diseases, such as Ebola and COVID-19, have a significant proportion of infected individuals that do not present symptoms, though they can still transmit the disease. Including an exposed and an asymptomatic compartment allows us to have a more precise mathematical representation of the diseases' biology and has implications for disease control. Another critical assumption of the SIR model

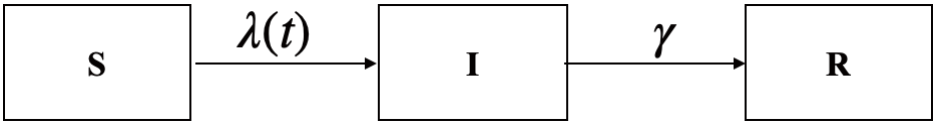

(a) Classic SIR model with exponentially distributed infectious stage.

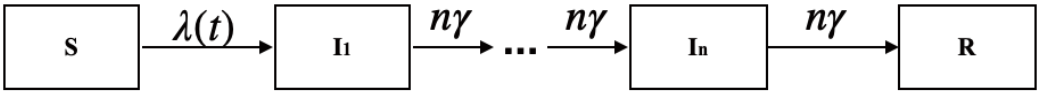

(b) SIR model with a gamma distributed infectious period.

Figure 1.1.: S is the number of susceptible individuals, I is the total number of infective individuals, which equals the sum of the infective individuals, I_j, in each of the n stages. The gamma distribution is determined by its mean $(1/\gamma)$ and the parameter n. The mean duration of infection is kept fixed to allow comparison between models.

is that the infectious period is exponentially distributed with a mean equal to $1/\gamma$. Although convenient, this assumption is equivalent to assuming that the probability of recovery in a given interval of time remains constant, irrespective of the time since infection. In an biological sense, this assumption is not realistic [2, 3]. Assuming this particular distribution overestimates the number of individuals with infectious periods that vary significantly from the mean value. In reality, an infected individual has a greater chance of recovery as time passes. Consequently, to include a more realistic infectious period distribution, a gamma instead of an exponential is more appropriate [4] (see Figure 1.1).

Simplifying assumptions play an important role in model predictions; they allow us to draw conclusions about disease dynamics while keeping the system as simple as possible. However, biologically sound models sometimes require increasing model complexity to represent diseases adequately. Thus, if a disease has an exposed period (an individual contracted the disease but has not exhibited symptoms yet and cannot transmit the pathogen) of significant length, it is necessary to include a compartment for exposed individuals. Similarly, certain diseases present a wide array of symptoms, some infected people do not exhibit all the symptoms, and sometimes they are asymptomatic carriers. Each disease's biology must be carefully studied to include a compartment for asymptomatic individuals in a mathematical model.

1.1 Important concepts in the modelling of infectious diseases

One of the advantages of using compartmental models to study infectious disease outbreaks is that individuals are separated depending on their health status, and every individual in a compartment is assumed to have the same characteristics. Therefore, we can track how each subgroup (susceptible, infected, and recovered) vary over time. Some of the questions pertain to disease persistence, whether there are any constant solutions to the system or oscillations. To analyze the dynamical systems' trajectories, i.e., what happens with the system after a long time, we need to introduce the concepts of fixed points' stability. The constant solutions to a system of differential equations are the fixed points of the system. One such equilibrium point is the disease-free equilibrium; that is, there are no infected individuals in the population at this steady state.

1.1.1 On the stability of equilibrium points and bifurcations

An equilibrium point's stability determines whether the solutions near said point get further, closer, or remain nearby. A differential equation system may contain several equilibrium points, and each of these could be locally stable. Saying an equi-

librium point is locally stable implies that the point remains stable if initial conditions that start near an equilibrium point stay in that point's vicinity. We say a point is locally asymptotically stable if it is stable, and all the nearby trajectories converge to the equilibrium point as time goes to infinity. An equilibrium point is globally asymptotically stable if the system eventually approaches the equilibrium point regardless of the initial condition.

The notion of local stability is tied to the concept of the basic reproduction number, $\mathcal{R}_0$, which is defined as the number of secondary infections when an infected individual is introduced to a completely susceptible population of hosts [5]. If there are control measures or interventions implemented at the start of an epidemic, the reproduction number is called the effective reproduction number, which we denote by $\mathcal{R}_e$. Several approaches have been developed to derive an analytical expression for $\mathcal{R}_0(\mathcal{R}_e)$ [5, 6]. One of the most common methods to obtain this value is the next-generation matrix method. Consider a compartmental model with n compartments, where m of those contain infected individuals. Let $\bar{x} = x_i$, $i = 1, \ldots, n$ denote the vector of the proportions of individuals in the ith compartment. Then, we can define $F_i(\bar{x}_i)$, which is the rate of appearance of new infections in the ith compartment. Further, let V_i^+ and V_i^- be the rates of transfer of individuals into and out of the ith compartment by other means besides infection, respectively. Note that the difference of $F_i(\bar{x}_i) - V_i(\bar{x}_i)$, where $V_i(\bar{x}_i) = V_i^- - V_i^+$, is the rate of change of x_i. If F_i and V_i satisfy the conditions detailed in [5, 6], we can obtain the next generation matrix operator FV^{-1}, where

$$F = \left[\frac{\partial F_i(x_0)}{\partial x_j}\right], \; V = \left[\frac{\partial V_i(x_0)}{\partial x_j}\right],$$

$i, j = 1, \ldots, m$ and x_0 is the disease-free equilibrium of the system. Thus, the entries of the matrix FV^{-1} give the rate at which infected individuals x_j produce new infections in x_i multiplied by the average length of time that individuals spend in compartment

j. $\mathcal{R}_0$ is the spectral radius of the next-generation matrix, that is, the dominant eigenvalue of the matrix.

Feng and Thieme [7] formulated a SEIQR model for childhood diseases to study the impact of isolation on periodic outbreaks. The dynamics of the system that Feng and Thieme proposed are dependent on the basic reproduction number. They showed that if $\mathcal{R}_0 < 1$, then the system has only a disease-free (trivial) equilibrium, which is globally asymptotically stable. Also, if $\mathcal{R}_0 > 1$, then there exists a unique endemic equilibrium (non-trivial). The expression that they obtain for $\mathcal{R}_0$ does not depend on the length of the isolation period. When the length of the isolation period is either very short or very long, the endemic equilibrium attracts all the system's solutions. Two different parameter values were identified at which the periodic solutions bifurcate from the equilibrium, i.e., a Hopf bifurcation occurs at two values of the length of the isolation period.

Feng and Thieme's work used the Hopf-bifurcation theorem to show the existence of periodic solutions and a center manifold reduction to show the stability of the solutions. A Hopf bifurcation occurs when a periodic solution surrounding an equilibrium point arises or disappears as a parameter varies. The details of the proof can be found in the paper *Recurrent Outbreaks of Childhood Diseases Revisited: The Impact of Isolation* by Feng and Thieme [7]. In Chapter 3, we reformulate this theorem for the gamma-distributed system that we use to model childhood diseases. For simplicity, here we state a version of the Hopf bifurcation theorem in two dimensions [8]:

Theorem 1.1.1 (Hopf bifurcation Theorem) *Consider the planar system*

$$\begin{aligned} \dot{x} &= f_\mu(x, y), \\ \dot{y} &= g_\mu(x, y), \end{aligned}$$

where μ is a parameter. Suppose the system has an equilibrium point, without loss of generality assume it is $(x, y) = (0, 0)$. Let the eigenvalues of the linearized system about the equilibrium point be given by $\lambda(\mu), \bar{\lambda}(\mu) = \alpha(\mu) \pm i\beta(\mu)$. Suppose further that

for a certain value of μ (we may assume the value to be 0), the following conditions are satisfied:

(i) Non hyperbolicity condition: conjugate pair of eigenvalues, i.e.,
$\alpha(0) = 0$, $\beta(0) = \omega \neq 0$, *where* $sgn(\omega) = sgn[(\frac{\partial g_\mu}{\partial x})]$;

(ii) Transversality condition: the eigenvalues cross the imaginary axis with non-zero speed, i.e.,
$$\frac{d\alpha(\mu)}{d\mu}|_{\mu=0} = d \neq 0;$$

(iii) Genericity condition:
$a \neq 0$, *with* $a = \frac{1}{16}(f_{xxx} + f_{xyy} + g_{xxy} + g_{yyy}) + \frac{1}{16\omega}(f_{xy}(f_{xx} + f_{yy}) - g_{xy}(g_{xx} + g_{yy}) - f_{xx}g_{xx} + f_{yy}g_{yy})$, *where* $f_{xy} = \left(\frac{\partial^2 f_\mu}{\partial_x \partial_y}\right)|_{\mu=0}(0,0)$, *etc.*

Then a unique curve of periodic solutions bifurcates from the origin into the region $\mu > 0$ if $ad < 0$ or $\mu < 0$ if $ad > 0$. The origin is a stable fixed point for $\mu > 0$ ($\mu < 0$) respectively, and an unstable fixed point for $\mu < 0$ ($\mu > 0$) respectively, if $d < 0$ ($d > 0$) respectively, whilst the periodic solutions are stable (unstable) if the origin is unstable (stable) on the side of $\mu = 0$ where the periodic solutions exist. The amplitude of the periodic orbits grows like $\sqrt{|\mu|}$ whilst their periods tend to $2\pi/|\omega|$ as $|\mu| \to 0$.

1.1.2 On age-structured models

Simple SIR models that are homogeneous with respect to age may fail to represent a pathogen's transmission between hosts accurately. The difference in contacts between different age groups can make a difference in model estimates and intervention strategies. We represent the different contacts via a contact matrix that contains the number of contacts per day a person of age i has with a person of age j. Thus, the system consists of individuals divided into age groups, and each age group is divided by health status into different compartments. The different groups interact with each other through the mixing matrix. The contacts per age group are country dependent;

we obtain country dependent contact matrices from [9], which were produced using social surveys to quantify contacts. We follow Busenberg and Castillo-Chavez's definition of c_{ij} : contacts that members of the ith group have with members of group j, given that i has contacts. The criteria that mixing models should meet are the following:

1. $c_{ij} \geq 0$,
2. $\sum_{j=1}^{k} c_{ij} = 1,\ j = 1, \ldots, k,$ and
3. $A_i N_i c_{ij} = A_j N_j c_{ji}$,

where N_i are the number of individuals in each group and A_i are the average per capita contact rates of the groups, also called activities. Studies of encounters by which respiratory diseases were transmitted suggest that individuals of the same age group mix preferentially. Thus, the contacts individuals from group i have with other groups is given by:

$$c_{ij} = e_i \delta_{ij} + (1 - e_i) f_j, \quad f_j = \frac{(1 - e_j) A_j(t) N_j}{\sum_k (1 - e_k) A_k(t) N_k}, \ \ i, j = 1, 2, 3, 4.$$

The parameter $e_i \in [0, 1]$ is the fraction of contacts an individual has with members of his age group, and δ_{ij} is the Kronecker delta (1 when i=j and 0 otherwise). The function f_j is proportional to the contacts outside of one's group $1 - e_{ij}$, and describes random mixing [10].

1.2 Outline of the thesis

Chapter 1 introduces the standard epidemiological models of SIR and SEIR type and some extensions considered in this thesis. First, simple models consisting of ordinary differential equations (ODEs) and their dynamical behavior is presented. Then, examples are discussed to illustrate the importance of considering extensions of these simple models, particularly the inclusion of population structures by age, either the chronological age or the age (or time spent) within a disease stage.

Chapter 2 introduces an age-structured COVID-19 model, a slightly modified version from Feng and Zhao's model [11], and uses case data from Ecuador to fit the model parameters. The model includes a compartment for asymptomatic individuals and uses a synthetic contact matrix. Parametrization of the model involved fitting the uncontrolled portion of the outbreak and estimating the impact that social distancing measures had on the epidemiological processes in each age group considered. We explore two release policies and compare them to a benchmark policy to evaluate prevented deaths and cases. This chapter shows that control measures targeting specific age groups can protect the most vulnerable individuals.

Chapter 3 introduces a general model with arbitrarily distributed disease stages that includes a compartment for isolated individuals. The ordinary differential equations system is obtained from the integrodifferential equations system once we assume a Gamma distributed infectious period. We compare this model with an ODE model with an exponentially distributed infectious period and show that isolating infected children is a potential mechanism that causes oscillatory incidence.

Chapter 4 presents an Ebola model that includes moderately and severely symptomatic individuals and is based on previous work by Zheng [12]. The model reconstructs the 2014-25 Ebola outbreak in Liberia by calibrating the model to case data. We compare the model considering moderate and severe symptoms to one that considers only typical symptoms and conclude that modeling the spectrum of Ebola symptoms is relevant for policy-making. Some of the detailed mathematical proofs for results presented in Chapters 2-4 are included in Supplementary Materials.

2. A MODEL OF THE NOVEL CORONAVIRUS OUTBREAK AND REOPENING STRATEGIES IN ECUADOR

2.1 Abstract

There have been many modeling studies on the spread and control of the COVID-19 epidemic. All of these models focus on specific countries, including the US, China, and others [13–18]. A few modeling studies have focused on Ecuador [19–21]. The study presented in this chapter was motivated by strict non-pharmaceutical interventions that Ecuador's government implemented during the COVID-19 pandemic. The objective is to use an age-structured model to evaluate various reopening policies after the lockdown and imposition of strict social distancing policies. The consideration of multiple age groups is based on the reported fact that younger people have a much lower disease severity and mortality than the elderly. Thus, age- and risk-dependent releasing policies might be beneficial for increasing economic activities while reducing the overall disease deaths. In this chapter, a mathematical model is used to evaluate these policies and identify the more appropriate timing and the level of relaxation of the restrictive measures on social distancing.

2.2 Introduction

The novel Severe Acute Respiratory Syndrome (SARS-CoV-2), which emerged in China in late 2019, spread to Ecuador on (or before) February 29, 2020. Since March, Ecuador has relied on lockdowns and other social distancing measures to control the virus's spread. Since June, many of the restrictions have been lifted in several provinces. The physical distancing interventions that were implemented, such

as school closures and social distancing at the workplace, have changed the usual interactions between different age groups.

The high variability in contact networks, where some individuals or groups have more contacts than average, has been shown to affect the course of outbreaks [11, 13, 22]. Specific interventions, such as school closures, change social networks and require models that account for the changes in contact patterns. Zhao and Feng recently published an SEIR-type model with a crude age structure to analyze the cost-benefit of implementing policy that would relax restrictions of younger individuals who face lower risk from COVID-19 [11].

In April, Ecuador was described as the "epicenter" of the pandemic in Latin America. The health care system in the country's largest city, Guayaquil, was overwhelmed with cases and fatalities such that officials struggled to dispose of bodies [23]. As of August 8, 2020 Ecuador had reported 93,572 cases and 16,051 active cases, as well as one of the highest excess mortality per million people in the world until June 17, 2020. On March 12, the government decreed a state of sanitary emergency and rolled out control measures to stop the virus's spread. Some of these measures included imposing isolation for all travelers arriving to the country, increased control at points of entry, and encouraging people to avoid large gatherings [24]. The Ecuadorian government decreed a lockdown period from March 17 until April 5 that prohibited movement between 9 pm and 5 am. Further, circulation was limited to 3 days a week depending on license plate number [25].

From March 17, 2020 to June 3, 2020, approximately 70% of the productive sector in Ecuador had remained paralyzed [26]. Starting on June 3, businesses in the capital city, Quito, were allowed to operate at half capacity and restaurants at a third capacity and by June 8, half of all the provinces in the country had relaxed restrictions [27]. Simultaneously releasing the entire population ignores the impact that each age group has on the spread of the disease and its severity, which varies by age group. For example, individuals over the age of 50 have a higher risk of needing mechanical ventilation once hospitalized. Similarly, the percentage of deaths among

hospitalized individuals (non-ICU and ICU admissions) is 2% in people between 18-49 years old, 9.8% among people aged 50 to 64 years, and 28.1% among individuals older than 65 years old [28]. Also, younger individuals have a higher probability of being asymptomatic (79%) than people aged more than 70 years (30%) [29].

Ecuador's economy has been particularly affected by the pandemic; partly due to the types of jobs that the majority of the population performs. According to data obtained from the national poll of employment, unemployment, and sub-employment (ENEMDU), by December 2019, 80% of people in poverty worked in the informal economic sector, and 64% of people worked as nonqualified workers (workers with elementary school education level), service workers, in sales and essential occupations. Most of the previously mentioned activities have not been able to return to complete normalcy after the shutdown [30].

In this study, we simulate the virus's transmission dynamics in different age groups and fit the model to case data to assess the cost-benefit of the lockdown and analyze the gradual release of specific age groups. This study aims to estimate population and age-dependent parameters, assess social distancing measures currently in place, and evaluate the effectiveness of a staggered-release policy for Ecuador, which may provide the twofold benefit of protecting vulnerable sectors of the population while gradually expanding economic activity.

2.3 Age-structured model

The composition of a country's population is an essential factor in designing control policies, particularly when the disease affects older individuals more than other age groups. The model described in this section is based on the age-structured SEIR-type model proposed by Zhao and Feng with preferential mixing between age groups [11]. We divide the population into four age groups: G1 consists of younger individuals (under 19 years old), G2 comprises individuals between 20 and 49 years, G3 includes individuals between 50 and 64 years old, and G4 includes individuals

over 65 years old. The choice to divide the population into these groups was based on the published, age-dependent parameter values by the CDC [28]. Ecuador has not published age-specific data, therefore, we used CDC values. About 80% of Ecuador's population is in the lower-risk groups G1 and G2, 12% of the people are in G3, and 7% are in G4 [31]. More detailed demographic information about the population is summarized in Table 2.1 and illustrated in Fig. 2.1.

Table 2.1.: Age groups in Ecuador.

Age	Percentage	Number of people	Total
0 - 19 years	38.9%	6,636 159	17,510 643
20 - 49 years	42.36%	7,417 490	
50 - 64 years	12.26%	2,146 697	
over 65	7.48%	1,310 297	

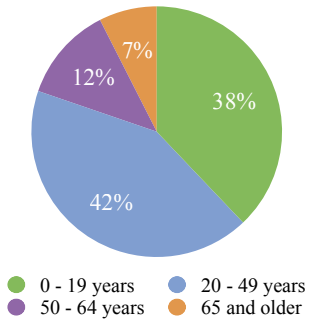

(a) Age distribution pie chart.

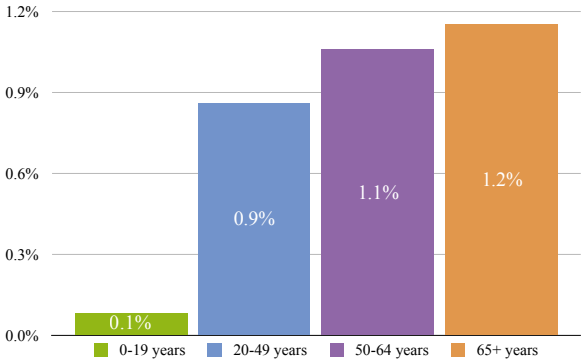

(b) Percentage of COVID cases by age groups (infected individuals in G_i/individuals in G_i).

Figure 2.1.: Estimated distribution of Ecuador's population by age for the year 2020 divided in four age groups and the percentage of total COVID cases per age group.

We further divide each of the age groups $i = 1, 2, 3, 4$ into the following classes: susceptible (S_i), exposed (E_i), infected symptomatic (I_i), infected asymptomatic (J_i), hospitalized (H_i), deaths associated with the disease (D_i), and recovered (R_i) individuals as in Figure 2.2.

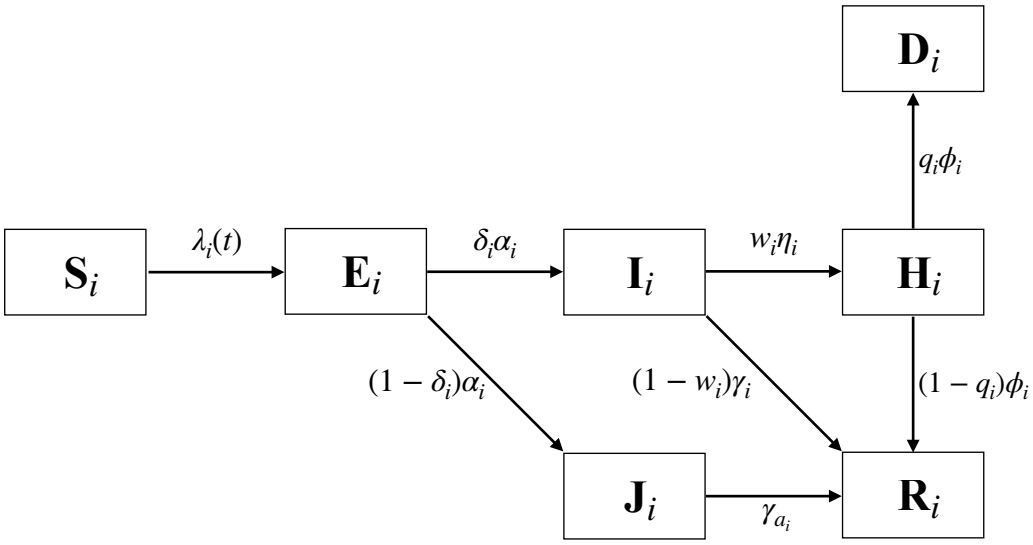

Figure 2.2.: Age-structured modified SEIR model of the ith age group; the groups interact through the force of infection term $\lambda_i(t)$, which includes the mixing function in (2.4)

.

Because this study focuses on a single outbreak, births and deaths are not considered. The model equations for age group i are as follows:

$$\begin{aligned}
\frac{dS_i}{dt} &= -\lambda_i(t)S_i(t), & \frac{dH_i}{dt} &= \eta_i I_i(t) - \phi_i H_i(t),\\
\frac{dE_i}{dt} &= \lambda_i(t)S_i(t) - \alpha_i E_i(t), & \frac{dJ_i}{dt} &= (1-\delta_i)\alpha_i E_i(t) - \gamma_{ai} J_i(t),\\
\frac{dI_i}{dt} &= \delta_i\alpha_i E_i(t) - [\mu_i + \eta_i + \gamma_i]I_i(t), & \frac{dD_i}{dt} &= q_i\phi_i H_i(t) + \mu_i I_i(t),\\
\frac{dR_i}{dt} &= \gamma_{ai} J_i(t) + \gamma_i I_i(t) + (1-q_i)\phi_i H_i(t),
\end{aligned} \tag{2.1}$$

where $\lambda_i(t)$ denotes the force of infection (FOI) and is given by

$$\lambda_i(t) = \beta_i A_i(t) \sum_{j=1}^{4} c_{ij} \frac{I_j(t) + \varepsilon_{1j} J_j(t)}{N_j}. \tag{2.2}$$

When the epidemic begins, all individuals are in the susceptible class and transition to the exposed class via contact with symptomatic or asymptomatic individuals of any age group, depends on (i) mixing between groups, which is described by the

mixing function c_{ij}, (ii) the activity level of group i, denoted by A_i, and (iii) the probability of infection per contact, denoted by β_i. After a latent period $(1/\alpha_i)$, an exposed individual develops symptoms with probability δ_i or is asymptomatic with probability $(1-\delta_i)$. Asymptomatic individuals recover after an infective period of $1/\gamma_{a_i}$. A proportion w of symptomatic individuals is hospitalized at rate η_i; ϕ_i is the rate at which a proportion, $(1-q_i)$, of hospitalized individuals recover, or die with proportion q_i. The proportion of infected individuals who recover without hospitalization is $(1-w)$; they have an infective period of $1/\gamma$.

We denote the infectivity ratio of J_i (asymptomatic individuals) to I_i (infected and symptomatic individuals) individuals by ε_1. The model in [11] includes the death rate of infected individuals that were not hospitalized (μ_i). There is no reliable data on the number of individuals that died outside of hospitals in Ecuador; thus, we assume that $\mu_i = 0$ for all four groups. The force of infection of each group i is $\lambda_i(t)$, where $c_{i,j}$ represents the proportion of the ith group's contacts with members of group j. Zhao and Feng lump together the probability of infection by contact per group (β_i) and the contact rate of each group (A_i) in one term called the *per capita* effective contact rate a_i; that is, each contact that leads to a new infection. Separating the activity (A_i) from the probability of infection per contact (β_i) allows us to obtain the A_i values from the contact matrix and estimate β_i from the case data.

Note that this model satisfies the three criteria of a mixing model [32]:

$$\begin{aligned} &1.\ c_{ij} \geq 0, \\ &2.\ \textstyle\sum_{j=1}^{k} c_{ij} = 1,\ j = 1, \ldots, k, \text{ and} \\ &3.\ A_i N_i c_{ij} = A_j N_j c_{ji}, \end{aligned} \tag{2.3}$$

where N_i are the number of individuals in each group and A_i are the average per capita contact rates of the groups, also called activities. Thus, the contacts individuals from group i have with other groups is given by:

$$c_{ij} = e_i \delta_{ij} + (1-e_i) f_j, \quad f_j = \frac{(1-e_j) A_j(t) N_j}{\sum_k (1-e_k) A_k(t) N_k}, \ \ i, j = 1, 2, 3, 4. \tag{2.4}$$

The parameter $e_i \in [0,1]$ is the fraction of contacts an individual has with members of his age group, and δ_{ij} is the Kronecker delta (1 when i=j and 0 otherwise). Note that the function f_j is proportional to the contacts outside of one's group $1 - e_{ij}$, and so describes mixing that is random [10]. Before any interventions are applied and without considering hospitalization, the reproduction number of each group i is

$$\mathcal{R}_{0i} = \beta_i A_i^0 \left[\frac{\delta_i}{\gamma_i} + \frac{\varepsilon_1(1-\delta_i)}{\gamma_{ai}} \right] \text{ for } t \leq T_1.$$

We denote the baseline value of the contact rate of each group by A_i^0; that is, the value A_i^0 is the number of contacts group members have before any control measures are applied. T_1 is the date when lockdown measures were implemented (March 17, 2020), school was canceled and social distancing measures started being enforced rigorously. The social distancing measures implemented in Ecuador were relaxed after June 3 (T_2) in the capital city, and a partial reopening of the country began though it was up to local officials to determine these policies [26]. The activity level of each group, $A_i(t)$, varies depending on the policies enacted. As in [11], we model these changes using a step function defined in the following way:

$$A_i(t) = \begin{cases} A_i^0, & t \leq T_1 \\ (1-s_1^i)A_i^0, & T_1 < t \leq T_2 \quad \text{(lockdown)} \\ (1-s_2^i)A_i^0, & T_2 < t \leq T_3 \quad \text{(reopening phase 1)} \\ (1-s_3^i)A_i^0, & T_3 < t \leq T_4 \quad \text{(reopening phase 2)} \\ (1-s_4^i)A_i^0, & T_4 < t \leq T_5 \quad \text{(reopening phase 3).} \end{cases} \tag{2.5}$$

The parameter s_1^i in (2.5) represents the percent reduction of contacts for group i from the baseline contacts before the lockdown period. After restrictions were relaxed, contacts have a reduction of s_2^i. The staggered release policies that we explore are reflected in parameters s_3^i and s_4^i and explained in section 2.5.

2.4 Data sources and parametrization of the model

We reconstruct the evolution of the COVID-19 outbreak in Ecuador using incidence data of each age group obtained from the Ministerio de Salud Pública del Ecuador [33]. In addition to case data, we obtained the dates when policies changed from the Servicio Nacional de Gestión de Riesgos y Emergencias (COE) in Ecuador [27].

All parameter values used in the simulations are listed in Table 2.2. Some parameter values were extracted from the literature directly, such as ε_1, $1/\alpha$, δ_i, $1/\gamma_{a_i}$ and $1/\gamma$. Others, such as the mean duration of hospitalization (w_i), were obtained using a weighted average of the CDC values listed for ICU stays and non-ICU stays per age group [28]. Disease-related death rates per group ($1/\phi_i$) were extracted from the databases [33].

2.4.1 Social Contact Matrices

The information on the contacts between different age groups was obtained from the social contact matrices produced by Prem et al., which used household level data from demographics, health surveys, and socio-demographic factors from online databases for 152 countries [9]. This matrix provides a mixing pattern of Ecuador and includes contacts at different levels, such as school, work, home, and other locations for 16 age groups (5-year intervals). The authors provide an Excel file with the synthetic matrices in their supplementary material of [9]. To reduce the 16×16 matrix into a 4×4 with the selected age intervals, we take the original age groups divided by 5-year intervals and group them by summing over the columns (contacts per group). We then do a weighted average over the groups (rows) with the age distributions of the country as weights. The age profile of the population was taken from Ecuadorian government databases [31]. We balance the reduced matrices using the formula provided by [39] to ensure reciprocity in the contacts; that is, that the contacts group i has with group j are the same as the contacts group j has with group

Table 2.2.: Definition of the parameters in model (2.1), and the ranges of their values used in numerical simulations.

Symbol	Definition	Value (Range)	Reference
	Group-independent parameters		
ε_1	Infectivity ratio of mildly infected to severely infected individuals	0.75 (0.25, 1)	[28]
$1/\alpha$	Mean latent period	5 (4.2, 6) days	[34]
δ	Proportion of symptomatic individuals	varies	[28, 35]
$1/\gamma_a$	Mean infectious period for J class	6 days	[28, 36]
$1/\gamma$	Mean infectious period for I class	6 (5, 10) days	[28, 36]
μ	Disease-related death rate for non-hospitalized individuals in the I class	0	assumed
	Group-dependent parameters		
β_i	probability of infection by contact (fitted to data)		
$\mathbf{1/\eta}$	Hospitalization rate of symptomatic individuals if alive (fixed)		
$1/\eta_1$		6 (3, 9) days	[33, 37]
$1/\eta_2$		6 (3, 9) days	[37]
$1/\eta_3$		6 (2, 9) days	[37]
$1/\eta_4$		3 (0, 7) days	[37]
$\boldsymbol{w_i}$	Proportion of infected individuals hospitalized		
w_1	0.0202 %		[38]
w_2	2.71%		[38]
w_3	9.63%		[38]
w_4	14.17%		[38]
$\mathbf{1/\phi_i}$	mean duration in H before disease death or recovery (fixed)		[28]
$1/\phi_1$		3	
$1/\phi_2$		4.6 days	
$1/\phi_3$		7.62 days	
$1/\phi_4$		8.1 days	
$\boldsymbol{q_i}$	Proportion of disease related deaths from the H class		
q_1		0.6%	[28]
q_2		2%	[28]
q_3		9.8%	[28]
q_4		28.1%	[28]
$\mathbf{A_i}$	Average per-capita contact rates of groups		computed
A_1		19.8	
A_2		18.5	
A_3		6.8	
A_4		3.07	
$\mathbf{e_i}$	preference level of each group		computed
e_1		0.469103	
e_2		0.10001	
e_3		0.22897	
e_4		0.130304	

i. Thus, the balanced matrix (2.3) satisfies the third condition in the criteria of a mixing model.

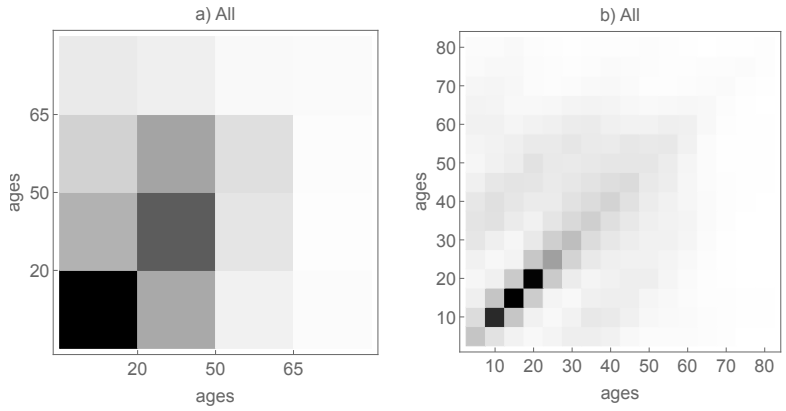

Figure 2.3.: Contact matrices from Ecuador: b) original matrices obtained from [9] for 16 age groups we used to obtain a) the matrix of the 4 age groups we are considering.

2.4.2 Estimation of β_i and the group-specific $\mathcal{R}_{0i}$

This study's fitting portion aims to reconstruct the dynamics of COVID-19 in Ecuador between February 15, 2020, and August 22, 2020, across three different periods defined by non-pharmaceutical interventions. Then, using those estimates evaluate different staggered release policies. The fitting was done in two phases: first, we fit the uncontrolled, initial outbreak data ($T_0 - T_1$) to estimate β_i, and then we estimated the control parameters (s_2^i and s_3^i).

Case data before March 17, 2020, is suitable for estimating the reproduction number because there were no significant interventions in place to alter the epidemic curve [27]. Using the data between February 15, 2020, and March 17, 2020, we estimate the baseline transmission rate of each group β_i for $i = 1, \ldots, 4$, which then remain constant throughout the epidemic. All other parameters were obtained from the literature or directly from the data and are listed in Table 2.2. We obtain the estimates of $\mathcal{R}_{0_i}$ for each age group using the formula (2.3) given our estimate of β_i. The reported cases are assumed to be Poisson samples from the model, which is appropriate for modelling the stochasticity in count data. We use Poisson Negative Log-likelihood and the package odeint to solve the differential equations.

The percentage of symptomatic individuals (δ_i) has been estimated from case data [14, 28, 40, 41] and from prediction models [29, 42, 43]. However, there is wide variation in the estimates, according to a comprehensive review by Kronbichler et al., the percentage of asymptomatic cases in case-series was 24.2% and ranged from 9.2% to 69% in prediction models [42]. The choices for the age dependent δ_i were based on estimates in [29]. The group with younger population G1, has a lower percentage of symptomatic individuals: $\delta_1 = 0.21$, while the older age group, G4, has $\delta_4 = 0.69$, i.e. 69% of symptomatic individuals. We set $\delta = 0.5$ for G2 and G3.

We fit the values of β_i for each age group and the results of these fittings are detailed in Table 2.3. We also compute the reproduction number of all groups using the formula in the supplementary material (A.1); note that the reproduction number of all age groups is within the confidence interval of the reproduction number for Ecuador, 3.95 (3.7-4.21) estimated by Caicedo-Ochoa et al. [44]. The calculation of the overall reproduction number for the entire population is detailed in supplementary material (A.1).

Table 2.3.: Transmission rates estimates with varying δ_i (proportion of symptomatic individuals).

Parameter	**G1**	**G2**	**G3**	**G4**	$\mathcal{R}_0$	Reference
δ_i	0.21	0.5	0.5	0.69	4.2	[29]
β_i	0.014	0.051	0.21	0.29		fitted value

2.5 Estimates of the control parameters

The efforts to contain the COVID-19 pandemic have relied mainly on non-pharmaceutical interventions due to the lack of a vaccine and effective treatment. The first case in Ecuador was identified in February, and a state of emergency declared in early March, but the government did not enforce strict social distancing until March 17, 2020, when a nighttime lockdown was imposed countrywide. Schools were closed,

non-essential workers were directed to work from home, and traffic was restricted to essential activities such as grocery shopping [27].

Using the transmission rates obtained in the first phase of the fit, we then estimate the reductions in contacts s_1^i for $i = 1, \ldots, 4$ during lockdown: $t \in (T_1 - T_2]$. Similarly, after the restrictive measures were lifted and phase 1 of the reopening process started ($t \in (T_2 - T_3]$), we estimate s_2^i for $i = 1, \ldots, 4$. We assume no reduction of the baseline contacts between groups in the first phase of the epidemic following the piecewise definition of the contacts function (2.5). In the lockdown phase, most groups have significant reductions in contacts (Table 2.4), which adequately reflect the restrictions placed by the government. Once some mobility restrictions were lifted after June 3, 2020, there was an increase contact rates by age group. Notably, the largest increase in contacts (lower contact reduction) occurs in G1. This is reflected in the steep increase of cases in that age group after reopening, probably due to low compliance with mask use in this population segment. In addition, upon analyzing Google Mobility reports of the country, specifically parks, and recreational areas, we observe an increase in mobility to these areas after lockdown ended [45]. Thus, we speculate that increased mobility of this age class or low adherence to social distancing rules may play a role in this significant decrease of contact reduction.

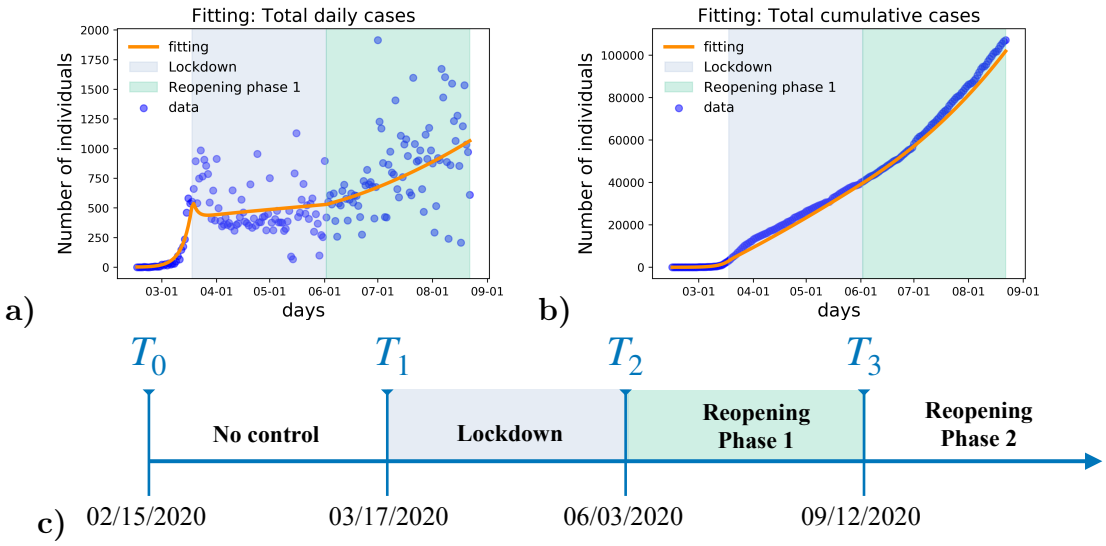

Figure 2.4.: Parameters were estimated by fitting data from February 15 to August 22. **a)** Fitting of the total daily cases (all groups) of the first three periods: before control, lockdown and reopening phase 1. **b)** Fitting of total cumulative cases of all age groups of the first three periods. **c)** Timeline of interventions implemented in Ecuador since the start of the outbreak.

Table 2.4.: Percent reduction of the contact rates A_i defined in (2.5) before lockdown ($T_0 - T_1$), during lockdown ($T_1 - T_2$), and reopening phase 1 ($T_2 - T_3$).

	Parameter	G1	G2	G3	G4
		$\delta_1 = 0.21$	$\delta_2 = 0.5$	$\delta_3 = 0.5$	$\delta_4 = 0.69$
$T_0 - T_1$	no reduction				
$T_1 - T_2$	s_1^i	0.716	0.743	0.764	0.614
$T_2 - T_3$	s_2^i	0.52	0.73	0.76	0.615

2.6 Evaluation of two different control policies

Reducing the number of daily cases in the most vulnerable groups (G3 and G4) is vital to keep mortality as low as possible in a country like Ecuador, which has a limited hospital bed capacity [46]. In addition to reducing the peak daily incidence, reducing the total number of infected individuals of the most vulnerable age groups is also important to reduce disease-related mortality. We explore two release policies' impact on the numbers of cases overall as well as by age group: 1) **delayed-release**

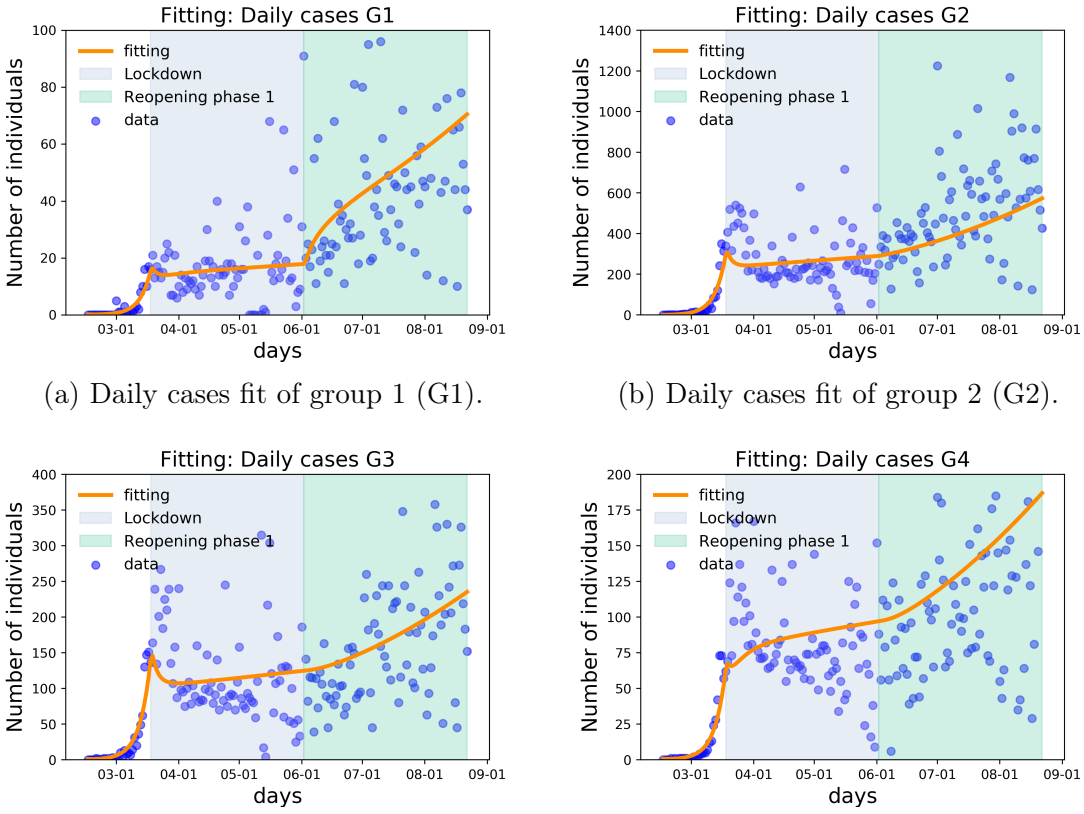

(a) Daily cases fit of group 1 (G1).

(b) Daily cases fit of group 2 (G2).

(c) Daily cases fit of group 3 (G3).

(d) Daily cases fit of group 4 (G4).

Figure 2.5.: Fitting of daily cases by age group of the first three periods of the outbreak between February 15 and August 22 reflecting the impact of the contact variation in each group over time.

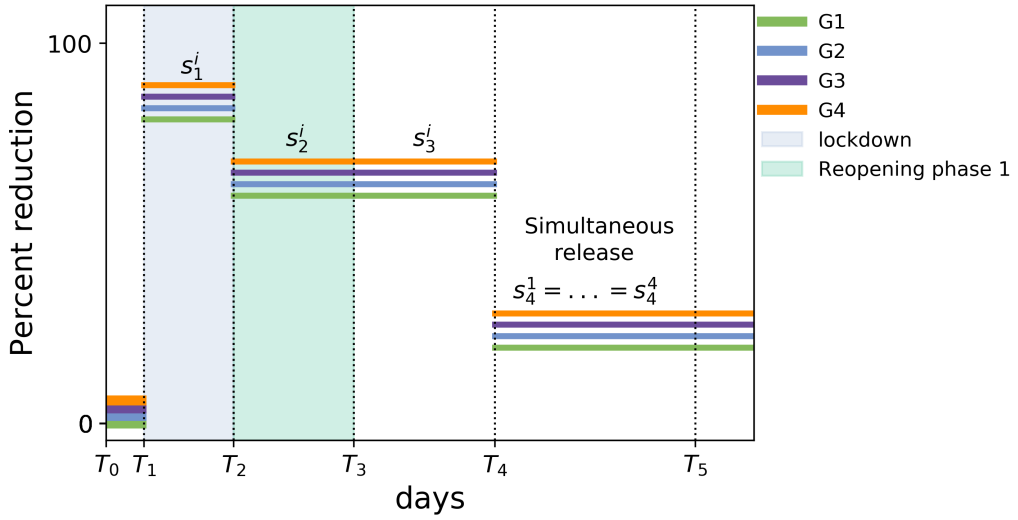

(a) **Benchmark delayed-release scenario**: all groups maintain restriction level $s_2^i = s_3^i$, $i = 1, \ldots, 4$ until T_4, after which all groups are simultaneously released.

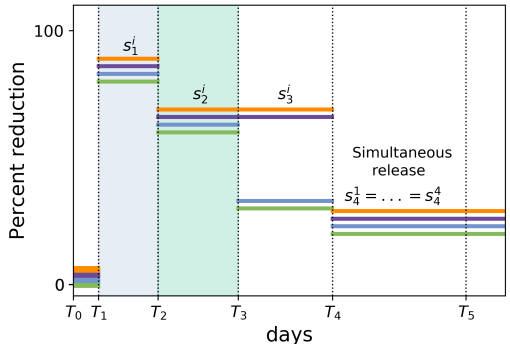

(b) **Staggered release A**: G1 and G2 are released first for a period of 120 days, afterwards all groups are released with $s_4^i = 0.2$, $i = 1, \ldots, 4$ for $t \in (T_4 < t)$.

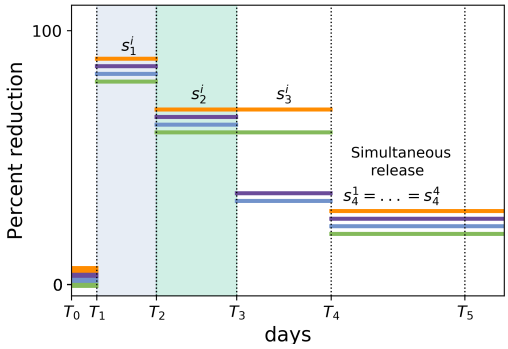

(c) **Staggered release B**: G2 and G3 are released first for a period of 120 days, afterwards all groups are released with $s_4^i = 0.2$, $i = 1, \ldots, 4$ for $t \in (T_4 < t)$.

Figure 2.6.: Different control strategies applied after reopening phase 1 is over, $t \geq T_3$.

and 2) **staggered-release** (Figure 2.6). The control policies studied take place after September 12, 2020 (start of reopening phase 2). The delayed-release policy consists of releasing all groups after T_4 until the end of the epidemic. This policy assumes that all groups are released at once with only a 20% reduction in contacts until the end of the outbreak $s_4^i = 0.2$ for $i = 1, \ldots, 4$ for $t \geq T_4$. The benchmark delayed-release policy assumes that a relatively high level of restrictions remain in place for an extended period of time (120 days after T_3). We use the delayed simultaneous-release policy as the benchmark policy against which to compare the other policies.

Staggered-release strategies A and B

The decision to release a specific age group before others has important consequences in the dynamics of the epidemic and the country's economy [26, 30]. We assess two staggered-release strategies: staggered-release strategy A allows G1 and G2 higher activity levels during the time interval $(T_3 - T_4)$; similarly, staggered-release strategy B allows G2 and G3 higher activity levels during the same time interval. After T_4, both strategies release individuals with contact restrictions of $s_4^1 = 0.2$ for $i = 1, \ldots, 4$ until the end of the epidemic. With these two strategies, we aim to study the consequences of releasing the country's economic workforce versus releasing the younger population (school, university re-openings), a large proportion of which is not economically active. We also analyze different scenarios within each strategy by varying the reduction in contacts for each age group under consideration (see Table 2.5). We assume 120 days for the reopening phase 2 because reducing the number of days does not significantly decrease the peak size of the epidemic curve once all groups are released after T_4. The benchmark scenario is depicted in every plot by a dotted orange line.

Table 2.5.: Different scenarios of the two staggered-release strategies during reopening stage 2.

	Parameter	G1	G2	G3	G4	Scenario
Staggered-release A						
$(T_3 - T_4) = 120$ days	s_3^i	s_2^1 - 0.1	s_2^2-0.1	s_2^3	s_2^4	1
		s_2^1 - 0.2	s_2^2-0.2	s_2^3	s_2^4	2
		s_2^1 - 0.3	s_2^2-0.3	s_2^3	s_2^4	3
		0.2	0.2	0.2	0.2	Benchmark
$T_4 - T_{\text{end}}$	s_4^i	0.2	0.2	0.2	0.2	
Staggered-release B						
$(T_3 - T_4) = 120$ days	s_3^i	s_2^1	s_2^2 - 0.1	s_2^3 - 0.1	s_2^4	1
		s_2^1	s_2^2 - 0.2	s_2^3 - 0.2	s_2^4	2
		s_2^1	s_2^2 - 0.3	s_2^3 - 0.3	s_2^4	3
		0.2	0.2	0.2	0.2	Benchmark
$T_4 - T_{\text{end}}$	s_4^i	0.2	0.2	0.2	0.2	

2.7 Analysis and Results

The delayed simultaneous-release policy, where all groups maintain post lockdown contact levels, is used as a baseline to compare the strategies considered. One of the main disadvantages of maintaining high levels of restriction is that, when all groups are released simultaneously, there is a high risk of a second wave if other control measures are not implemented. To analyze the impact of the strategies chosen, we evaluate the peak daily incidence, the epidemic's final size, and how many cases/deaths can be prevented with different control strategies. Zhao and Feng evaluate the strategies considered based on the reduction in each group's cumulative deaths compared to the benchmark policy [11]. We follow the same approach and compute this quantity, which they call "efficacy"

$$\mathcal{F}_i = \frac{D_{Bi} - D_i}{D_{Bi}}, \text{ where } D_i = \int_{T_0} [q_i \phi_i H_i(t) + \mu_i I_i(t)] dt, \quad i = 1, 2, 3, 4, \tag{2.6}$$

where B_i is the benchmark delayed-release policy. Let $\mathcal{F}_0 = \sum_{i=1}^{4} \mathcal{F}_i$ denote the efficacy over all groups.

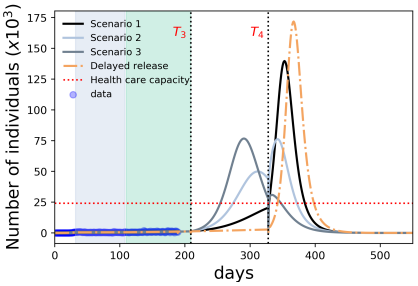

(a) **Staggered release A:** daily cases of all groups.

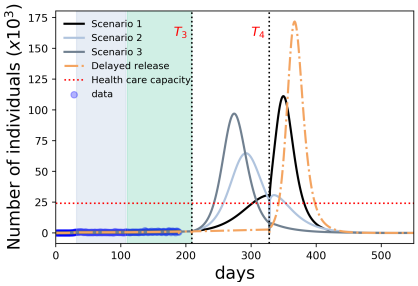

(b) **Staggered release B:** daily cases of all groups.

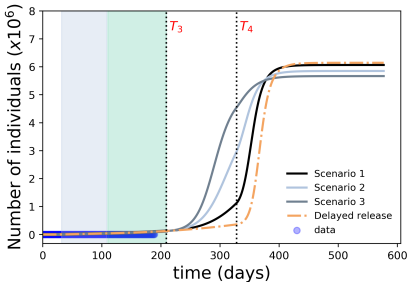

(c) **Staggered release A:** cumulative cases of all groups.

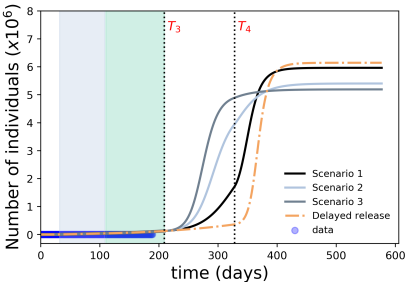

(d) **Staggered release B:** cumulative cases of all groups.

Figure 2.7.: Effects of staggered-release strategies in all groups.

2.7.1 Results of staggered-release A

In this section, we analyze the effects of staggered-release A (see Fig. 2.6), which consists of releasing G1 and G2 before G3 and G4 for 120 days (reopening phase 2). The restriction levels of G3 and G4 during reopening phase 2 ($T_3 - T_4$) are maintained at the levels fitted for reopening phase 1 ($T_2 - T_3$) and we explore three different scenarios for the restriction levels of G1 and G2. We decrease the fitted values of the percent reduction of contacts for G1 and G2 during reopening phase 1 (s_2^1 and s_2^2) by 10, 20, and 30% during reopening phase 2; after T_4 contact restrictions are lowered to 20% until the end of the epidemic in T_5.

The daily cases in all groups are shown in Figure 2.7, and the three different scenarios considered are plotted against the benchmark delayed-release scenario. Scenario 1 (see Table 2.5) shows the number of cases per day if G1 and G2 increase

by 10%; the small increase in contacts during reopening phase 2 translates to few infections during that period, but results in a high peak once all groups are simultaneously released after T_4. Scenario 2 and 3 have a maximum 55% reduction from the benchmark policy in daily cases. The peak of scenario 2 is reached in reopening phase 2, while scenario 3 reaches its peak on reopening phase 3.

Therefore, to minimize peak size on both reopening phases, a careful study should be done to spread the cases as evenly as possible to prevent exceeding hospital surge capacity. The red dotted line in Figure 2.7 represents Ecuador's total health care capacity, i.e., the total number of beds available. Reducing the daily cases as much as possible will reduce the strain on the healthcare system.

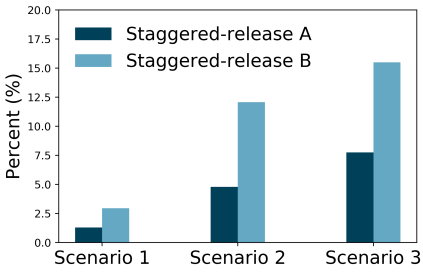

(a) Cases prevented by staggered relative to simultaneous-release policies.

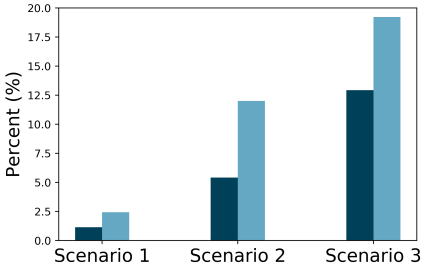

(b) Percent "efficacy" ($\mathcal{F}_0 * 100$), i.e., deaths prevented by staggered-relative to simultaneous-release policies.

Figure 2.8.: Percentage of deaths and cases prevented when employing a staggered-release strategy versus the delay-release benchmark policy.

There is no significant reduction of the cumulative cases with staggered-release strategy A relative to the delayed-release benchmark policy (Figure 2.8 (a)); for instance, scenario 3 reduces the final size by 8%, and all other scenarios reduce the cumulative cases by less than 5%. In Figure 2.8 (b), we plot the percent "efficacy" ($\mathcal{F}_i * 100$) of each scenario considered in staggered-release strategy A for all groups (2.6). Scenario 3 prevents about 7% of cases; however, the biggest difference is in $\mathcal{F}_0 * 100$ which is around 13%.

2.7.2 Results of staggered-release B

Staggered-release B consists of releasing G2 and G3 before G1 and G4 for 120 days, which allows the economically active sector of the population to resume activities during reopening phase 2, while the most vulnerable group, G4, remains with a high level of restrictions until reopening phase 3. Similarly to staggered-release A, we maintain the fitted restriction levels of G1 and G4 from reopening phase 1 and explore lowering three different restriction levels for G2 and G3 (Table 2.5).

On Figure 2.7 (b), we see how all the scenarios of staggered-release B reduce the peak size of the curve of the daily cases; and scenario 2 has the smallest peak size. However, when we look at the cumulative cases in Figure 2.7 (d), we observe that scenario 3 prevents the most cases. Moreover, Figure 2.8 b) demonstrates that it also prevents the most deaths out of all scenarios (20%). Peak size is an important factor to consider in any control policy, because hospital beds always are limited. Further study is needed to design the optimal scenario within staggered-release strategy B, given that Scenario 3 prevents the most cases and deaths, but has a higher peak than Scenario 2. The risk of overwhelming the health care system is that deaths might increase due to a lack of available hospital beds. We did not include hospitalization capacity in our model, so do not include such deaths. Therefore, it is crucial to strike a balance between preventing deaths (if we assume all patients have access to health care) and minimizing daily cases simultaneously.

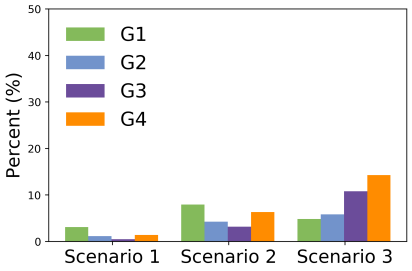

(a) Percent "efficacy" ($\mathcal{F}_i * 100,\ i = 1, 2, 3, 4$) employing staggered-release strategy A.

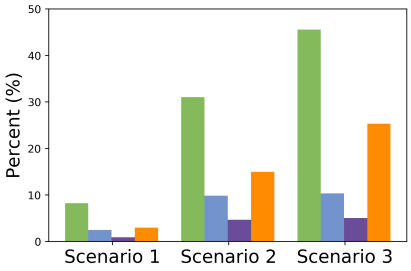

(b) Percent "efficacy" ($\mathcal{F}_i * 100,\ i = 1, 2, 3, 4$) employing staggered-release strategy B.

Figure 2.9.: Percent reduction in cumulative deaths of each group relative to the benchmark scenario when we use staggered-release strategies.

2.8 Discussion

The spread of SARS-CoV-2 is highly dependent on the direct contact that susceptible individuals have with infected ones [47]. Our simulations show that social distancing measures can be useful in reducing both the total number of infected individuals and deaths, and lower the peak incidence of COVID-19 when appropriately applied. This study evaluates the effect that age-specific control measures have on the timing, final size, and overall deaths avoided (Figures 2.8 and 2.9). Zhao and Feng's work shows the advantages of a staggered-release strategy designed to avoid high incidence among the most vulnerable groups. Releasing age groups with low mortality and low risk of hospitalization allows them to achieve some population immunity and protect the most vulnerable groups. The younger groups may have a higher level of infections, but a significant portion are asymptomatic or mildly symptomatic, and a few require hospitalization.

The benchmark policy, which limits contacts (some groups maintaining lockdown levels) for 228 days, results in a very high number of infected individuals once all groups are simultaneously released in phase 3. Both staggered-release strategies considered produce better results as Figures 2.7–2.9 show, both in overall deaths and cases prevented. The staggered-release strategies studied represent practical control

measures that the Ecuadorian government could implement in the following months, such as reopening schools and universities and a percentage of workplaces (staggered-release A), or just allowing a percentage of the economically active population to return to work (staggered-release B).

Figure 2.7 (b) shows that staggered-release B scenario 3 has the highest overall efficacy $\mathcal{F}_0$, thus reducing the most deaths of the options considered. Staggered-release B scenario 3 releases the highest percentage of individuals from G2 and G3. However, this scenario is problematic because the peak incidence occurs in 120 days (reopening phase 2), producing a high number of infected individuals per day (see Figure 2.7 (b)). This result indicates that the timing at which individuals are released is vital for any control strategy. One reason why staggered-release B, scenario 2, is the most successful at minimizing peak sizes is because individuals are released when daily incidence is decreasing. However, decreasing daily incidence is not enough to guarantee small peak sizes. For example, scenario 2 of staggered-release A in Figure 2.7 (a) does not minimize peak size. Individuals are simultaneously released when the daily cases are declining in T_4, but because the release happens close to the peak, cases increase, and a higher peak occurs during phase 3. Therefore, releasing the population's economically active sector provides more benefits than releasing the youngest, lowest risk groups.

Zhao and Feng conclude in their work that releasing low-risk groups saves lives [11]. We agree with that conclusion, but differ in which groups should be released first. This difference could be a consequence of several country-specific factors, such as age distribution and the contact matrix. Furthermore, Zhao and Feng assume that all groups have the same restriction levels for the scenarios they consider, whereas we obtain such values from fitting the model to observations (2.4).

None of the strategies investigated brings the total daily incidence below the number of hospital beds available in Ecuador. Therefore, it would be useful to design an optimal control strategy to attain this goal. However, this paper aims to analyze the consequences of releasing specific groups earlier and contrast the outcomes resulting

from a more conservative control strategy, the delayed simultaneous-release policy. The conclusions from this study are qualitative; any official policy requires further study of the interventions' timing and what percentage of the economically active sector can return to work during reopening phase 2. In summary, releasing lower risk individuals allows the population to build some degree of immunity and protect vulnerable groups with higher disease-related death rates. An additional benefit of releasing G2 and G3 earlier is that it allows economic activity to resume earlier than the delayed simultaneous-release policy.

3. A MODEL FOR CHILDHOOD DISEASES WITH GAMMA DISTRIBUTED DISEASE STAGES

3.1 Background

Childhood diseases, such as measles, whooping cough, mumps and rubella, are an active area of research due to the significant number of cases per year, especially in underdeveloped countries [48]. Some childhood diseases, such as poliomyelitis, are near eradication due to extensive vaccination campaigns [49, 50]. However, in the past decade, measles cases, particularly in the U.S, have increased significantly due to anti-vaccination sentiment [51].

Consequently, understanding the dynamics of childhood diseases remains an active area of research. Among the features that make childhood diseases well suited for mathematical modeling is their relatively simple epidemiology, and in most cases low mortality rates and lifelong immunity after recovery. Outbreaks of most childhood diseases are recurrent; some exhibit highly regular annual or biennial patterns, while others present seemingly irregular outbreaks [52,53]. Therefore, one of the main goals of mathematical epidemiology has been to determine what causes these recurrent outbreaks and predict when they will occur (interepidemic interval). Since the nineteenth century, researchers have been searching for the causes of recurrent outbreaks. Seasonal variations of the pathogen's virulence were proposed as a hypothesis for recurrence by Brownlee [54]. Hirsch identified the density of susceptible individuals as an important factor for recurrence in the late 1800s [55]; however, mechanistic models were not used to explain reoccurring outbreaks in childhood diseases until the 1900s.

In 1929, Soper analyzed a discrete-time compartmental model that generated sustained oscillations when infectiousness was concentrated at the end of the incubation

period. However, when the infectivity was distributed over an interval of time, the oscillations damped and converged to the equilibrium [56]. In general, the SIR model alone cannot accurately simulate the reoccurring outbreaks of childhood diseases. Nevertheless, modifications of the simple SIR model have been successful in generating sustained oscillation patterns. Bauch classifies these modifications into two categories: endogenous and exogenous [57]. Exogenous mechanisms produce sustained oscillations by directly incorporating seasonal forcing of specific parameters and the forcing period is a model parameter. On the other hand, endogenous mechanisms do not directly incorporate the oscillation period in the model parameters and typically yield sustained oscillations by destabilizing the endemic equilibrium and generating stable limit cycles with period T.

One of such endogenous mechanism can be produced by combining alternative assumptions about the incidence term and isolation. Feng and Thieme consider that infected children who become infective at the end of the latency period get severe symptoms and have to stay at home [7]. Therefore, their infectiousness is considerably reduced, given that they are not making contacts outside their families. They proposed a modified SIR model that includes a class of isolated individuals (Q class) and an isolation-adjusted bilinear mass action infection term. The standard, mass action incidence term $\beta IS/N$ is modified by dividing βIS by the active section of the population; that is, individuals that are not isolated $(N - Q)$. This model, which we call a SIQR model, showed that isolation combined with the modified bilinear mass action term create self-sustained oscillations [7].

An interesting result shown in [7] is that isolation can be a possible mechanism responsible for the periodic recurrence of childhood diseases. The model is capable of generating periodic solutions via a supercritical Hopf bifurcations using the isolation period, denoted here by T, as a bifurcation parameter. However, when the model results are applied to common childhood diseases, the lower critical values T_c at which Hopf bifurcation occurs is outside realistic ranges, except for Scarlet fever, which is 2-3 weeks. In their study of an extended model with general disease stage

distributions [58, 59], some special scenarios are discussed, but the critical value T_c is still outside of realistic ranges for most childhood diseases.

In this chapter, we consider an extension of the simple model in [7] by generalizing the exponentially distributed disease stages to Gamma distributions. Detailed analyses of the existence and stability of equilibrium points as well as Hopf bifurcations are presented. It is demonstrated that the critical value T_c can be greatly improved and fall in realistic ranges for many childhood diseases.

The results presented in this chapter provide another example showing the shortcomings of simple epidemiological models with exponentially distributed sojourns. One of the main reasons in this case is that the standard deviation of the mean is identical to the mean. This may cause problems when the model is used for diseases with long latent or infectious periods when quarantine or isolation is imperfect. A significant number of researchers have tried to introduce a modeling framework that allows incorporating arbitrary length distributions to the various disease stages [60, 61]. One of the standard ways to construct these models is to obtain integro-differential equations from a continuous-time stochastic model [62–65]. It has been shown that models with different distributions of stage durations while keeping the same mean may significantly alter dynamics and evaluations of disease control strategies [64, 66]. For example, it is shown in [64] that more realistic assumptions than the exponential stage distribution need to be considered when an epidemiological model is used to assess the effectiveness of quarantine and isolation. Using a model with gamma-distributed disease stages, the authors illustrated that, for some parameter values, models with exponential and gamma distribution assumptions can generate inconsistent evaluations of intervention strategies.

In section 3.2, we extend the results in [7] by considering gamma-distributed infectious stages. We obtain the ODE model from a system of integro-differential equations when Gamma distributions replace the arbitrary stage distributions. In section 3.3, we study the model properties, including the relation between the existence and

stability, the basic reproduction number, and the bifurcation analysis. Section 3.4 contains some numerical results that support the analytical results obtained.

3.2 Model with general distributions for disease stages

Similar to [7], we divide the total population into four epidemiological classes: individuals susceptible to the disease, S; infective non-isolated individuals, I_i; infective isolated individuals Q_i; and recovered and immune individuals, R. The total population is $N = S + I + Q + R$ and the total non-isolated population, i.e., the active population is $A = S + I + R$. One of the model's main assumptions is that sick children stay at home and undergo a form of isolation that reduces their ability to infect others, so the force of infection is $\lambda(t) = \beta I/A$, where β is the per-capita rate of infection when contacting an infected individual. Other parameters used in [7] include: Λ, the recruitment rate at which individuals are born into the population; μ, the natural per capita mortality rate; γ and ω, the rates at which individuals leave the infected and isolation classes, respectively. The model in [7] assumes that the waiting time in the infected stage is exponentially distributed. Thus, $1/\gamma$ represents the mean length of the infective period before isolation, and $1/\omega$ represents the mean length of the isolation period.

To relax the exponential distribution assumption to allow Gamma distributions (with the shape parameter greater than 1), we first present the model with arbitrarily distributed disease stages. Let P_I, $P_Q : [0, \infty) \to [0, 1]$ describe the duration of the infected and isolated stages, respectively. Therefore, $P_i(s)\,(i = I, Q)$ gives the probability that a living individual remains in the ith stage s units of time since entering the stage. Figure 3.1 illustrates the transitions of individuals between stages with the arbitrary survival functions $P_I(t)$ and $P_Q(t)$. The derivative $-\dot{P}_i(s)\,(i =$

I, Q) gives the rate of exiting stage i at stage age s due to disease progression. The nonnegative functions $P_i(s)$ $(i = I, Q)$ have the following properties

$$P_i(0) = 1, \quad \dot{P}_i(s) \leq 0, \quad \int_0^\infty P_i(s)ds < \infty, \ i = I, Q. \tag{3.1}$$

For simplicity, assume an exponential survival function $P_m(s)$ with parameter μ, i.e., $P_m(s) = e^{-\mu s}$.

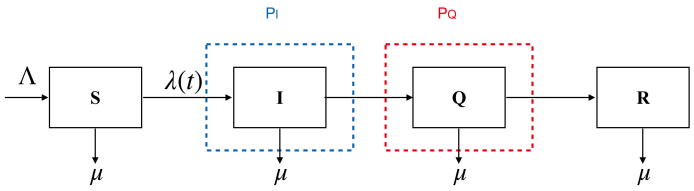

Figure 3.1.: Transition diagram of disease stages when the waiting times in the I and Q stages are described by the functions P_I and P_Q, respectively.

The equations for the S class is an ODE:

$$\frac{dS}{dt} = \Lambda - \lambda(t)S - \mu S, \tag{3.2}$$

where $\lambda(t)$ is the modified force of infection given by

$$\lambda(t) = \frac{\beta\ I}{S + I + R},$$

and $\lambda(t)S(t)$ gives the number of new infections at time t. The total number of infectious individuals is given by

$$I(t) = \int_0^t \lambda(s)S(s)P_I(t-s)e^{-\mu(t-s)}ds + I(0)P_I(t)e^{-\mu t}. \tag{3.3}$$

The first term in equation (3.3) represents the total number of individuals at time t who became infected $t-s$ units of time ago $(0 < s < t)$ and have not been isolated or died by time t. The second term represents the individuals who were infected at time

$t = 0$ and remain in the I compartment at time t. We assume that all individuals that are initially in the I compartment have stage age 0.

Differentiating equation (3.3) we obtain the input for the Q equation.

$$\begin{aligned} I'(t) &= \lambda(t)S(t) \\ &\quad -\Big[\int_0^t \lambda(t)S(s)\dot{P}_I(t-s)e^{-\mu(t-s)}ds - \mu P_I(t)e^{-\mu t}I(0) + \dot{P}_I(t)e^{-\mu t}I(0)\Big]. \end{aligned}$$

Similar to [65], we can obtain the equation $Q(t)$. Denote the random variables for the independent waiting times of the transitions from I to Q and from Q to R by T_{P_I} and T_{P_Q}, respectively. If s denotes the time at which individuals enter the isolated stage Q, then the conditional probability of remaining there at time $t > s$, given that the individual was isolated at time τ $(s < \tau < t)$, is given by:

$$P_Q(t-s|\tau-s) := \frac{\mathbb{R}[T_{P_Q} > t-s]}{\mathbb{R}[T_{P_Q} > \tau-s]} = \frac{P_Q(t-s)}{P_Q(\tau-s)}.$$

Thus, the number of individuals in the isolated class at time t is given by

$$\begin{aligned} Q(t) &= \int_0^t \Big[\int_0^\tau \lambda(s)S(s)e^{-\mu(\tau-s)}\dot{P}_I(\tau-s)\frac{e^{-\mu(t-s)}}{e^{-\mu(\tau-s)}} + I(0)e^{-\mu t}\dot{P}_I(\tau)\Big] \\ &\quad \times P_Q(\tau-s)P_Q(t-\tau|\tau-s)dsd\tau, \qquad (3.4) \\ &= \int_0^t \Big[\int_0^\tau \lambda(s)S(s)\dot{P}_I(\tau-s)e^{\mu(t-s)}ds + I(0)e^{-\mu t}\dot{P}_I(\tau)\Big]P_Q(t-\tau)d\tau. \end{aligned}$$

Differentiating the $Q(t)$ equation we obtain:

$$\begin{aligned} Q'(t) &= \int_0^t \lambda(s)S(s)e^{-\mu(t-s)}\dot{P}_I(t-s)ds + I(0)e^{-\mu t}\dot{P}_I(t) \\ &\quad + \int_0^t P_Q(t-\tau)\int_0^\tau \lambda(s)S(s)e^{-\mu(t-s)}\dot{P}_I(\tau-t)ds - I(0)e^{-\mu t}\dot{P}_I(\tau)d\tau \\ &\quad + \int_0^t \dot{P}_Q(t-\tau)\int_0^\tau \lambda(s)S(s)e^{-\mu(t-s)}\dot{P}_I(\tau-s)ds + I(0)e^{-\mu t}\dot{P}_I(\tau)d\tau, \end{aligned}$$

which provides the inflow to the R equation. After simplifications, we get:

$$R(t) = \int_0^t \int_0^u \dot{P}_Q(u-\tau)\Big[\int_0^\tau \lambda(s)S(s)e^{-\mu(t-s)}\dot{P}_I(\tau-s)ds + I(0)e^{-\mu t}\dot{P}_I(\tau)\Big]d\tau du. \tag{3.5}$$

Therefore, we obtain the following system of integro-differential equations for the model:

$$\begin{aligned}
\frac{dS}{dt} &= \Lambda - \lambda(t)S - \mu S, \\
I(t) &= \int_0^t \lambda(s)S(s)P_I(t-s)e^{-\mu(t-s)}ds + I(0)P_I(t)e^{-\mu t}, \\
Q(t) &= \int_0^t \Big[\int_0^\tau \lambda(s)S(s)\dot{P}_I(\tau-s)e^{-\mu(t-s)}ds + I(0)e^{-\mu t}\dot{P}_I(\tau)\Big]P_Q(t-\tau)d\tau, \\
R(t) &= \int_0^t \int_0^u \dot{P}_Q(u-\tau)\Big[\int_0^\tau \lambda(s)S(s)e^{-\mu(t-s)}\dot{P}_I(\tau-s)ds + I(0)e^{-\mu t}\dot{P}_I(\tau)\Big]d\tau du.
\end{aligned} \tag{3.6}$$

3.2.1 Reduction of the system (3.6) to a system of ODEs

The diagram in Fig. 3.2 delineates the 'linear chain trick' when the waiting times in both the I and the Q stages follow Gamma distributions. The primary motivation to use the linear chain trick is that it allows the system of integral or integro-differential equations to be rewritten as a system of ordinary differential equations.

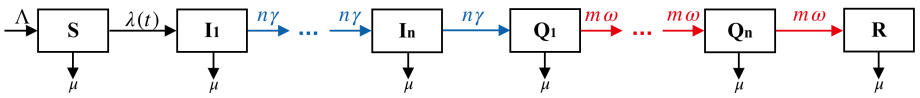

Figure 3.2.: Similar to Fig. 3.1, but for the case when the survival functions P_I and P_Q are Gamma with parameters (n,γ) and (m,ω), respectively, where n and m are the shape parameters, and $1/\gamma$ and $1/\omega$ are the means.

Consider the I equation in (3.3) with the survival function P_I given by

$$P_I(t) = G^n_{n\gamma}(t) = \sum_{j=1}^{n} \frac{(n\gamma t)^{j-1} e^{-n\gamma t}}{(j-1)!}. \tag{3.7}$$

Substitution of the function in (3.7) into (3.3) yields:

$$\begin{aligned}
I(t) &= \int_0^t \lambda(s)S(s)P_I(t-s)e^{-\mu(t-s)}ds + I(0)P_I(t)e^{-\mu t}, \\
&= \int_0^t \lambda(s)S(s)\sum_{j=1}^{n} \frac{(n\gamma(t-s))^{j-1}e^{-n\gamma(t-s)}}{(j-1)!}e^{-\mu(t-s)}ds + I(0)\sum_{j=1}^{n}\frac{(n\gamma t)^{j-1}e^{-n\gamma t}}{(j-1)!}e^{-\mu t}, \\
&= \sum_{j=1}^{n}\bigg(\int_0^t \lambda(s)S(s)\frac{(n\gamma(t-s))^{j-1}e^{-n\gamma(t-s)}}{(j-1)!}e^{-\mu(t-s)}ds + I(0)\frac{(n\gamma t)^{j-1}e^{-n\gamma t}}{(j-1)!}e^{-\mu t}\bigg), \\
&:= \sum_{j=1}^{n} I_j(t),
\end{aligned}$$

where

$$I_1(t) = \int_0^t \lambda(s)S(s)e^{-n\gamma(t-s)}e^{-\mu(t-s)}ds + I(0)e^{-n\gamma t}e^{-\mu t},$$

and

$$\begin{aligned}
I_j(t) &= \int_0^t \lambda(s)S(s)\frac{(n\gamma(t-s))^{j-1}e^{-n\gamma(t-s)}}{(j-1)!}e^{-\mu(t-s)}ds \\
&\quad + I(0)\frac{(n\gamma t)^{j-1}e^{-n\gamma t}}{(j-1)!}e^{-\mu t}, \text{ for } j = 1, \ldots, n.
\end{aligned}$$

Differentiating the $I_1(t)$ equation yields the first equation in (3.11).

$$\begin{aligned}
I_1'(t) &= \lambda(t)S(t) - (n\gamma+\mu)\bigg(\int_0^t \lambda(s)S(s)e^{-n\gamma(t-s)}e^{-\mu(t-s)}ds + I(0)e^{-n\gamma t}e^{-\mu t}\bigg), \\
&= \lambda(t)S(t) - (n\gamma+\mu)I_1(t).
\end{aligned} \tag{3.8}$$

For $j > 1$ we have

$$\begin{aligned}
I_j'(t) &= \lambda(t)S(t)e^{-\mu 0}0 + \int_0^t \lambda(s)S(s)\frac{d}{dt}\bigg(e^{-\mu(t-s)}\frac{(n\gamma(t-s))^{j-1}e^{-n\gamma(t-s)}}{(j-1)!}\bigg)ds \\
&\quad +I(0)\frac{d}{dt}\bigg(\frac{(n\gamma t)^{j-1}e^{-n\gamma t}}{(j-1)!}e^{-\mu t}\bigg), \\
&= \int_0^t \lambda(s)S(s)e^{-\mu(t-s)}\bigg(n\gamma\frac{(n\gamma(t-s))^{j-2}e^{-n\gamma(t-s)}}{(j-2)!} - n\gamma\frac{(n\gamma(t-s))^{j-1}e^{-n\gamma(t-s)}}{(j-1)!}\bigg)ds \\
&\quad -\mu\int_0^t \lambda(s)S(s)\frac{(n\gamma(t-s))^{j-1}e^{-n\gamma(t-s)}}{(j-1)!}e^{-\mu(t-s)}ds \\
&\quad +I(0)e^{-\mu t}\bigg(n\gamma\frac{(n\gamma t)^{j-2}e^{-n\gamma t}}{(j-2)!} - n\gamma\frac{(n\gamma t)^{j-1}e^{-n\gamma t}}{(j-1)!}\bigg) \\
&\quad -I(0)\mu e^{-\mu t}\frac{(n\gamma t)^{j-1}e^{-n\gamma t}}{(j-1)!}, \\
&= \int_0^t \lambda(s)S(s)e^{-\mu(t-s)}\bigg(n\gamma\frac{(n\gamma(t-s))^{j-2}e^{-n\gamma(t-s)}}{(j-2)!}\bigg)ds + I(0)e^{-\mu t}n\gamma\frac{(n\gamma t)^{j-2}e^{-n\gamma t}}{(j-2)!} \\
&\quad +\int_0^t \lambda(s)S(s)e^{-\mu(t-s)}\bigg(n\gamma\frac{(n\gamma(t-s))^{j-1}e^{-n\gamma(t-s)}}{(j-1)!}\bigg)ds + I(0)e^{-\mu t}n\gamma\frac{(n\gamma t)^{j-1}e^{-n\gamma t}}{(j-1)!} \\
&\quad -\mu\int_0^t \lambda(s)S(s)e^{-\mu(t-s)}\frac{(n\gamma(t-s))^{j-1}e^{-n\gamma(t-s)}}{(j-1)!}ds \\
&\quad -\mu I(0)e^{-\mu t}\frac{(n\gamma t)^{j-1}e^{-n\gamma t}}{(j-1)!}, \\
&= n\gamma I_{j-1}(t) - (\mu + n\gamma)I_j(t). \qquad (3.9)
\end{aligned}$$

From the $Q(t)$ equation in (3.4), with the survival function P_Q given by $P_Q(t) = G^m_{m\omega}(t) = \sum_{j=1}^m \frac{(m\omega t)^{j-1}e^{-m\omega t}}{(j-1)!}$, we obtain

$$\begin{aligned}
Q(t) &= \int_0^t \bigg[\int_0^\tau \lambda(s)S(s)\dot{P}_I(\tau - s)P_m(t-s)ds + I(0)P_m(t)\dot{P}_I(\tau)\bigg]P_Q(t-\tau)d\tau, \\
&= \int_0^t \sum_{j=1}^m \frac{(m\omega(t-\tau))^{j-1}}{(j-1)!}e^{-m\omega(t-\tau)}\bigg[\int_0^\tau \lambda(s)S(s)e^{-\mu(t-s)}\frac{(n\gamma(\tau-s))^{n-1}e^{-n\gamma(\tau-s)}}{(n-1)!}ds \\
&\quad +I(0)e^{-\mu t}\frac{(n\gamma\tau)^{n-1}e^{-n\gamma(\tau)}}{(n-1)!}\bigg]d\tau, \\
&= \sum_{j=1}^m \int_0^t \frac{(m\omega(t-\tau))^{j-1}}{(j-1)!}e^{-m\omega(t-\tau)}\bigg[\int_0^\tau \lambda(s)S(s)e^{-\mu(t-s)}\frac{(n\gamma(\tau-s))^{n-1}e^{-n\gamma(\tau-s)}}{(n-1)!}ds \\
&\quad +I(0)e^{-\mu t}\frac{(n\gamma\tau)^{n-1}e^{-n\gamma(\tau)}}{(n-1)!}\bigg]d\tau, \\
&= \sum_{j=1}^m Q_j(t).
\end{aligned}$$

Thus, for $j = 1$

$$\begin{aligned} Q_1(t) &= \int_0^t e^{-m\omega(t-\tau)}\left[\int_0^\tau \lambda(s)S(s)e^{-\mu(t-s)}\frac{(n\gamma(\tau-s))^{n-1}e^{-n\gamma(\tau-s)}}{(n-1)!}ds \right. \\ &\quad \left. + I(0)e^{-\mu t}\frac{(n\gamma\tau)^{n-1}e^{-n\gamma(\tau)}}{(n-1)!}\right]d\tau. \end{aligned}$$

Differentiating the previous equation we obtain

$$\begin{aligned} Q_1'(t) &= n\gamma\left[\int_0^t \lambda(s)S(s)\frac{(n\gamma(t-s))^{n-1}e^{-n\gamma(t-s)}}{(n-1)!}e^{-\mu(t-s)}ds + I(0)\frac{(n\gamma t)^{n-1}e^{-n\gamma t}}{(n-1)!}e^{-\mu t}\right] \\ &\quad -m\omega\int_0^t e^{-m\omega(t-\tau)}\left[\int_0^\tau \lambda(s)S(s)e^{-\mu(t-s)}\frac{(n\gamma(\tau-s))^{n-1}e^{-n\gamma(\tau-s)}}{(n-1)!}ds \right. \\ &\quad \left. + I(0)e^{-\mu t}\frac{(n\gamma\tau)^{n-1}e^{-n\gamma(\tau)}}{(n-1)!}\right]d\tau \\ &\quad -\mu\int_0^t e^{-m\omega(t-\tau)}\left[\int_0^\tau \lambda(s)S(s)e^{-\mu(t-s)}\frac{(n\gamma(\tau-s))^{n-1}e^{-n\gamma(\tau-s)}}{(n-1)!}ds \right. \\ &\quad \left. + I(0)e^{-\mu t}\frac{(n\gamma\tau)^{n-1}e^{-n\gamma(\tau)}}{(n-1)!}\right]d\tau, \\ &= n\gamma I_n(t) - m\omega Q_1(t) - \mu Q_1(t), \end{aligned}$$

which is the equation corresponding to $Q_1(t)$ in (3.11). For $j > 1$,

$$\begin{aligned} Q_j(t) &= \int_0^t \frac{(m\omega(t-\tau))^{j-1}}{(j-1)!}e^{-m\omega(t-\tau)}\left[\int_0^\tau \lambda(s)S(s)e^{-\mu(t-s)}\frac{(n\gamma(\tau-s))^{n-1}e^{-n\gamma(\tau-s)}}{(n-1)!}ds \right. \\ &\quad \left. + I(0)e^{-\mu t}\frac{(n\gamma\tau)^{n-1}e^{-n\gamma(\tau)}}{(n-1)!}\right]d\tau. \end{aligned}$$

Then,

$$\begin{aligned} Q_j'(t) &= \left[\int_0^t \frac{d}{dt}\Big(\frac{(m\omega(t-\tau))^{j-1}}{(j-1)!}e^{-m\omega(t-\tau)}\Big)\left[\int_0^\tau \lambda(s)S(s)e^{-\mu(t-s)}\frac{(n\gamma(\tau-s))^{n-1}e^{-n\gamma(\tau-s)}}{(n-1)!}ds \right. \right. \\ &\quad \left. \left. + I(0)e^{-\mu t}\frac{(n\gamma\tau)^{n-1}e^{-n\gamma(\tau)}}{(n-1)!}\right]d\tau\right] \end{aligned}$$

$$
\begin{aligned}
&+\Bigg[\int_0^t \frac{(m\omega(t-\tau))^{j-1}}{(j-1)!}e^{-m\omega(t-\tau)}\Bigg[\int_0^\tau \lambda(s)S(s)\frac{d}{dt}(e^{-\mu(t-s)})\frac{(n\gamma(\tau-s))^{n-1}e^{-n\gamma(\tau-s)}}{(n-1)!}ds\\
&+I(0)\frac{d}{dt}(e^{-\mu t})\frac{(n\gamma\tau)^{n-1}e^{-n\gamma(\tau)}}{(n-1)!}\Bigg]d\tau\Bigg],\\
=\;& m\omega Q_{j-1}(t)-m\omega Q_j(t)-\mu Q_j(t),
\end{aligned}
$$

which corresponds to the $Q_j(t)$ equation for $j>1$ in (3.11). Similarly, from equation (3.5), we obtain the equation for $R'(t)$:

$$
\begin{aligned}
R'(t) =\;& \int_0^t \dot{P}_Q(t-\tau)\Bigg[\int_0^\tau \lambda(s)S(s)P_m(t-s)\dot{P}_I(\tau-s)ds+I(0)P_m(t)\dot{P}_I\Bigg]d\tau\\
&+\int_0^t\int_0^u \dot{P}_Q(u-\tau)\Bigg[\int_0^\tau \lambda(s)S(s)\dot{P}_m(t-s)\dot{P}_I(\tau-s)ds+I(0)\dot{P}_m(t)\dot{P}_I(\tau)\Bigg]d\tau du,\\
=\;& \int_0^t \frac{m\omega(m\omega(u-\tau))^{m-1}e^{-m\omega(u-\tau)}}{(m-1)!}\Bigg[\int_0^\tau \lambda(s)S(s)(-\mu e^{-\mu(t-s)})\\
&\frac{n\gamma(n\gamma(\tau-s))^{n-1}e^{-n\gamma(\tau-s)}}{(n-1)!}ds+I(0)(-\mu e^{-\mu t})\frac{n\gamma(n\gamma(\tau))^{n-1}e^{-n\gamma(\tau)}}{(n-1)!}\Bigg]d\tau\\
&+m\omega\int_0^t\int_0^u \frac{(m\omega(u-\tau))^{m-1}e^{-m\omega(u-\tau)}}{(m-1)!}\Bigg[\int_0^\tau \lambda(s)S(s)e^{-\mu(t-s)}\\
&\frac{n\gamma(n\gamma(\tau-s))^{n-1}e^{-n\gamma(\tau-s)}}{(n-1)!}ds+I(0)e^{-\mu t}\frac{n\gamma(n\gamma(\tau))^{n-1}e^{-n\gamma(\tau)}}{(n-1)!}\Bigg]d\tau,\\
=\;& -muR(t)+m\omega Q_m(t).
\end{aligned}
$$

In summary, we obtained from the integro-differential equations system (3.6) the following ODE system:

$$
\begin{aligned}
\frac{dS(t)}{dt} &= \Lambda-\lambda(t)S(t)-\mu S(t),\\
\frac{dI_1(t)}{dt} &= \lambda(t)S(t)-(\mu+n\gamma)I_1(t),\\
&\vdots\\
\frac{dI_n(t)}{dt} &= n\gamma I_{n-1}(t)-(\mu+n\gamma)I_n(t),\\
\frac{dQ_1(t)}{dt} &= n\gamma I_n(t)-(\mu+m\omega)Q_1(t),\\
&\vdots\\
\frac{dQ_m(t)}{dt} &= m\omega Q_{m-1}(t)-(\mu+m\omega)Q_m(t),\\
\frac{dR(t)}{dt} &= m\omega Q_m(t)-\mu R(t),
\end{aligned}
\tag{3.10}
$$

where $\lambda(t) = \beta \sum_j I_j/A(t)$ and $A = S + \sum I_j + R$.

We observe from (3.10) that the effect of the assumption of Gamma distributed infective stages is that the single infective class (I) and isolated class (Q) in the previous SIQR model is replaced by n and m sub-stages. Susceptible individuals, once infected, enter the first I stage (I_1) and enter the first isolation stage on the n-th stage after passing through each I_j successively. A similar process occurs once individuals enter the isolated compartments and recover after they have exited the final Q_m stage. The waiting time in each infective sub-stage is identical and equal to the waiting time of the exponential distribution model divided by n. The definitions of all variables and parameters are also listed in Table 3.1.

Table 3.1.: State variables and parameters for model (3.10).

Variable	Definition
S	Susceptible individuals
I_i	Infectious non-isolated individuals in sub-stage i, $1 \leq i \leq n$
Q_i	Isolated individuals in sub-stage i, $1 \leq i \leq m$
R	Recovered individuals
Parameter	
Λ	Recruitment rate
μ	Per capita mortality rate, $1/\mu$ is the average life expectancy
β	Per capita infection rate
$1/\gamma$	Mean duration from onset to isolation
$1/\omega$	Mean duration of isolation

3.2.2 The system with scaled parameters and variables

For the purpose of demonstration, we will use the case of $m = 2$ and $n = 2$ for the analysis in the rest of the chapter. In this case, the system (3.10) has the following form:

$$\begin{aligned}
\frac{dS(t)}{dt} &= \Lambda - \lambda(t)S(t) - \mu S(t), \\
\frac{dI_1(t)}{dt} &= \lambda(t)S(t) - (\mu + 2\gamma)I_1(t), \\
\frac{dI_2(t)}{dt} &= 2\gamma I_1(t) - (\mu + 2\gamma)I_2(t), \\
\frac{dQ_1(t)}{dt} &= 2\gamma I_2(t) - (\mu + 2\omega)Q_1(t), \\
\frac{dQ_2(t)}{dt} &= 2\omega Q_1(t) - (\mu + 2\omega)Q_2(t), \\
\frac{dR(t)}{dt} &= 2\omega Q_2(t) - \mu R(t),
\end{aligned} \tag{3.11}$$

where

$$\lambda(t) = \beta \sum_{j=1}^{2} I_j/A(t), \quad A = S + \sum_{j=1}^{2} I_j + R.$$

The total population size is obtained by adding the equations in system (3.11) $N = S + I_1 + I_2 + Q_1 + Q_2 + R = A + Q_1 + Q_2$. Note that $\frac{d}{dt}N = \Lambda - \mu N$ and $N(t) \to \frac{\Lambda}{\mu}$ as $t \to \infty$. If we assume that the population has reached this limit, then $N \equiv \Lambda/\mu \equiv S + I_1 + I_2 + Q_1 + Q_2 + R$. This allows us to eliminate the S equation in the analysis.

The analysis can be simplified by scaling the parameters by β:

$$\nu = \frac{\mu}{\beta}, \qquad \Gamma = \frac{2\gamma}{\beta}, \qquad \Omega = \frac{2\omega}{\beta}, \tag{3.12}$$

and by considering proportions:

$$s = \frac{S}{A}, \qquad i_j = \frac{I_j}{A}, \qquad q_j = \frac{Q_j}{A}, \qquad r = \frac{R}{A}. \tag{3.13}$$

From $A = N - \sum_i Q_i = A = S + \sum I_j + R$ we have $A' = -\sum_j \frac{d}{dt} Q_j$. By differentiating (3.13) and substituting (3.12), we have the following system for the proportions:

$$\begin{aligned}
s' &= \nu(i_1 + i_2 + q_1 + q_2 + r) - s(i_1 + i_2) + s\big[\Gamma i_2 - (\nu + \Omega)(q_1 + q_2) + \Omega q_1\big], \\
i_1' &= (i_1 + i_2)(1 - i_1 - i_2 - r) - (\Gamma + \nu) i_1 + i_1\big[\Gamma i_2 - (\nu + \Omega)(q_1 + q_2) + \Omega q_1\big], \\
i_2' &= \Gamma i_1 - (\Gamma + \nu) i_2 + i_2\big[\Gamma i_2 - (\nu + \Omega)(q_1 + q_2) + \Omega q_1\big], \\
q_1' &= \Gamma i_2 - (\nu + \Omega) q_1 + q_1\big[\Gamma i_2 - (\nu + \Omega)(q_1 + q_2) + \Omega q_1\big], \\
q_2' &= \Omega q_1 - (\nu + \Omega) q_2 + q_2\big[\Gamma i_2 - (\nu + \Omega)(q_1 + q_2) + \Omega q_1\big], \\
r' &= \Omega q_2 - \nu r + r\big[\Gamma i_2 - (\nu + \Omega)(q_1 + q_2) + \Omega q_1\big],
\end{aligned}$$

which is equivalent to (noticing that $s + \sum_{j=1}^{2} i_j + r = 1$):

$$\begin{aligned}
i_1' &= (i_1 + i_2)(1 - i_1 - i_2 - r) - (\Gamma + \nu) i_1 + i_1\big[\Gamma i_2 - (\nu + \Omega)(q_1 + q_2) + \Omega q_1\big], \\
i_2' &= \Gamma i_1 - (\Gamma + \nu) i_2 + i_2\big[\Gamma i_2 - (\nu + \Omega)(q_1 + q_2) + \Omega q_1\big], \\
q_1' &= \Gamma i_2 - (\nu + \Omega) q_1 + q_1\big[\Gamma i_2 - (\nu + \Omega)(q_1 + q_2) + \Omega q_1\big], \\
q_2' &= \Omega q_1 - (\nu + \Omega) q_2 + q_2\big[\Gamma i_2 - (\nu + \Omega)(q_1 + q_2) + \Omega q_1\big], \\
r' &= \Omega q_2 - \nu r + r\big[\Gamma i_2 - (\nu + \Omega)(q_1 + q_2) + \Omega q_1\big].
\end{aligned} \tag{3.14}$$

3.3 Endemic equilibrium and reproduction number

System (3.14) always has the disease-free equilibrium (DFE) denoted by U_0:

$$s = 1,\ i_1 = i_2 = q_1 = q_2 = r = 0.$$

Let $U^* = (i_1^*, i_2^*, q_1^*, q_2^*, r^*)$ denote a positive or endemic equilibrium (EE) of (3.14) that satisfies (computation details are in supplementary material (B.2)):

$$\begin{aligned}
&i_1^* = \nu(\Gamma + \nu)(\Omega + \nu)^2 k, \quad i_2^* = \Gamma\nu(\Omega + \nu)^2 k, \\
&q_1^* = \Gamma^2\nu(\Omega + \nu)k, \qquad q_2^* = \Gamma^2\nu\Omega k, \qquad r^* = \Gamma^2\Omega^2 k,
\end{aligned} \tag{3.15}$$

where

$$k = \frac{(1-\nu)(2\Gamma+\nu) - \Gamma^2}{(2\Gamma+\nu)(\Gamma^2\Omega^2 + (\nu+\Omega)^2(2\Gamma\nu+\nu^2))}. \tag{3.16}$$

Before proceeding, we define the effective reproduction number, a quantity that will help the biological interpretation of the stability analysis. The model we are considering (3.14) includes an isolated compartment, thus, a control measure is already included in the model. Therefore we define an effective reproduction number instead of the basic reproduction number. The effective reproduction number, $\mathcal{R}_e$, derived in Supplementary material (B.1) is defined as:

$$\mathcal{R}_e = \frac{\beta(4\gamma+\mu)}{(2\gamma+\mu)^2} = \frac{2\Gamma+\nu}{(\Gamma+\nu)^2}.$$

Note on $\mathcal{R}_e$: we can rewrite the effective reproduction number in the following way:

$$\mathcal{R}_e = \frac{\beta}{2\gamma+\mu} + \beta\frac{2\gamma}{2\gamma+\mu}\frac{1}{2\gamma+\mu}.$$

The first and second terms represent the contributions from individuals in the I_1 and I_2 stages, respectively. Note that, $1/(2\gamma+\mu)$ is the death-adjusted mean duration in each of the I_i stage, and $2\gamma/(2\gamma+\mu)$ is the probability that an infectious individual survived and entered the I_2 stage.

We can write k defined in (3.16) in the following form:

$$k = \frac{(\Gamma+\nu)^2(\mathcal{R}_e-1)}{(2\Gamma+\nu)(\Gamma^2\Omega^2 + (\nu+\Omega)^2(2\Gamma\nu+\nu^2))}. \tag{3.17}$$

To obtain a non-negative equilibrium U^*, distinct from the disease-free equilibrium U_0, we require $k > 0$. Therefore, $k > 0$ if and only if $\mathcal{R}_e > 1$.

The model we are considering, (3.14), includes an isolated compartment, thus, a control measure is already included in the model. However, the effective reproduction number, $\mathcal{R}_e$, is independent of the isolation period $1/\omega$.

The result below shows that $\mathcal{R}_e = 1$ is the threshold value for the stability of U_0 and the existence of U^*.

Theorem 1 (Local stability of U_0 and existence of U^*)
If $\mathcal{R}_e < 1$ then System (3.14) has only the disease-free equilibrium U_0, which is locally asymptotically stable. If $\mathcal{R}_e > 1$, there is a unique endemic equilibrium U^* given by (3.15).

The stability of U^* is discussed in the next section.

3.3.1 Stability of the Endemic Equilibrium

To analyze the stability of the endemic equilibrium (EE), we linearize the system of ODE's around the endemic equilibrium. Let $U = (i_1, i_2, q_1, q_2, r)^T$ and rewrite (3.14) as $U' = F(U)$. The Jacobian of F at the EE U^* is given by

$$DF(U^*) = \begin{pmatrix} J_{1,1} & J_{1,2} & -i_1^*\nu & -i_1^*(\nu+\Omega) & -i_1^* - i_2^* \\ \Gamma & (i_2^*-1)\Gamma - \nu & -i_2^*\nu & -i_2^*(\nu+\Omega) & 0 \\ 0 & q_1^*\Gamma + \Gamma & -(q_1^*+1)\nu - \Omega & -q_1^*(\nu+\Omega) & 0 \\ 0 & q_2^*\Gamma & \Omega - q_2^*\nu & -(q_2^*+1)(\nu+\Omega) & 0 \\ 0 & r^*\Gamma & -r^*\nu & -r(\nu+\Omega)+\Omega & -\nu \end{pmatrix},$$

where $J_{1,1} = -2(i_1^* + i_2^*) - r - \Gamma - \nu + 1$ and $J_{1,2} = \Gamma i_1^* - 2(i_1^* + i_2^*) - r + 1$. The characteristic polynomial from the Jacobian matrix has the form

$$|yI - DF(U^*)| = y^5 + ay^4 + by^3 + cy^2 + dy + e.$$

Due to the length of the coefficients, they are included in the supplementary material (B.2). The parameters that the coefficients depend on are $\nu = \frac{\mu}{\beta}$, $\Gamma = \frac{2\gamma}{\beta}$,and $\Omega = \frac{2\omega}{\beta}$. The average longevity denoted by $1/\mu$ is on the scale of years, while the infectious $(1/\gamma)$ and isolation periods $(1/\omega)$ are on the scale of days; this allows us to conclude that ν is much smaller than Γ and Ω. Note that the components of the

endemic equilibrium $U^* = (i_1^*, i_2^*, q_1^*, q_2^*, r^*)$ as given in (3.15) are analytic functions of $\nu > -\delta$ for some $\delta > 0$ and

$$\begin{aligned}
i_1^* &= \left(\frac{1}{\Gamma} - \frac{1}{2}\right)\nu - \frac{\nu^2\left(4\Gamma^2 + \Gamma(\Omega-8) + 4\Omega\right)}{4\left(\Gamma^2\Omega\right)} + O\left(\nu^3\right), \qquad (3.18)\\
i_2^* &= \left(\frac{1}{\Gamma} - \frac{1}{2}\right)\nu + \frac{\nu^2\left(-4\Gamma^2 + \Gamma(\Omega+8) - 8\Omega\right)}{4\Gamma^2\Omega} + O\left(\nu^3\right),\\
q_1^* &= \frac{(2-\Gamma)\nu}{2\Omega} + \frac{\nu^2\left(-2\Gamma^2 + \Gamma(\Omega+4) - 8\Omega\right)}{4\Gamma\Omega^2} + O\left(\nu^3\right),\\
q_2^* &= \frac{(2-\Gamma)\nu}{2\Omega} + \frac{(\Gamma-8)\nu^2}{4\Gamma\Omega} + O\left(\nu^3\right),\\
r^* &= \left(1 - \frac{\Gamma}{2}\right) + \left(\frac{1}{4} - \frac{2}{\Gamma}\right)\nu + \nu^2\left(\frac{3}{\Gamma^2} - \frac{\Omega+32}{8\Gamma\Omega} + \frac{2}{\Omega}\right) + O\left(\nu^3\right).
\end{aligned}$$

Similarly, the coefficients of the characteristic polynomial are analytic functions of $\nu > -\delta$ and have the form:

$$\begin{aligned}
a(\nu) &= \frac{3\Gamma}{2} + \left(\frac{2}{\Gamma} + \frac{13}{4}\right)\nu + 2\Omega + O(\nu^2), \qquad (3.19)\\
b(\nu) &= \Omega(3\Gamma + \Omega) + \nu\left(\frac{4\Omega}{\Gamma} + \frac{5\Gamma}{2} + \frac{9\Omega}{2} + 4\right) + O\left(\nu^2\right),\\
c(\nu) &= \frac{3\Gamma\Omega^2}{2} + \frac{1}{4}\left(2(-2+\Gamma)^2\Gamma + 8(4+\Gamma)\Omega + \left(5 + \frac{8}{\Gamma}\right)\Omega^2\right)\nu + O\left(\nu^2\right),\\
d(\nu) &= \left((\Gamma-2)^2\Gamma\Omega + \left(4 - \frac{\Gamma}{2}\right)\Omega^2\right)\nu + O\left(\nu^2\right),\\
e(\nu) &= \Gamma\Omega^2\left(2-\Gamma\right)\nu + O\left(\nu^2\right).
\end{aligned}$$

The characteristic polynomial's coefficients are positive because $(2-\Gamma) > 0$ for biologically reasonable parameters; thus, we can conclude that for small $\nu > 0$, there are five distinct roots. The characteristic equation for $\nu = 0$ is

$$y^5 + a(0)y^4 + b(0)y^3 + c(0)y^2 = 0,$$

which has the following roots:

$$y_{1,2} = 0, \qquad y_{3,4} = -\Omega, \qquad y_5 = -\frac{3\Gamma}{2}. \tag{3.20}$$

By the implicit function theorem, $y_{3,4}(\nu)$ and $y_5(\nu)$ are analytic functions of ν and have the following series expansion

$$y_{3,4}(\nu) = -\Omega + \sum_{j=1}^{\infty} y_j \nu^j, \qquad y_5(\nu) = -\frac{3\Gamma}{2} + \sum_{j=1}^{\infty} y_j \nu^j.$$

From Kato [67], the roots of this polynomial have expansions

$$y(\nu) = \sum_{j=1}^{\infty} y_j \nu^j, \qquad y(\nu) = \sum_{j=1}^{\infty} y_j \nu^{j/2}.$$

Substituting these expansions into the characteristic polynomial eliminates the first expansion possibility, thus the second possibility with $\epsilon = \nu^{1/2}$ allows us to rewrite the coefficients in the following form.

$$\begin{aligned} a &= a(\Omega, \epsilon^2) = \frac{3\Gamma}{2} + 2\Omega + a_1(\Omega, \epsilon^2)\epsilon^2, \\ b &= b(\Omega, \epsilon^2) = \Omega(3\Gamma + \Omega) + b_1(\Omega, \epsilon^2)\epsilon^2, \\ c &= c(\Omega, \epsilon^2) = \frac{3\Gamma\Omega^2}{2} + c_1(\Omega, \epsilon^2)\epsilon^2, \\ d &= d(\Omega, \epsilon^2) = d_1(\Omega)\epsilon^2 + d_2(\Omega, \epsilon^2)\epsilon^4, \\ e &= e(\Omega, \epsilon^2) = e_1(\Omega)\epsilon^2 + e_2(\Omega, \epsilon^2)\epsilon^4. \end{aligned} \tag{3.21}$$

Thus, we will look for eigenvalues of $DF(U^*)(\nu)$ of the form $y = \epsilon\tilde{y}$, where $\epsilon = \nu^{1/2}$. Substituting the coefficients in the characteristic polynomial,

$$(\epsilon\tilde{y})^5 + a(\epsilon\tilde{y})^4 + b(\epsilon\tilde{y})^3 + c(\epsilon\tilde{y})^2 + d(\epsilon\tilde{y}) + (e_1(\Omega)\epsilon^2 + e_2(\Omega, \epsilon^2)\epsilon^4) = 0.$$

After some algebraic manipulations, we obtain the following five roots (details presented in supplementary section (B.4))

$$y_{1,2}(\nu) = \pm i\nu^{1/2}\sqrt{\frac{2(2-\Gamma)}{3}} + \nu\frac{\frac{6\Gamma^2(2-\Gamma)}{\Gamma+16} - \Omega}{3\Gamma\Omega} + O(\nu^{3/2}), \tag{3.22}$$

$$y_{3,4}(\nu) = -\Omega + O(\nu), \qquad y_5(\nu) = -\frac{3\Gamma}{2} + O(\nu).$$

If we use Ω as a bifurcation parameter, the roots $y_{1,2}$ cross the imaginary axis from left to right when Ω crosses a number close to $\Omega^* = \frac{6\Gamma^2(2-\Gamma)}{\Gamma+16}$ from left to right; by the implicit function theorem, we can show the crossing is transversal.

Theorem 3.3.1 *There is a function $\Omega_0(\nu)$ defined for small $\nu > 0$,*

$$\Omega_0(\nu) = \frac{6\Gamma^2(2-\Gamma)}{\Gamma+16} + O(\nu)^{1/2},$$

such that the system (3.11) satisfies the following property:

(a) The endemic equilibrium is locally asymptotically stable if $\Omega > \Omega_0(\nu)$ and unstable if $\Omega < \Omega_0(\nu)$, as long as Ω does not become too small.

(b) There is a Hopf bifurcation of periodic solutions at $\Omega = \Omega_0(\nu)$ for small enough $\nu > 0$. The periods are approximately

$$T = \frac{2\pi}{|\Im y_\pm|} \approx \frac{2\pi}{\sqrt{\frac{2(2-\Gamma)}{3}}\nu^{1/2}},$$

in the neighborhood of the Hopf bifurcation point.

(c) The stability of the bifurcating periodic solution is given by the sign of the following expression

$$\alpha = \frac{1}{16}\left(g^{(1)}_{rrr} + g^{(1)}_{rss} + g^{(2)}_{rrs} + g^{(2)}_{sss}\right) - \frac{1}{16\Im y_+(\Omega_0(0))}\left[g^{(1)}_{rs}\left(g^{(1)}_{rr} + g^{(1)}_{ss}\right) - g^{(2)}_{rs}\left(g^{(2)}_{rr} + g^{(2)}_{ss}\right) - g^{(1)}_{rr}g^{(2)}_{rr} + g^{(1)}_{ss}g^{(2)}_{ss}\right]\Big|_{r=s=\lambda=0},$$

where all partial derivatives are evaluated at the bifurcation point. The bifurcating periodic solution is locally asymptotically stable if $\alpha < 0$ *(supercritical case); it is unstable if* $\alpha > 0$.

To determine the stability of the Hopf bifurcation in Theorem 3.3.1, we use the center manifold reduction and determine that the Hopf bifurcation is supercritical and the bifurcating branch consists of stable periodic solutions in the neighborhood of the bifurcation point. The details of the proof are included in Supplementary Material (B.5).

3.4 Numerical Simulations

In this section, we analyze the model numerically using Mathematica to illustrate that the model with Gamma distributed infectious stages can provide more realistic critical value of the isolation period for the appearance of periodic solutions via Hopf bifurcation. We assume a longevity $(1/\mu)$ of 65 years and an infectious period before isolation $(1/\gamma)$ of 3 days. From these parameter values, we can estimate the transmission rate ($\beta = 2.133$) from the expression for the effective reproduction number $\mathcal{R}_e$ in Theorem 1.

As in [7], we choose $\mathcal{R}_e = 6.4$. From Theorem 3.3.1, we can approximate the isolation periods, $1/\omega_0 = \frac{\beta(\gamma+8\beta)}{12\gamma^2(\beta-\gamma)} \approx 15.5$ days, at which the endemic equilibrium becomes unstable. Figure 3.3 is a bifurcation generated by numerical simulations with the isolation period as the bifurcation parameter. The vertical axis shows the proportion $(I_1 + I_2)/N$ at the endemic equilibrium and, for $1/\omega > 1/\omega_0 \approx 15.5$, the maximum/minimum magnitude of the periodic solution.

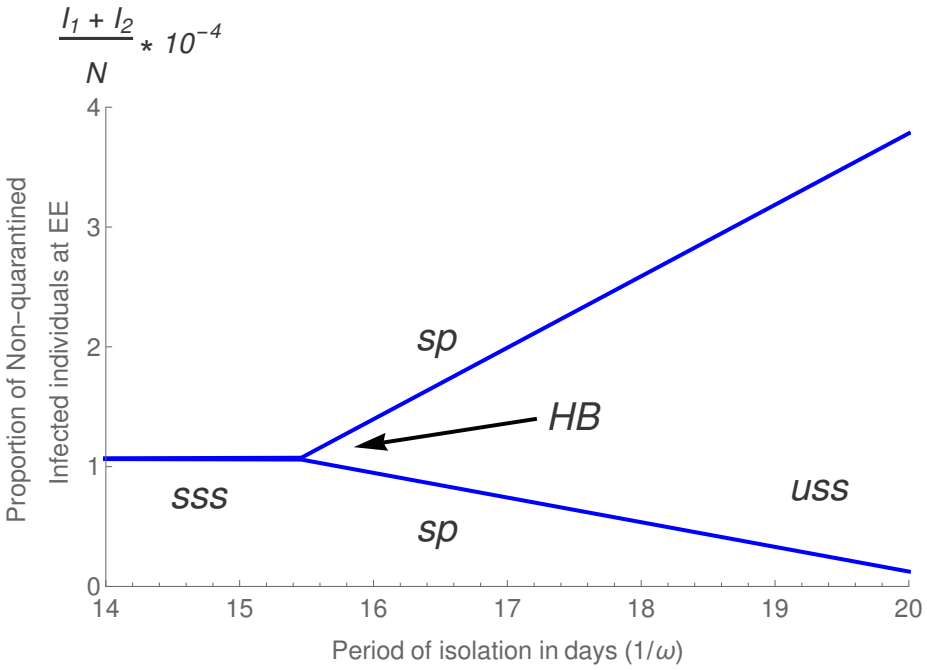

Figure 3.3.: A bifurcation diagram generated by numerical simulations, showing the fraction of individuals in the I stage at the endemic equilibrium vs the isolation period $1/\omega$. The portion of the line labeled with "sss" and "uss" denote the stable and unstable (endemic) steady-state, respectively, and "sp" denotes stable periodic solution. The two branches of the curves represent lower and upper amplitudes of the periodic solutions.

The Hopf bifucation can also be illustrated by plotting time-varying solutions for several values of isolation period near the bifurcation point $1/\omega_0 \approx 15.5$ days. This is shown in Figure 3.4. Similar to Figure 3.3, the proportion of individuals $(I_1 + I_2)/N$ is plotted as a function of time. Plots in (a)-(d) are for $1/\omega = 1$, 6, 16, and 30 days. We observe in (a) and (b) that the solutions converge to the endemic equilibrium as $t \to \infty$, and that the convergence takes longer as $1/\omega$ increases. In (c), the stable periodic solution appears due to the stability switch of the endemic equilibrium.

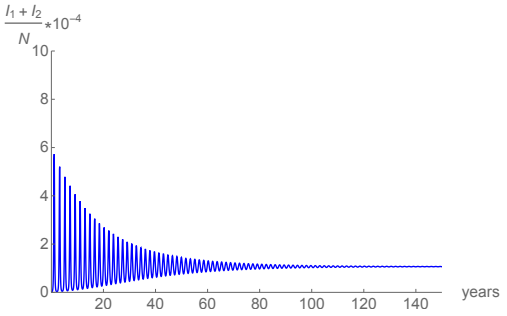

(a) Fraction of infected individuals $(I_1+I_2)/N$ over time with length of the isolation period $1/\omega = 1$ days.

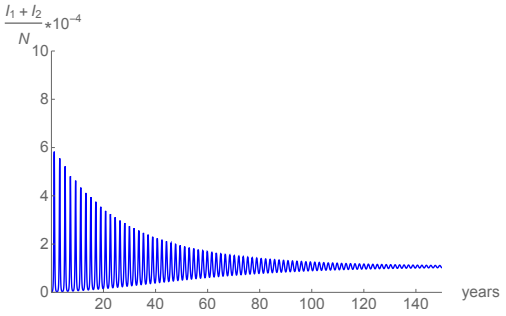

(b) Fraction of infected individuals $(I_1 + I_2)/N$ over time with length of the isolation period $1/\omega = 6$ days.

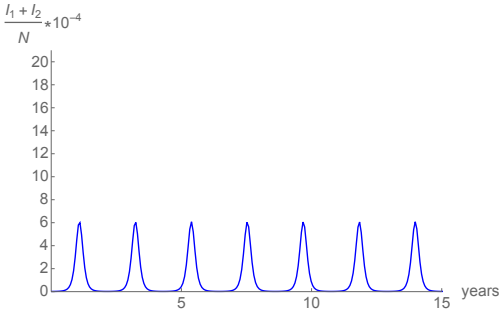

(c) Fraction of infected individuals $(I_1+I_2)/N$ over time with length of the isolation period $1/\omega = 16$ days.

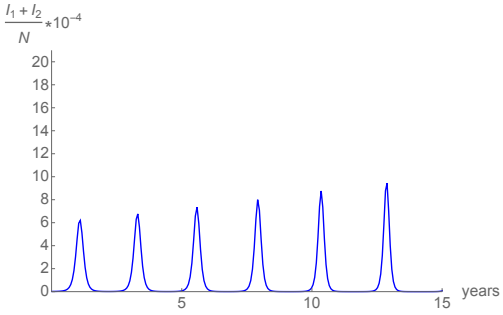

(d) Fraction of infected individuals $(I_1 + I_2)/N$ over time with length of the isolation period $1/\omega = 30$ days.

Figure 3.4.: Numerical solutions to the system of equations defined in Equation (3.11) for different values of the isolation period $1/\omega$.

3.5 Discussion

Childhood disease modeling remains an active research area, and the models have become increasingly sophisticated. Among the results of models that consider endogenous mechanisms to produce oscillations is that of Soper in 1929 [56], though his model is structurally unstable, and the oscillations are marginally stable. The modeling approach in [7] of using a SIQR model by including isolation (the Q compartment) and a modified incidence term provided a possible mechanism for producing sustained oscillations. However, due to the assumption of exponentially distributed infectious period, the condition required for the periodic solution to occur is too large for most childhood diseases. Using scarlet fever as an example, the authors showed that a stable periodic solution exists when the isolation period is greater than 23 days. By

relaxing the exponential distribution assumption and allowing Gamma distributions for the disease stages, the critical isolation period for sustained oscillations is reduced from 23 days to 15.5 days, which is in more realistic ranges for most childhood diseases.

The incorporation of a more realistic Gamma distribution for the infectious stage in the SIQR model made analysis more difficult, particularly proving the existence of a Hopf bifurcation and stability of the bifurcating periodic solution. The Jacobian matrix at the unique endemic equilibrium U^* has a polynomial of degree 5. By taking advantage of the different time scales of model parameters, the coefficients of leading terms of the eigenvalues of the characteristic equation are calculated, which allowed us to show that there are two complex and three negative eigenvalues. Moreover, the real part of the complex eigenvalues switches sign at a critical value of the isolation period $1/\omega$, which is shown to correspond to a Hopf bifurcation. By applying the Center Manifold Theorem, we show that the bifurcation is supercitical.

4. ASSESSING THE EFFECTS OF MODELING THE SPECTRUM OF CLINICAL SYMPTOMS ON THE DYNAMICS AND CONTROL OF EBOLA

This chapter has been adapted from J. Ponce,Y. Zheng, G. Lin, Z. Feng, Assessing the effects of modeling the spectrum of clinical symptoms on the dynamics and control of Ebola, *Journal of Theoretical Biology* 467 (2019) 01013. doi:10.1016/j.jtbi.2019.01.013 [68]. This work is included with permission from Elsevier.

4.1 Introduction

The 2014-15 Ebola outbreak in West Africa, which presented a serious threat to global public health, was declared a "public health emergency of international concern" by the WHO on August 8, 2014 [69]. The Ebola virus is transmitted among humans through close contact with bodily fluids of infected ill and dead persons, including blood, secretions, etc. [70]. Symptoms of Ebola infection vary widely, but commonly include fever, fatigue, loss of appetite, vomiting, diarrhea, and headache, as well as hemorrhagic symptoms [70]. For the 2014-15 West African Ebola outbreak, 87% of infected individuals exhibited fever, the most commonly reported symptom. And some hemorrhagic symptoms are rarely reported (<5.7%) [70]. This suggests that infected individuals experience a range of symptoms from mild to severe. Asymptomatic infections are quite possible, as shown in previous Ebola outbreaks [71, 72].

In the past year, two studies analyzed minimally symptomatic and asymptomatic ebola in the 2014-15 outbreak. Bower et al. tested 933 people in Kerry town, Sierra Leone, and found evidence of asymptomatic ebola in roughly 2.6% of the population studied. Additionally, 12% reported some symptoms and although they were undiagnosed, tested positive for Ebola antibodies [73]. A slightly smaller survey by

Richardson et al. on minimally symptomatic Ebola reported that up to 25% of Ebola infections may have been minimally symptomatic [74], which is consistent with previous outbreaks estimates [71, 72].

The 2014-15 Ebola outbreak in West Africa has been very well studied, the basic reproduction number has been computed, and control measures have been evaluated [75–82]. However, most models do not consider individuals who did not exhibit symptoms during the outbreak but tested positive for antibodies once swab studies were performed. Bellan et al. modeled asymptomatic individuals, though they did not assume post-mortem transmission of the disease and concluded that models without asymptomatic infection overestimate epidemic size [83]. Pandey et al. [84] included asymptomatic infection in their model but studied only its influence on epidemic sizes with different possible control measures. In addition, those authors did not study moderately symptomatic individuals, who might have reduced infectivity. The consequences of including moderately symptomatic individuals in the model warrants detailed study.

To model the spectrum of clinical symptoms of Ebola infection, Zheng developed a model with compartments for asymptomatic, mildly symptomatic, and severely symptomatic individuals [12]. This work considers a simplified version of that model, which considers infections with moderate and severe symptoms. However, that model did not provide significantly different results from the case without considering multiple levels of symptoms. This chapter analyzes the simpler model with moderate and severe symptoms, which improves the outcomes. We omit some of the derivation's details in this chapter, and we refer the reader to [12] for the complete information. For completeness, some of the similar derivations are included in this chapter; we emphasize new results and the modified model's aspects.

A Gamma distribution is adopted for a more realistic, yet mathematically tractable, infectious period. Once an individual becomes exposed to the disease, they can develop either severe or moderate symptoms. If an individual develops moderate symptoms, we assume they recover without needing to seek medical treatment. In

addition, we assume that those moderately symptomatic individuals from the exposed class probably are infectious, but less so than those with severe symptoms.

These moderately symptomatic people are important in estimating basic reproduction number and evaluating control effectiveness. For example, early outbreak data from Liberia are used to estimate the basic reproduction number (there were limited effects of control measures before the middle of September, 2014 [70, 84]) as 1.83 from the model with 30% moderate infections, which is consistent with the WHO estimate via a different approach. If moderate symptoms are disabled, however, the estimated reproduction number is 1.94, which is 6% higher. This shows that models without considering moderate infections might overestimate the basic reproduction number. In addition, the model without moderately symptomatic infections overestimates the reduction in transmission rates in the community, hospitals and after death due to international interventions. This implies that credit given to control measures may actually be due to moderately symptomatic infections.

4.2 A new model with severe and moderate infections

The objective of this paper is to enhance our understanding of the effects of including minimally symptomatic individuals on Ebola modeling. A compartmental model is developed by including a compartment for infected individuals with moderate symptoms. One of the important control measures for Ebola is isolation, which will be considered in our model as well. It has been demonstrated that, when control measures such as isolation are included in epidemiological models, one must consider disease sojourns that are more realistic than exponential distributions to avoid biased evaluations of disease control and prevention programs [64]. It has also been pointed out in [85] that, depending on the underlying assumptions on the epidemiological processes (e.g., recovery, hospitalization, disease induced death, etc.), the transition diagram between epidemiological classes can be very different, leading to significantly different model equations (see Models I, II and III and the corresponding

transition diagrams in [85]). In this paper, we adopt the same underlying assumption as for Model II in [85], which assumes that, from individuals with severe infections, the transitions to hospitalization and disease progression (recovery or death) are independent. Intuitively, the waiting times of these transitions are measured by two independent clocks. If the hospitalization clock chimes before recovery or death, the clock of disease progression continues to run until either recovery or death. If the disease progression clock chimes before hospitalization, the individual dies with probability f and recovers with probability $1-f$. More detailed explanations can be found in [85] including the reduction of this model from a system of integro-differential equations (with arbitrary stage durations) to a system of ordinary differential equations (ODEs) when waiting times follow Gamma distributions. When disease progression follows a Gamma distribution with shape parameter $n \geq 1$ and rate parameter γ, the hospitalization process follows an exponential distribution with parameter χ (a gamma distribution with shape parameter equal to 1) and disease progression for the moderate infections follows a Gamma distribution with shape parameter $m \geq 1$ and rate parameter γ_a; the transition diagram is depicted in Figure 4.1.

The total population is divided into the following epidemiological classes: susceptible S, latent (exposed) E, infectious with severe symptoms I_j, $j = 1, 2, \ldots, n$, infectious with moderate symptoms J_k, $j = 1, 2, \cdots, m$, hospitalized H_j, $j = 1, 2, \cdots, n$, disease-induced death and not safely buried D, and recovered R. The total population is $N = S + E + I + J + H + R$, where $I = \sum_{j=1}^{n} I_j(t)$, and $H = \sum_{j=1}^{n} H_j(t)$, and $J = \sum_{k=1}^{m} J_k(t)$. A diagram for transitions between classes is shown in Figure 4.1.

For new infections, depending on the outcome of viral replication and host immunological response, individuals could be mildly infectious with moderate symptoms (with a fraction δ) or fully infectious with severe symptoms (with a fraction $1 - \delta$). The force of infection, denoted by $\lambda(t)$, is given by

$$\lambda(t) = \frac{\beta_I \big[I(t) + \varepsilon J(t) \big] + \beta_H H(t) + \beta_D D(t)}{N(t)},$$

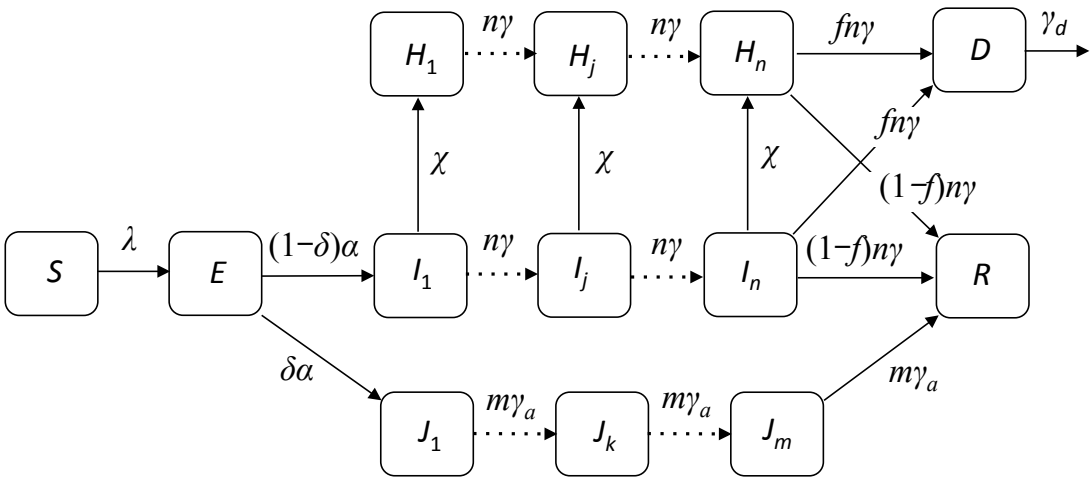

Figure 4.1.: Transition diagram between epidemiological classes under the assumption of Gamma distributed infectious stages for severe infections (I_j, $j = 1, 2, \cdots, n$) and moderate infections (J_k, $k = 1, 2, \cdots, m$) with shape parameters n and m, respectively. The mean infectious periods of these two types of infections are $1/\gamma$ and $1/\gamma_a$, and the mean duration from the time of death to burial is $1/\gamma_d$. The *per-capita* rate of hospitalization for individuals with severe infections is χ; this is the rate at which individuals in the I_j compartment enter the H_j compartment. The proportion of deaths for severe infections is f.

where β_I, β_H, and β_D are transmission rates in the community, hospital and at funerals (deceased but not yet safely buried), respectively, and ε is a factor ($0 \leq \epsilon \leq 0.2$) representing the reduced infectivity of individuals with moderate symptoms (or the ratio of infectivities of moderate and severe infections). The infectious periods of moderate and severe symptoms are assumed to follow Gamma distributions with shape parameters m and n, and mean infectious periods $1/\gamma_a$ and $1/\gamma$, respectively. This is equivalent to considering m and n sub-stages with transition rates from each sub-stage to the next equal to $m\gamma_a$ and $n\gamma$ (see Figure 4.1). Individuals with severe infections may be hospitalized at rate χ while at each of the n sub-stages. Deaths due to infection only occur at the last sub-stage of severe infections. Because this is an epidemic model for a single outbreak, demographic processes (births and natural deaths) are ignored.

The model consists of the following differential equations:

$$
\begin{aligned}
\frac{dS}{dt} &= -\lambda(t)S, \\
\frac{dE}{dt} &= \lambda(t)S - \alpha E, \\
\frac{dI_1}{dt} &= (1-\delta)\alpha E - (n\gamma + \chi)I_1, \\
\frac{dI_j}{dt} &= n\gamma I_{j-1} - (n\gamma + \chi)I_j, \quad j = 2, \ldots, n, \\
\frac{dH_1}{dt} &= \chi I_1 - n\gamma H_1, \\
\frac{dH_j}{dt} &= \chi I_j + n\gamma H_{j-1} - n\gamma H_j, \quad j = 2, \ldots, n, \\
\frac{dJ_1}{dt} &= \delta\alpha E - m\gamma_a J_1, \\
\frac{dJ_k}{dt} &= m\gamma_a J_{k-1} - m\gamma_a J_k, \quad k = 2, \ldots, m, \\
\frac{dD}{dt} &= fn\gamma I_n + fn\gamma H_n - \gamma_d D, \\
\frac{dR}{dt} &= (1-f)n\gamma I_n + (1-f)n\gamma H_n + m\gamma_a J_m,
\end{aligned}
\tag{4.1}
$$

where δ is the fraction of infections with moderate symptoms; $1/\gamma$ and $1/\gamma_a$ are the average periods for infections with severe and moderate symptoms; $1/\alpha$ is the latent period; χ is rate at which individuals with severe symptoms are hospitalized; and f is the fraction of severe infections resulting in death. As discussed in [85], the parameter γ can be chosen to be the weighted average of the interval from disease onset to recovery, $1/\gamma_{IR}$, and from onset to death, $1/\gamma_{ID}$, as follows:

$$
\frac{1}{\gamma} = (1-f)\frac{1}{\gamma_{IR}} + f\frac{1}{\gamma_{ID}}. \tag{4.2}
$$

All parameters with their definitions and ranges are listed in Table 4.1. The WHO Ebola Response Team published estimates for the 2014-15 Ebola outbreak in West African [70]. Authors of recently published studies estimated the reproduction number by fitting models to symptom onset dates during the initial stage of this outbreak [75, 78], and estimated parameters and evaluated interventions by calibrating models using these data [81,84]. Similar studies for previous outbreaks include [86,87]

and [79], which focused on estimates from the 1995 Congo and 2000 Uganda outbreaks, respectively.

Table 4.1.: Definition of the parameters in model 4.1, and the ranges of their values used in numerical simulations and sensitivity analysis.

Symbol	Definition	Value (Range)	References
β_I	Community transmission rate	0.319 (0.3, 0.33)	estimated
β_H	Hospital transmission rate	0.6 (0.55, 0.65)β_I	[78]
β_D	Traditional burial transmission rate	1.2 (1, 1.25)β_I	[84, 88]
ε	Ratio of infectivities of moderate to severe infections	0.1 (0, 0.2)	assumed
$1/\chi$	Mean time from disease onset to hospitalization	4.9 (4.8, 5.3) days	[70, 79, 87]
$1/\gamma_{ID}$	Mean time from disease onset to death	7.9 (7.5, 8.5)days	[79, 87]
$1/\gamma_{IR}$	Mean time from disease onset to recovery	9 (8.5, 9.5)days	[84]
$1/\gamma$	Mean of the Gamma distribution for severe infection	$= \frac{1-f}{\gamma_{IR}} + \frac{f}{\gamma_{ID}}$	[85]
$1/\gamma_a$	Mean of the Gamma distribution for moderate infection	3.1 (3, 7) days	assumed
$1/\gamma_d$	Mean time from deceased to buried	2.02 (1.5, 2.5) days	[79, 84, 87]
$1/\alpha$	Latent period	9.5 (9, 12)days	[70, 84, 86]
δ	Proportion of infections with moderate symptoms	0.3 (0.1, 0.42)	[83]
f	Proportion of disease death for severe infections	0.6966 (0.69, 0.73)	[70, 86]

4.3 Derivation of the basic and control reproduction numbers

The basic (control) reproduction number was calculated in [12] for the more extensive system. Here, we present the results applied to this simplified version of that model 4.1 and omit the details of the derivation. As with the more complex model, we can write the reproduction number as a weighted average of the reproduction number of severely symptomatic and moderately symptomatic individuals in the following way:

$$\mathcal{R}_c = (1-\delta)\mathcal{R}_{c1} + \delta\mathcal{R}_{c2}, \tag{4.3}$$

where $\mathcal{R}_{c1}$ and $\mathcal{R}_{c2}$ represent secondary infections produced by individuals with severe and moderate symptoms, respectively, given by

$$\begin{aligned}\mathcal{R}_{c1} &= (1-\delta)\left\{\beta_I \tfrac{1}{\chi}\left[1-\left(\tfrac{n\gamma}{n\gamma+\chi}\right)^n\right]+\beta_H\left(\tfrac{1}{\gamma}-\tfrac{1}{\chi}\left[1-\left(\tfrac{n\gamma}{n\gamma+\chi}\right)^n\right]\right)+\beta_D\tfrac{f}{\gamma_d}\right\},\\ \mathcal{R}_{c2} &= \frac{\delta\varepsilon\beta_I}{\gamma_a}.\end{aligned} \tag{4.4}$$

Therefore, from (4.3) and (4.4) we have

$$\mathcal{R}_c = (1-\delta)\left\{\beta_I\frac{1}{\chi}\left[1-\left(\frac{n\gamma}{n\gamma+\chi}\right)^n\right]+\beta_H\left(\frac{1}{\gamma}-\frac{1}{\chi}\left[1-\left(\frac{n\gamma}{n\gamma+\chi}\right)^n\right]\right)+\beta_D\frac{f}{\gamma_d}\right\}+\frac{\delta\varepsilon\beta_I}{\gamma_a}. \tag{4.5}$$

It can be verified that this expression for $\mathcal{R}_c$ is equivalent to that obtained using the next generation matrix method. The effects of disease control measures are represented by reduced transmission rates β_i $(i = I, H, D)$, interval from death to burial $1/\gamma_d$, and rate of hospitalization χ. In the absence of these parameter values, formula (4.5) provides an expression for the basic reproduction number $\mathcal{R}_0$.

Denote the four components of $\mathcal{R}_c$ associated with I, H, D, and J by $\mathcal{R}_c^I$, $\mathcal{R}_c^H$, $\mathcal{R}_c^D$, and $\mathcal{R}_c^J$, respectively. Then the expression in (4.5) can also be written as

$$\mathcal{R}_c = \mathcal{R}_c^I + \mathcal{R}_c^H + \mathcal{R}_c^D + \mathcal{R}_c^J,$$

where

$$\begin{aligned}\mathcal{R}_c^I &= (1-\delta)\beta_I\frac{1}{\chi}\left[1-\left(\frac{n\gamma}{n\gamma+\chi}\right)^n\right],\\ \mathcal{R}_c^H &= (1-\delta)\beta_H\left(\frac{1}{\gamma}-\frac{1}{\chi}\left[1-\left(\frac{n\gamma}{n\gamma+\chi}\right)^n\right]\right),\\ \mathcal{R}_c^D &= (1-\delta)\beta_D\frac{f}{\gamma_d},\\ \mathcal{R}_c^J &= \frac{\delta\varepsilon\beta_I}{\gamma_a}.\end{aligned} \tag{4.6}$$

These expressions in (4.6) can be helpful for examining how various factors may affect $\mathcal{R}_c$.

Remark: In the case when moderate infections are not considered, i.e., $\delta = 0$, the reproduction number given in (4.5) becomes $\mathcal{R}_c = \mathcal{R}_{c1}$ (see (4.4)), which is exactly the same as the reproduction number for Model II in [85]. This allows us to compare the models with and without moderate infections.

4.4 Data fitting and parameter estimation

We will use the situation in Liberia based on the WHO reports [89] to calibrate the model equations in 4.1. For demonstration purposes, we consider the model for the case of $n = 2$ and $m = 1$. The data corresponding to the initial phase of exponential growth is used to estimate the transmission parameters β_i $(i = I, H, D)$, which are then used to determine $\mathcal{R}_0$ using formula (4.5). By fitting the model to reports after control started, we can estimate the reductions in the transmission rates and the control reproduction number, $\mathcal{R}_c$, which then allows us to evaluate alternative control measures.

4.4.1 Estimation of transmission rates and the reproduction number

We use data from the 2014 Ebola outbreak in Liberia and obtained data from the CDC's website [90], extracted from the WHO situation reports [89]. Before September 14, 2014, the data are suitable to estimate the basic reproduction number because the local efforts to contain the outbreak from the middle of August 2014 were not significant [84] and the epidemic curve was not affected [70]. Therefore, we used the data from June 5, 2014, to September 14, 2014, to calibrate the models and estimate the basic reproduction number [70, 84].

The only parameters that we estimate are the transmission rates before control measures were implemented. We used the estimates obtained by the WHO Ebola Response Team [70] and the values listed in Table 4.1 for other parameters. We assume that the data from Liberia are Poisson samples and use the R package *bbmle* to perform the maximum likelihood estimation and *deSolve* to solve the system of

differential equations. The confidence intervals of the fitted parameters are computed using bootstrapping. The bootstrapping approach we used was resampling residuals, which fits the model, retains the fitted values and residuals. And then, it reassembles the data by pairing predictions and randomly resampled residuals and refits; finally refitting the model to the resampled data.

We use the initial outbreak data (before September 14th) to estimate the transmission rates β_i $(i = I, H, D)$, from which we estimated $\mathcal{R}_0$ using formula (4.5). Furthermore, we fix β_H and β_D to be proportional to β_I with the proportions in certain ranges (see Table 4.1) so that β_I is the only transmission rate estimated.

We noticed that the curve fitting is particularly sensitive to the choice of the initial and end points of the selected time period for the exponential growth. To account for this issue, we performed an 8-fold cross validation, which was chosen to have similarly sized sub-samples. The analysis was performed on datasets with 25 points and 26 points, excluding and including the last point. The 25-point dataset with the minimum average error (RMSE) was chosen. In addition, because the fitted values will depend on the choice of the proportion of moderate infections δ, for which there is no commonly accepted value, we obtain estimates for several values of δ including the case of no moderate infections ($\delta = 0$). We use Bower et al.'s [73] estimate that 12% of infections are moderately symptomatic as a lower bound for the value δ and Bellan et al.'s [83] estimate of 40% as an upper bound. We considered four scenarios in this section: (a) $\delta = 0$; (b) $\delta = 0.15$; (c) $\delta = 0.3$; and (d) $\delta = 0.5$. The corresponding estimates of $\mathcal{R}_0$ are 1.94, 1.89, 1.83, and 1.71 (these values and the confidence intervals are also listed in Table 4.2). For these four cases (a)–(d), the fitted curves are illustrated in Figure 4.2. These fitted curves generates estimates of β_I values with corresponding confidence intervals equal to 0.244 (0.232,0.25), 0.275 (0.26, 0.28), 0.319 (0.309, 0.33), and 0.409 (0.39, 0.42), respectively. We used the Akaike information criterion (AIC) to compare the models and evaluate which value of δ returns the best fit. The AIC estimates the relative quality of a statistical model for a given dataset by estimating the likelihood of a model to predict future values.

The four different values of δ are analyzed as different models, the best model is the one with the minimum AIC ($\delta = 0.3$) among the candidate models.

Although the estimates of $\mathcal{R}_0$ in all cases of (a)–(d) are in the range of existing estimates [86, 87], the estimate in (c), i.e., $\mathcal{R}_0 = 1.83$ (95% CI, 1.76 to 1.88), is the most consistent with the estimate from WHO response team (obtained using other statistical methods). In addition, for case (c), we estimate that community transmission, $\mathcal{R}_0^I = 0.78$ contributes the most to $\mathcal{R}_0$ at 42%. Contributions from other transmissions are $\mathcal{R}_0^H = 0.64$, $\mathcal{R}_0^D = 0.38$, and $\mathcal{R}_0^J = 0.03$, which consist of about 35%, 21%, and 1.6% of $\mathcal{R}_0$, respectively.

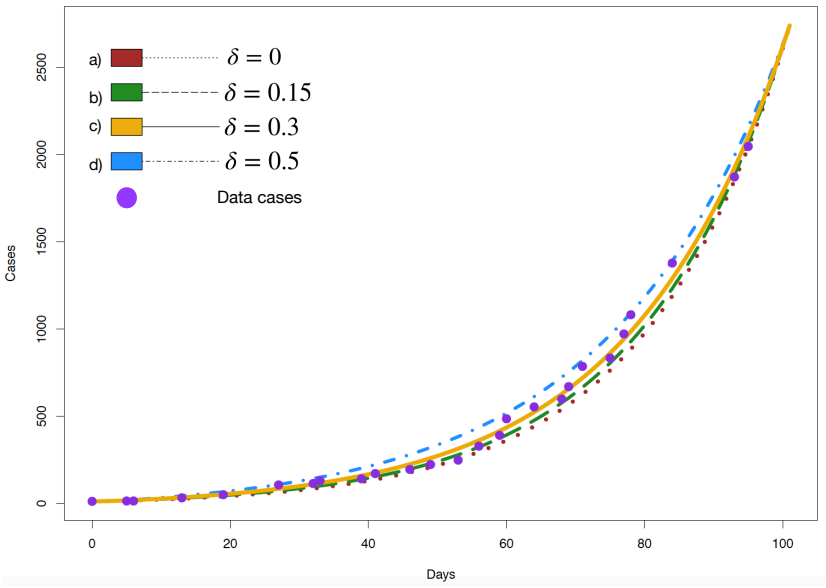

Figure 4.2.: Fitting of model 4.1 to the 2014 Ebola reports before control (i.e., from June 5th to September 8th). The line plots correspond to different proportions of moderate infections: (a) $\delta = 0$, (b) $\delta = 0.15$, (c) $\delta = 0.3$ (d) $\delta = 0.5$. For the cases (a)–(d), the Akaike information criterion (AIC) are 325, 281, 267, and 341, respectively.

Table 4.2.: Estimates of $\mathcal{R}_0$ corresponding to the model fitting presented in Figure 4.2 for four cases with different proportions of moderate infections: (a) $\delta = 0$, (b) $\delta = 0.15$, (c) $\delta = 0.3$, (d) $\delta = 0.5$. Estimates of the components $\mathcal{R}_0^i$ $(i = I, H, D, J)$ of $\mathcal{R}_0$ are also provided.

Case	$\mathcal{R}_0$ (95% CI)	$\mathcal{R}_0^I$ (95% CI)	$\mathcal{R}_0^H$ (95% CI)	$\mathcal{R}_0^D$ (95% CI)	$\mathcal{R}_0^J$ (95% CI)
(a)	**1.94** (1.84, 2.01)	**0.84** (0.79, 0.86)	**0.69** (0.66, 0.71)	**0.41** (0.38, 0.43)	**0**
(b)	**1.89** (1.79, 1.93)	**0.81** (0.76, 0.82)	**0.67** (0.63, 0.68)	**0.4** (0.38, 0.42)	**0.012** (0.012, 0.013)
(c)	**1.83** (1.76, 1.88)	**0.78** (0.74, 0.8)	**0.64** (0.62, 0.66)	**0.38** (0.36, 0.39)	**0.03** (0.028, 0.031)
(d)	**1.71** (1.62, 1.75)	**0.71** (0.67, 0.73)	**0.59** (0.56, 0.60)	**0.35** (0.32, 0.36)	**0.064** (0.06, 0.065)

CI: Confidence Interval.

4.4.2 Estimates of the control parameters

In countries with widespread and intense spreading, the West African Ebola outbreak's containment relied on non-pharmaceutical interventions due to ineffective treatment options. Non-pharmaceutical interventions include social mobilization, use of personal protective equipment (PPE) in healthcare facilities, safe burials, contact-tracing and quarantine. The social mobilization control measures implemented include information campaigns to raise awareness of the disease's transmission mode, social distancing from infected individuals, timely hospitalization, and safe handling of deceased individuals. Personal protective equipment can significantly lower the risk of infections in hospitals and healthcare facilities. Contact tracing programs allow probable cases to be identified and isolated early. Similarly, safe burials conducted by trained teams can help reduce transmission from deceased people. These interventions are linked to one or more parameters in the model; thus, a natural question is whether considering moderate symptoms in the model affects the estimated effectiveness of these interventions and to what extent ignoring this may contribute to biased evaluations.

Let t_c denote the time when intervention started in mid September, which for convenience is chosen to be 100 days from June 5th, 2014. To estimate the effect of control measures, we assume that the transmission rates for community (β_I), hospital

(β_H), and funeral (β_D) are reduced by factors z_I, z_H, and z_D, respectively. That is, the transmission rates for $t > t_c$ will be $\beta_i(1 - z_i)$, $i = I, H, D$. This change can be described by using piecewise-constant functions:

$$\beta_i(t) = \begin{cases} \beta_i & \text{for } t < t_c, \\ \beta_i(1 - z_i) & \text{for } t \geq t_c,\ i = I, H, D. \end{cases}$$

In addition, the time from onset to hospitalization ($1/\chi$) is assumed to be reduced by 0.25, i.e., around 1.2 days earlier in hospitalization due to control [76].

The estimated values of reductions z_i in the transmission rates are shown in Table 4.3 for (i) $\delta = 0$ and (ii) $\delta = 0.3$. We observe that the reductions in case (i) is larger than that in (ii), implying that models that do not explicitly include moderate infections (case (i)) may overestimate the effectiveness of the control measures considered here.

Figure 4.3 shows the comparison between fitted model curves and reports for both the period before intervention ($t < t_c = 100$), which is the same as the curves shown in Figure 4.2, and after ($t > t_c = 100$). We observe that, when moderate infections are considered ($\delta > 0$), particularly for the case of $\delta = 0.3$ (see (ii)), this model fits the data much better than the model without considering moderate infections explicitly (see (i)). These results suggest again that considering moderate infections is necessary to estimate the effects of interventions for policy-making.

Table 4.3.: Estimates of reductions (z_i, $i = I, H, D$) in transmission rates for four cases based on the proportion δ for moderate infections.

	Estimates (95% CI)	
Cases	(i) $\delta = 0$	(ii) $\delta = 0.3$
z_I	**0.987** (0.738, 1)	**0.83** (0.675, 0.945)
z_H	**0.514** (0.326, 0.652)	**0.49** (0.263, 0.51)
z_D	**0.23** (0, 0.527)	**0.217** (0, 0.259)

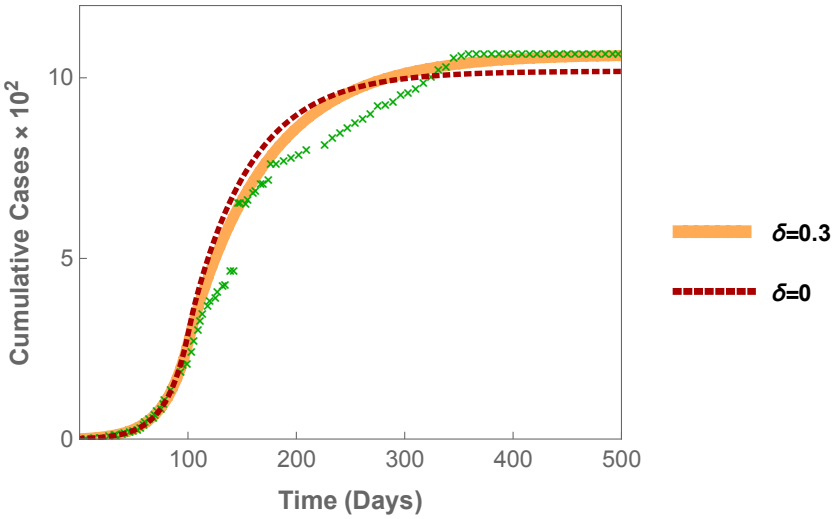

Figure 4.3.: Fitting of the model 4.1 to the 2014 Ebola data for the period between June 5th, 2014 and October 8th, 2015. For $t < t_c = 100$, the fit is the same as in Figure 4.2, whereas the fit for $t > t_c = 100$ is used for estimating the control reduction parameters z_i $(i = I, H, D)$. The two cases are for δ values: (i) $\delta = 0$ and (ii) $\delta = 0.3$. The jump in cases between day 100 and day 200 is due to a catch up in monitoring and reporting in Liberia [91].

4.5 Evaluation of alternative control scenarios

Using the parameters estimated in the previous sections, we can experiment different scenarios for alternative control strategies. For example, if the reduction factors z_i $(i = I, H, D)$ were higher or lower than the estimated values, and/or if the time of control t_c started earlier or was delayed, how much that would have affected the disease outcomes in terms of final epidemic size, peak size, and duration. Apparently these evaluation results will be depend on the choice of other parameter values. Thus, we will also examine the sensitivity of the reproduction number $\mathcal{R}_c$ and other measures (final size, peak size, etc.) to various model parameters.

4.5.1 The effects of timing of interventions

The timing of interventions is critical for disease control. Let T denote the time of intervention, and consider $T = t_c = 100$ (days) as the baseline scenario. We first investigate earlier or later starting times and examine how they may affect the results of the outbreak using measures including final epidemic size, peak size, duration of outbreak, and total number of deaths.

In Figure 4.4, the epidemic curves and cumulative cases for various scenarios are plotted. Early intervention corresponds to the starting time $T = 86$ and 93 while late intervention corresponds to $T = 107$ and 114. This is for the case of 30% moderate infections (i.e., $\delta = 0.3$, the case (c) in Table 4.2). All other parameter are fixed at the same values, and z_i correspond to case (ii) in Table 4.3.

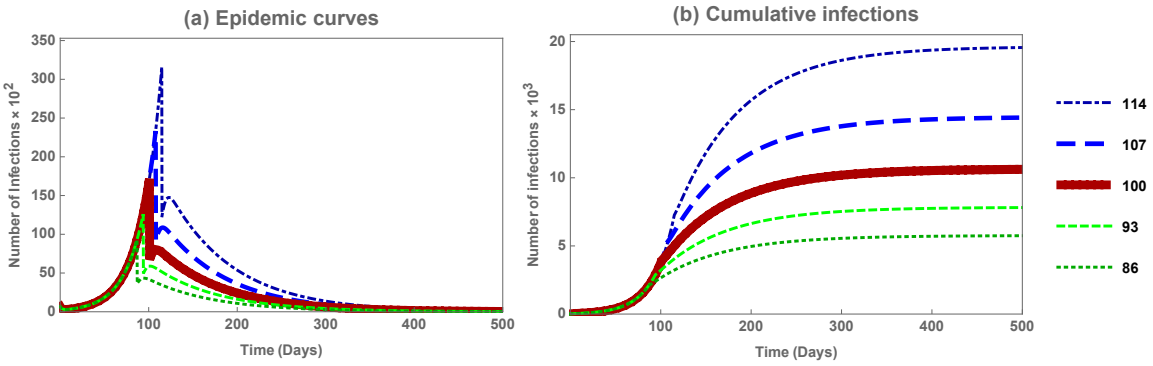

Figure 4.4.: Plots of (a) epidemic curves and (b) cumulative infections for various times to intervention T: The baseline scenario $T = t_c = 100$ (thicker solid line), with one or two weeks early intervention $T = 86$ and 93 and one or two weeks delayed intervention $T = 107$ and 114.

We observe in Figure 4.4 that the difference in both peak sizes and final sizes are very large between early and late interventions. For example, the peak and final size values of early intervention are a half of the baseline scenario (the thick solid curve) values. Similarly, the peak and final sizes double when control is applied two weeks later than the hundredth day. The reduction that we observe in the epidemic curves

in Figure 4.4 and Figure 4.5 close to day 100 is due to the application of control measures at different times.

We can also compare models with different proportions of moderate infections, including the case when moderate infections are not explicitly considered (i.e., $\delta = 0$). Figure 4.5 shows simulation results corresponding to the same set of two δ values as before. The cumulative and epidemic curves are shown in the top and bottom rows, respectively. The three columns are for (a) early intervention by one week ($T = 93$ days), (b) the baseline scenario $T = t_c = 100$ days), and (c) late intervention by one week ($T = 107$ days). It suggests again that the model with $\delta = 0$ overestimate the effects of early and delayed interventions. We observe in Figure 4.5 that, although the two models produce similar cumulative curves, they produce very different peak sizes for all three intervention times. Particularly, the peak size decreases with increasing δ, and the model without moderate infections ($\delta = 0$) produces the highest peak size, approximately 20% higher than the model with $\delta = 0.3$.

These differences between the two models are more transparent in Figure 4.6. The bar chart for peak sizes (a) shows that the reduction in peak sizes with one week early intervention are 70 for $\delta = 0$ and 51 for $\delta = 0.3$ and the increase in peak sizes with one week late intervention are 88 for $\delta = 0$ and 62 for $\delta = 0.3$. The plot in (b) shows that changes in final sizes generated by the two models do not differ significantly.

It can be helpful to derive a functional relationship between the time to intervention and the final epidemic size. By fitting the regression line

$$FS(t) = FS(t_0)exp(k(t - t_0)),$$

to the final size we obtained the values k=0.0488, 0.04375 for the cases of $\delta = 0$ and $\delta = 0.3$, respectively, as shown in Figure 4.7 (a). Figure 4.7 (b) is obtained using the formula $\frac{FS(t)-FS(t_c)}{FS(t_c)} * 100$. It shows that the final size percentage increases or decreases as control is applied for different values of t. If control is applied a week early ($t = t_c - 7$) where $t_c = 100$, the percentage of cases per day is negative. That is,

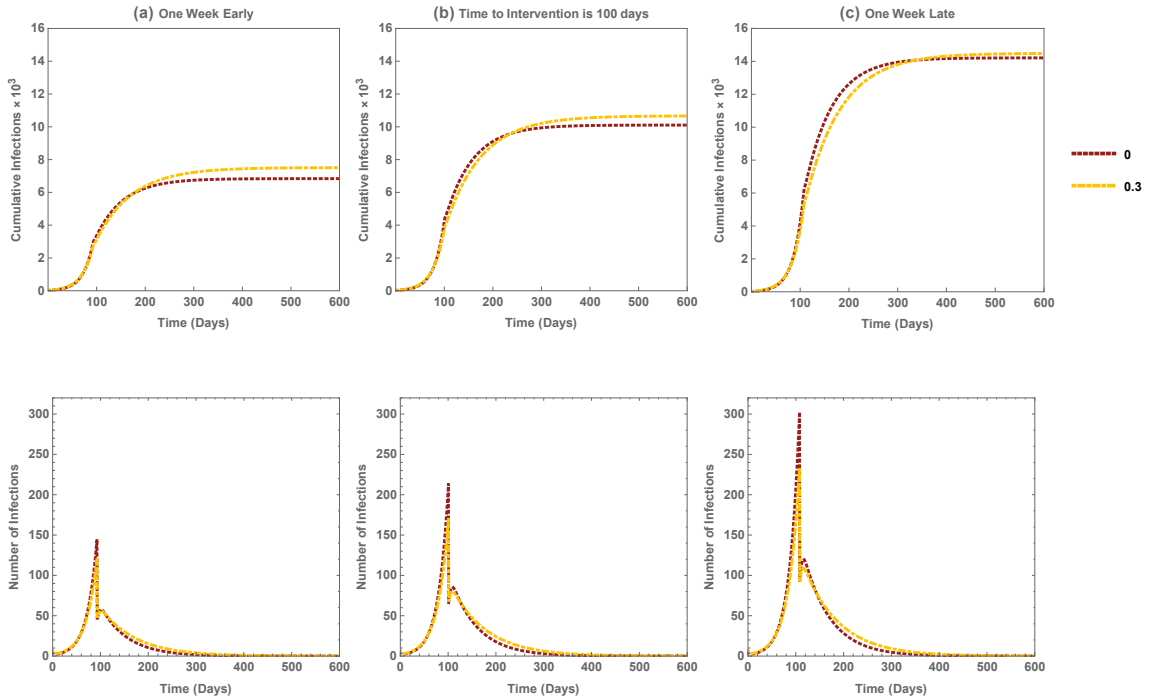

Figure 4.5.: Comparison of models with different proportions (δ) of moderate infections and timing T of intervention: (a) $T = 93$ (one week early), (b) $T = t_c = 100$, and (c) $T = 107$ (one week late). The curves show cumulative infections for different δ values: $\delta = 0$ and 0.3.

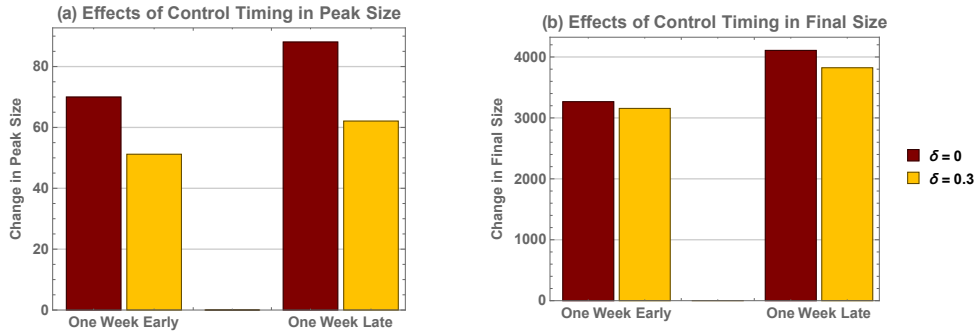

Figure 4.6.: Changes by one week earlier or later than the baseline scenario (i.e., $T = t_c = 100$ days) in (a) peak size and (b) final size for $\delta = 0$ and $\delta = 0.3$. All parameter values are the same as in Figures 4.4 and 4.5.

by applying control earlier, we have prevented roughly 27% of cases. Similarly, if we apply control measures a week later, the percentage is positive; the percentage increase

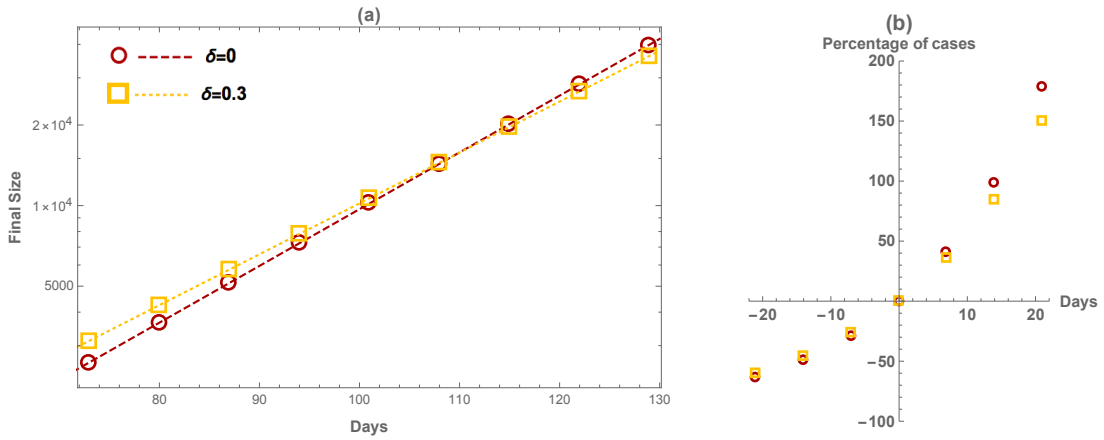

Figure 4.7.: Percentage of change of final sizes as a function of time of intervention with respect to the baseline scenario ($T = t_c = 100$ days) corresponding to different fractions of moderate infections δ.

is roughly 37%. We observe that the model without asymptomatic infections ($\delta = 0$) predicts a lower or higher final size for earlier or later interventions, respectively.

4.6 Sensitivity analysis of $\mathcal{R}_0$

A sensitivity analysis of $\mathcal{R}_0$ provides important information regarding how uncertainty and variability of model parameters may affect results and which parameters are most influential. The analysis is based on the Latin hypercube sampling method with 1000 points selected from assigned parameter ranges corresponding to the case of 30% moderate infections (see Table 4.1). The parameters considered in this analysis include transmission rates ($\beta_I, \beta_H, \beta_D$), progression rates from onset to recovery or hospitalization (γ, γ_a, γ_d, χ), and factors related to moderate infections (δ and ε), and death fraction (f).

A probability distribution (PDF) was assigned to each parameter to describe the range of possible values and their probabilities. The PDFs were chosen based on the biology of the disease and depending on whether the parameter was estimated or obtained from existing literature. The parameter ϵ was fixed, as well as the proportions

for β_H and β_D, because only β_I was estimated and the others are proportional to β_I. For all parameters except δ, a triangular distribution was used because it is recommended for situations in which a most likely value and a range for each parameter is estimable [92]. In the case of δ, a uniform distribution was used because studies provide a wide range for this parameter. Partial rank relation coefficients (PRCC) were computed between the values of the seven parameters that identified the independent effect of each parameter on $\mathcal{R}_0$. In this study, we assume statistical independence of the input parameters.

The results are illustrated in Figure 4.8.

4.6.1 Sensitivity analysis of peak and final epidemic sizes

Under the control measures corresponding to z_i $(i = I, H, D, \chi)$ in case (ii) of Table 4.3, deterministic simulations generate the peak and final sizes shown in Figure 4.4. When parameters are selected based on LHS with 1000 simulated epidemics, the distributions of the peak and final sizes are illustrated in Figure 4.9. The parameter ranges correspond to cases (c) in Table 4.2 and (ii) in Table 4.3, and the time to intervention is the baseline scenario (i.e., $t_c = 100$ days). We observe that, although the means for both the peak (a) and the final (b) sizes are consistent with those shown in Figure 4.4 (the thick solid curve), the variances are large.

4.6.2 Control measures and their effects on the time course

To assess the importance of various control measures for future outbreaks, we conducted a time course sensitivity analysis based on the 2014-15 Liberia outbreak. This is done again through Latin hypercube sampling of the control parameters represented by z_I, z_H, and z_D (reductions in β_I, β_H, and β_D) and the timing of intervention, denoted by T. The partial rank correlation coefficients (PRCC) are presented in Figure 4.10. The ranges for z_I, z_H, and z_D are same as the confidence intervals estimated in Table 4.3. The range for T is chosen to be between 1 week before and 1 week after

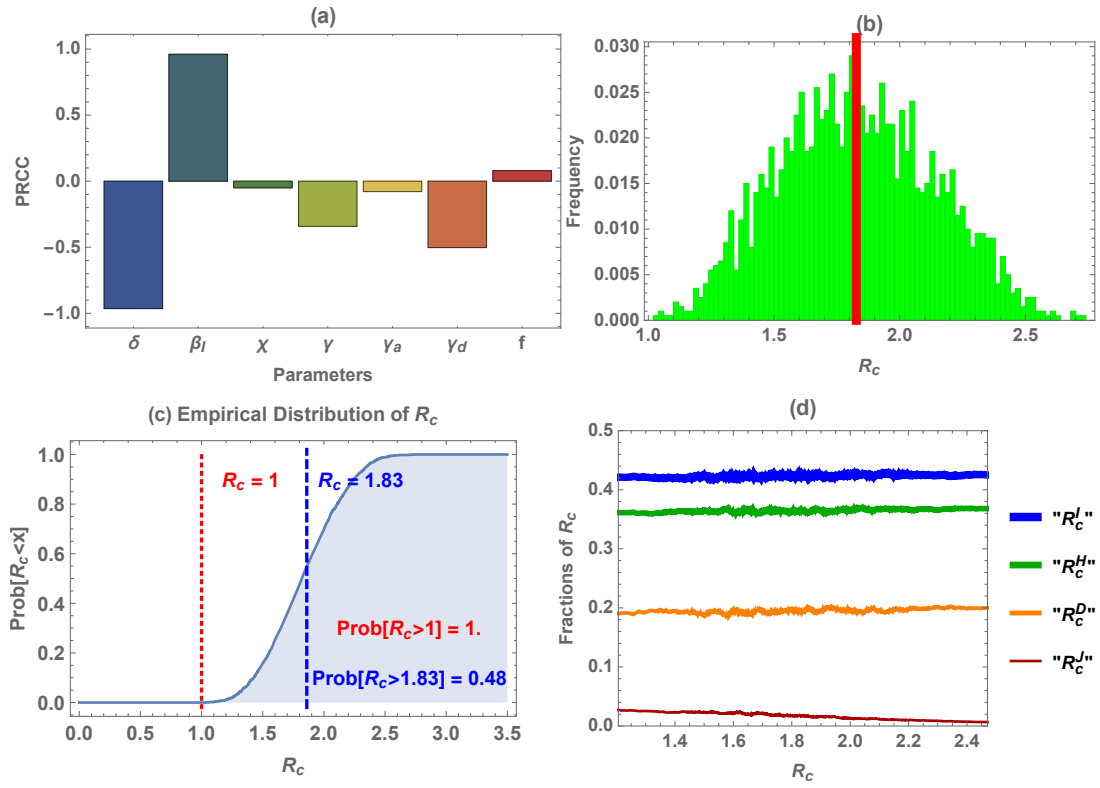

Figure 4.8.: Sensitivity and uncertainty analyses of the basic reproduction number $\mathcal{R}_c$ with respect to model parameters. Values of the parameters are chosen using the Latin hypercube sampling method, with the ranges around the values corresponding to the case of 30% moderate infections as listed in Table 4.1. The plots in the top row show the PRCC values of these parameters (left) and the distribution of $\mathcal{R}_c$ (right). The bottom row shows the empirical CDF of $\mathcal{R}_c$ (left) and the contributions of $\mathcal{R}_c^i$ $(i = I, H, D, J)$ to $\mathcal{R}_c$ (right).

the baseline scenario $t_c = 100$ (days), and the range for the reduction parameter z_χ (time from onset to hospitalization) is (0, 0.3).

We observe that the PRCC curves of control parameters are similar and close to zero before implementation of control measures. Once control measures were implemented, the PRCC curves of different control parameters quickly approach relatively stable values. The first PRCC curve to approach 1 is the timing of control measures, which is positively correlated with cumulative cases. This is because the later that

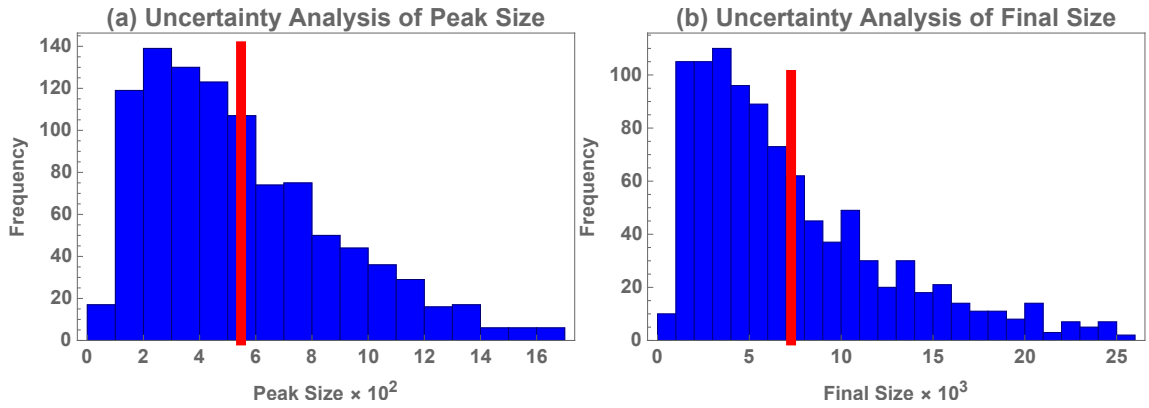

Figure 4.9.: Similar to Figure 4.8(b) but results of the uncertainty analysis for the peak and final sizes. This figure illustrates distributions of the peak and final sizes of 1000 simulated epidemics with parameters selected using LHS from ranges corresponding to the case of 30% moderate infections.

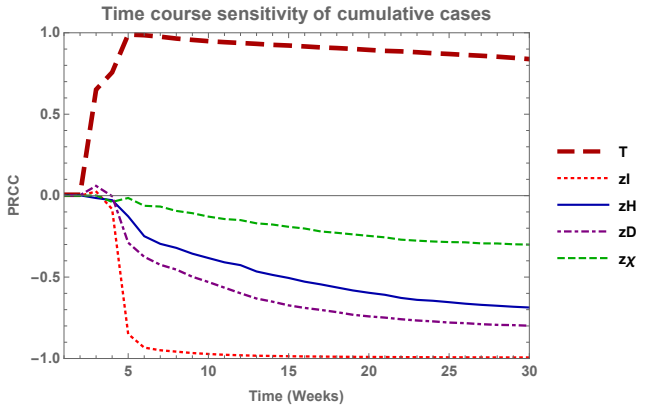

Figure 4.10.: Time course sensitivity with respect to control parameters.

control measures are implemented, the larger the outbreak. Early implementation of control measures is very important in the exponential growth phase of any outbreak. As time increases, the influence of time to intervention diminishes. All other control measures are negatively correlated, which implies that implementing these control measures mitigates the outbreak. The most influential measures are the reductions in community and hospital transmission (z_I and z_D), followed by z_H and z_χ.

4.7 Discussion

To investigate the impact of a spectrum of symptoms of Ebola infection, we modeled Ebola infections with moderate and severe symptoms. Those with moderately symptomatic infections from the exposed class have some viral replication, which is controlled due to strong innate immunity plus successful adaptive immunity. These individuals are not very infectious despite moderately symptomatic infections, because they have few viruses circulating within their bodies. Individuals with severe symptoms have higher viral load and therefore are more infectious than people with moderately infections. Various levels of moderately symptomatic infections are considered in our analysis based on estimates by Bower et al. [73], Bellan et al. [83] and Richardson et al. [74].

The model developed in this paper extends Model II in [85] by explicitly including moderate infections. The formulation and its underlying assumptions are demonstrated via integro-differential equations and their reduction to ordinary differential equations in [85]. The merit of this model is that it retains the infection history even after hospitalization. This is important in determining times of recovery and death, especially when no treatment is available. The Gamma assumption also provides a realistic infectious period, and infectious individuals recover or die in the later stage of the infection, but not sooner.

The results in this paper illustrate the importance of considering infections with moderate symptoms. First, the estimated basic reproduction number $\mathcal{R}_0$ for the model with 30% moderate infections ($\delta = 0.3$) is 1.83, which is the most consistent (among the models with different δ values) with WHO's empirical estimate (see Table 4.2). It is worth noting that our reproduction numbers are obtained by fitting our models directly to cases using maximum likelihood estimation. Alternatively, one can estimate the exponential growth rate of early cases and connect the rate to reproduction number by assuming a generation interval [93]. The estimate of $\mathcal{R}_0$ can be inflated when excluding moderate infections in the model ($\delta = 0$). However,

uncertainty analysis of $\mathcal{R}_0$ of the model with 30% moderate infections could lead to reproduction numbers from 1.2 to 2.4 (see Figure 4.8). We show that the sensitivity of $\mathcal{R}_0$ to δ (percentage of moderately symptomatic individuals) is higher than to most other parameters (see Figure 4.8(a)), and that the most influential components of $\mathcal{R}_0$ is $\mathcal{R}_0^I$ followed by $\mathcal{R}_0^H$ (see Figure 4.8(d)).

Second, the effectiveness of interventions is over-estimated when ignoring the moderate infections. We demonstrate in Figures 4.4–4.6 that, although models with various δ values provide similar evaluations of the effect of control measures on the final epidemic sizes, the model with $\delta = 0$ predicts a much higher effectiveness of early intervention than models with $\delta = 0.3$. Thus, without considering moderately symptomatic infections, extra credit is given to implemented control measures. The sensitivity analysis also shows that the variances in the peak and final epidemic sizes are relatively large (Figure 4.9) and that the reduction in β_I (among all β_i's, $i = I, H, D, \chi$) is the most influential to the cumulative number of cases over the entire time course, while the timing of interventions diminishes (see Figure 4.10).

In addition, the timing of interventions is of great importance to mitigate final epidemic size. Because final size is an exponential function of the time to intervention, early interventions could significantly reduce epidemic size. An empirical regression equation linking final size and timing of interventions could be useful for policy-making.

It is necessary to stratify infections by severity of clinical symptoms in modeling. This permits reasonable estimates of the reproduction number and effectiveness of control measures, especially when infected persons present with various symptoms. More epidemiological investigation of moderately symptomatic infections of Ebola will be helpful to estimate their fractions of the total infection and infectivity. These are crucial to more useful modeling of future outbreaks.

5. SUMMARY

In this thesis, I developed models that help understand how assumptions affect predictions, parameter estimations, and control measures using different diseases as examples. The models explore the impact of age structure, inclusion of asymptomatic individuals in the model and, different distributions for the infectious period. In chapter 2, an age-structured COVID-19 model was introduced, based on Chao and Feng's work [11]. The system divides the population into different age groups and health status, which allows us to analyze targeted policies. In this case, the importance of including different age groups in a population is that results obtained for one country do not necessarily extend to another. The difference in societal structures is reflected in the contact matrix for each country and policies that should be implemented to minimize transmission. We fitted the model to age stratified infections reported from Ecuador during the COVID-19 outbreak and analyzed two distinct policies against a baseline delayed-release policy. We found that releasing the active workforce is better than reopening schools while continuing to restrict the active workforce. The measures used to evaluate the different policy options were: total cases and deaths prevented and minimizing daily cases to prevent peaks in incidence. We conclude that releasing the population's economically active sector provides more benefits than releasing the youngest, lowest risk groups. In addition, we determine that timing is of great importance for the implementation of control measures. Control measures applied for a short period followed by loosening restrictions for all age groups cause high subsequent waves.

Chapter 3 was motivated by recurrent childhood disease outbreaks with relatively short infectious periods. We follow Feng and Thieme, who obtained oscillations by combining alternative assumptions about the incidence term (isolated individuals were removed) and isolation. This chapter considers a general model with arbitrarily

distributed infectious and quarantine stages and then recovers the ODE model when Gamma distributions are used for infected and quarantined stages. Changing the distribution from an exponential to Gamma allows the critical point (isolation period) necessary for sustained oscillations to be reduced from 3 [7] to 2 weeks, which makes this model applicable to many more childhood diseases. We analyze the system's stability, identify the critical value of the isolation period, and prove the existence of a Hopf bifurcation, which is consistent with the results from [7].

In chapter 4, we developed a model including moderate and severe symptoms based on previous work by Zheng [12], which takes into account the possibility that individuals could be asymptomatic or have moderately symptomatic infections, as reported during previous Ebola outbreaks. We fit the model to capture the dynamics of the recent outbreak of Ebola in Liberia, and estimate the basic reproduction number as 1.83 (CI: 1.72, 1.86), consistent with the WHO response team's empirical estimate. We compare the model to one with typical symptoms by excluding moderate ones. The model with only typical symptoms overestimates the basic reproduction number and effectiveness of control measures and exaggerates peak size changes attributable to interventions' timing. In this study, we show that including asymptomatic Ebola infections may have crucial implications for policy-making.

Some of the limitations of chapter 2 include parameter identifiability issues, both practical and structural, which can be addressed by performing identifiability analysis on the model. Finally, given recent vaccine developments, a vaccination strategy could also be considered when designing the policies. The mathematical model could be adapted to include vaccinated individuals in a separate compartment.

Computing the interepidemic periods in the model (3.11)in chapter 3 would allow us to understand when outbreaks are likely to occur. Furthermore, we could compare how the Gamma distribution impacts these estimates. The Ebola model studied in chapter4 includes Gamma distributed infectious period with shape parameter 2. This allowed simpler simulations; however, further study is required to decide the specific number of sub-compartments needed for the infectious period of both symptomatic

and asymptomatic individuals. Similarly, the numerical solutions of the childhood disease model studied in chapter 4 could also benefit from using a disease-specific value for the shape of the Gamma distributions considered.

REFERENCES

[1] W. O. Kermack and A. G. McKendrick. A Contribution to the Mathematical Theory of Epidemics. *Proceedings of the Royal Society A: Mathematical, Physical and Engineering Sciences*, 115(772):700–721, 8 1927.

[2] KJ Gough. The estimation of latent and infectious periods. *Biometrika*, 64(3):559–565, 1977.

[3] Norman TJ Bailey. A statistical method of estimating the periods of incubation and infection of an infectious disease. *Nature*, 174(4420):139–140, 1954.

[4] Dorothy Anderson and Ray Watson. On the spread of a disease with gamma distributed latent and infectious periods. *Biometrika*, 67(1):191–198, 1980.

[5] O. Diekmann, J A P. Heesterbeek, and J A J Metz. On the definition and the computation of the basic reproduction ratio R0 in models for infectious diseases in heterogeneous populations. *Journal of Mathematical Biology*, 28(4):365–382, 6 1990.

[6] P. Van Den Driessche and James Watmough. Reproduction numbers and subthreshold endemic equilibria for compartmental models of disease transmission. *Mathematical Biosciences*, 180(1-2):29–48, 2002.

[7] Zhilan Feng and Horst R Thieme. Recurrent outbreaks of childhood diseases revisited: the impact of isolation. *Mathematical Biosciences*, 128(1-2):93–130, 1995.

[8] Stephen Wiggins. *Introduction to applied nonlinear dynamical systems and chaos*, volume 2. Springer Science & Business Media, 2003.

[9] Kiesha Prem, Alex R Cook, and Mark Jit. Projecting social contact matrices in 152 countries using contact surveys and demographic data. *PLoS computational biology*, 13(9):e1005697, 2017.

[10] Zhilan Feng and John W Glasser. Mixing in meta-population models. In *The Dynamics of Biological Systems*, pages 99–126. Springer, 2019.

[11] Henry Zhao and Zhilan Feng. Staggered release policies for covid-19 control: Costs and benefits of relaxing restrictions by age and risk. *Mathematical biosciences*, page 108405, 2020.

[12] Yinqiang Zheng. *Mathematical Models of Ebola Virus Disease and Vaccine Preventable Diseases*. PhD thesis, Purdue University, 2016.

[13] Juanjuan Zhang, Maria Litvinova, Yuxia Liang, Yan Wang, Wei Wang, Shanlu Zhao, Qianhui Wu, Stefano Merler, Cécile Viboud, Alessandro Vespignani, et al. Changes in contact patterns shape the dynamics of the covid-19 outbreak in china. *Science*, 2020.

[14] Michael Day. Covid-19: identifying and isolating asymptomatic people helped eliminate virus in italian village. *Bmj*, 368:m1165, 2020.

[15] Talha Burki. Covid-19 in latin america. *The Lancet Infectious Diseases*, 20(5):547–548, 2020.

[16] Otmani M. Covid-19: First results of the voluntary screening in iceland – nordic life science – the leading nordic life science news service. nordic life science – the leading nordic life science news service. Available at `https://nordiclifescience.org/covid-19-first-results-of-the-voluntary-screening-in-iceland/` (2020).

[17] Sijia Tian, Nan Hu, Jing Lou, Kun Chen, Xuqin Kang, Zhenjun Xiang, Hui Chen, Dali Wang, Ning Liu, Dong Liu, et al. Characteristics of covid-19 infection in beijing. *Journal of Infection*, 2020.

[18] WW Sun, F Ling, JR Pan, J Cai, ZP Miao, SL Liu, W Cheng, and EF Chen. Epidemiological characteristics of 2019 novel coronavirus family clustering in zhejiang province. *Zhonghua yu Fang yi xue za zhi [Chinese Journal of Preventive Medicine]*, 54:E027–E027, 2020.

[19] Miguel Reina Ortiz and Vinita Sharma. Modeling the covid-19 outbreak in ecuador: Is it the right time to lift social distancing containment measures? *medRxiv*, 2020.

[20] Carlos Enrique Bustamante Orellana, Jordy Jose Cevallos Chavez, Cesar Montalvo, Jeff Sullivan, Edwin Michael, and Anuj Mubayi. Modeling and preparedness: The transmission dynamics of covid-19 outbreak in provinces of ecuador. *medRxiv*, 2020.

[21] Irene Torres and Fernando Sacoto. Localising an asset-based covid-19 response in ecuador. *The Lancet*, 395(10233):1339, 2020.

[22] John A Jacquez, Carl P Simon, James Koopman, Lisa Sattenspiel, and Timothy Perry. Modeling and analyzing hiv transmission: the effect of contact patterns. *Mathematical Biosciences*, 92(2):119–199, 1988.

[23] Anthony Faiola and Ana Herrero. Uncollected bodies lie for days in the streets of ecuador: The emerging epicenter of the coronavirus in latin america. *Stuff/Fairfax*, 2020.

[24] Agencia EFE El Comercio. Gobierno decreta emergencia sanitaria en ecuador por covid-19. *El Comercio*, 2020.

[25] Victor Serrano. Toque de queda parcial se inicia desde este martes en el ecuador. *El Universo*, 2020.

[26] Associated Press. Quito retoma actividad tras largo confinamiento por covid-19. *The San Diego Union-Tribune*, 2020.

[27] Servicio Nacional de Gestión de Riesgos y Emergencias. Resoluciones coe. Technical report, Servicio Nacional de Gestión de Riesgos y Emergencias, 2020.

[28] CDC. Covid-19 pandemic planning scenarios. Available at `https://www.cdc.gov/coronavirus/2019-ncov/hcp/planning-scenarios.html`(10-July-2020), July 2020.

[29] Nicholas G Davies, Petra Klepac, Yang Liu, Kiesha Prem, Mark Jit, Rosalind M Eggo, CMMID COVID-19 working group, et al. Age-dependent effects in the transmission and control of covid-19 epidemics. *MedRxiv*, 2020.

[30] Ronny Correa-Quezada, Leonardo Izquierdo, and Diego Garcia-Velez. Informe de economía de ecuador: Enero-mayo 2020 impacto del covid-19 en ecuador. Technical report, Universidad Técnica Particular de Loja, 2020.

[31] INEC. Proyecciones poblacionales. *Instituto Nacional de Estadisticas y Censos*, 2020.

[32] Stavros Busenberg and Carlos Castillo-Chavez. A general solution of the problem of mixing of subpopulations and its application to risk-and age-structured epidemic models for the spread of aids. *Mathematical Medicine and Biology: A Journal of the IMA*, 8(1):1–29, 1991.

[33] Ministerio de Salud Pública del Ecuador. Boletines epidemiológicos coro- navirus covid-1. Technical report, Ministerio de Salud Pública del Ecuador, 2020.

[34] Ruiyun Li, Sen Pei, Bin Chen, Yimeng Song, Tao Zhang, Wan Yang, and Jeffrey Shaman. Substantial undocumented infection facilitates the rapid dissemination of novel coronavirus (sars-cov-2). *Science*, 368(6490):489–493, 2020.

[35] Daniel P Oran and Eric J Topol. Prevalence of asymptomatic sars-cov-2 infection: A narrative review. *Annals of Internal Medicine*, 2020.

[36] Roman Wölfel, Victor M Corman, Wolfgang Guggemos, Michael Seilmaier, Sabine Zange, Marcel A Müller, Daniela Niemeyer, Terry C Jones, Patrick Vollmar, Camilla Rothe, et al. Virological assessment of hospitalized patients with covid-2019. *Nature*, 581(7809):465–469, 2020.

[37] CDC. Covid-19 laboratory-confirmed hospitalizations. Available at `https://gis.cdc.gov/grasp/COVIDNet/COVID19_5.html`(25-July-2020), July 2020.

[38] Robert Verity, Lucy C Okell, Ilaria Dorigatti, Peter Winskill, Charles Whittaker, Natsuko Imai, Gina Cuomo-Dannenburg, Hayley Thompson, Patrick GT Walker, Han Fu, et al. Estimates of the severity of coronavirus disease 2019: a model-based analysis. *The Lancet infectious diseases*, 2020.

[39] Niel Hens, Girma Minalu Ayele, Nele Goeyvaerts, Marc Aerts, Joel Mossong, John W Edmunds, and Philippe Beutels. Estimating the impact of school closure on social mixing behaviour and the transmission of close contact infections in eight european countries. *BMC infectious diseases*, 9(1):1–12, 2009.

[40] Kenji Mizumoto, Katsushi Kagaya, Alexander Zarebski, and Gerardo Chowell. Estimating the asymptomatic proportion of coronavirus disease 2019 (covid-19) cases on board the diamond princess cruise ship, yokohama, japan, 2020. *Eurosurveillance*, 25(10):2000180, 2020.

[41] Xian Zhou, Yang Li, Tao Li, and Wenhong Zhang. Follow-up of asymptomatic patients with sars-cov-2 infection. *Clinical Microbiology and Infection*, 2020.

[42] Andreas Kronbichler, Daniela Kresse, Sojung Yoon, Keum Hwa Lee, Maria Effenberger, and Jae Il Shin. Asymptomatic patients as a source of covid-19 infections: A systematic review and meta-analysis. *International Journal of Infectious Diseases*, 98:180–186, 2020.

[43] Hiroshi Nishiura, Tetsuro Kobayashi, Takeshi Miyama, Ayako Suzuki, Sungmok Jung, Katsuma Hayashi, Ryo Kinoshita, Yichi Yang, Baoyin Yuan, Andrei R Akhmetzhanov, et al. Estimation of the asymptomatic ratio of novel coronavirus infections (covid-19). *medRxiv*, 2020.

[44] Yaset Caicedo Ochoa, David E Rebellón Sanchez, Marcela Peñaloza, Hector F Cortes Motta, and Yardany R Méndez-Fandiño. Effective reproductive number estimation for initial stage of covid-19 pandemic in latin american countries. *International Journal of Infectious Diseases*, 2020.

[45] Google LLC. Google covid-19 community mobility reports. Available at `https://www.google.com/covid19/mobility/` (09/12/2020).

[46] Instituto Nacional de Estadísticas y Censos. Camas y egresos hospitalarios. Available at `https://www.ecuadorencifras.gob.ec/camas-y-egresos-hospitalarios/` (2020).

[47] M. Alexander Otto. Covid-19 update: Transmission 5% or less among close contacts. Available at `https://www.the-hospitalist.org/hospitalist/article/218769/coronavirus-updates/covid-19-update-transmission-5-or-less-among-close`(11-March-2020), March 2020.

[48] World Health Organization. Measles fact sheet. Available at `https://www.who.int/news-room/fact-sheets/detail/measles`(5-Dec-2019), December 2019.

[49] Frank Fenner, Donald Ainslie Henderson, Isao Arita, Zdenek Jezek, Ivan D Ladnyi, et al. *Smallpox and its eradication*, volume 6. World Health Organization Geneva, 1988.

[50] Olen M Kew, Roland W Sutter, Esther M de Gourville, Walter R Dowdle, and Mark A Pallansch. Vaccine-derived polioviruses and the endgame strategy for global polio eradication. *Annu. Rev. Microbiol.*, 59:587–635, 2005.

[51] Olivia Benecke and Sarah Elizabeth DeYoung. Anti-vaccine decision-making and measles resurgence in the united states. *Global Pediatric Health*, 6:2333794X19862949, 2019.

[52] David JD Earn, Pejman Rohani, Benjamin M Bolker, and Bryan T Grenfell. A simple model for complex dynamical transitions in epidemics. *science*, 287(5453):667–670, 2000.

[53] Chris T Bauch and David JD Earn. Transients and attractors in epidemics. *Proceedings of the Royal Society of London. Series B: Biological Sciences*, 270(1524):1573–1578, 2003.

[54] John Brownlee. Statistical studies in immunity: the theory of an epidemic. *Proceedings of the Royal Society of Edinburgh*, 26(1):484–521, 1906.

[55] August Hirsch. *Handbook of geographical and historical pathology*, volume 1. New Sydenham Society, 1883.

[56] Herbert E Soper. The interpretation of periodicity in disease prevalence. *Journal of the Royal Statistical Society*, 92(1):34–73, 1929.

[57] Chris T Bauch. The role of mathematical models in explaining recurrent outbreaks of infectious childhood diseases. In *Mathematical Epidemiology*, pages 297–319. Springer, 2008.

[58] Zhilan Feng and Horst R Thieme. Endemic models with arbitrarily distributed periods of infection i: Fundamental properties of the model. *SIAM Journal on Applied Mathematics*, 61(3):803–833, 2000.

[59] Zhilan Feng and Horst R Thieme. Endemic models with arbitrarily distributed periods of infection ii: Fast disease dynamics and permanent recovery. *SIAM Journal on Applied Mathematics*, 61(3):983–1012, 2000.

[60] Frank Hoppensteadt. An age dependent epidemic model. *Journal of the Franklin Institute*, 297(5):325–333, 1974.

[61] F Hoppensteadt. Mathematical theories of populations: Demographics, genetics and epidemics, siam reg. In *Conf. Series in Appl. Math*, 1975.

[62] William Ogilvy Kermack and Anderson G McKendrick. A contribution to the mathematical theory of epidemics. *Proceedings of the royal society of london. Series A, Containing papers of a mathematical and physical character*, 115(772):700–721, 1927.

[63] Herbert W Hethcote and David W Tudor. Integral equation models for endemic infectious diseases. *Journal of mathematical biology*, 9(1):37–47, 1980.

[64] Zhilan Feng, Dashun Xu, and Haiyun Zhao. Epidemiological models with non-exponentially distributed disease stages and applications to disease control. *Bulletin of mathematical biology*, 69(5):1511–1536, 2007.

[65] Zhilan Feng, Yiqiang Zheng, Nancy Hernandez-Ceron, Henry Zhao, John W Glasser, and Andrew N Hill. Mathematical models of ebola—consequences of underlying assumptions. *Mathematical biosciences*, 277:89–107, 2016.

[66] Olga Krylova and David JD Earn. Effects of the infectious period distribution on predicted transitions in childhood disease dynamics. *Journal of The Royal Society Interface*, 10(84):20130098, 2013.

[67] Tosio Kato. Perturbation theory for linear operators, grundlehren der mathematischen wissenschaften, 1976.

[68] Joan Ponce, Yiqiang Zheng, Guang Lin, and Zhilan Feng. Assessing the effects of modeling the spectrum of clinical symptoms on the dynamics and control of ebola. *Journal of theoretical biology*, 467:111–122, 2019.

[69] WHO Statement on the first meeting of the IHR Emergency Committee on the 2014 Ebola outbreak in West Africa.

[70] WHO Ebola Response Team. Ebola Virus Disease in West Africa — The First 9 Months of the Epidemic and Forward Projections. *New England Journal of Medicine*, 371(16):1481–1495, October 2014.

[71] R. T. Heffernan, B. Pambo, R. J. Hatchett, P. A. Leman, R. Swanepoel, and R. W. Ryder. Low Seroprevalence of IgG Antibodies to Ebola Virus in an Epidemic Zone: Ogooué-Ivindo Region, Northeastern Gabon, 1997. *Journal of infectious diseases*, 191(6):964–968, March 2005.

[72] E. M. Leroy, S. Baize, V. E. Volchkov, S. P. Fisher-Hoch, M-C. Georges-Courbot, J. Lansoud-Soukate, M. Capron, P. Debré, A. J. Georges, and J. B. McCormick. Human asymptomatic Ebola infection and strong inflammatory response. *The Lancet*, 355(9222):2210–2215, June 2000.

[73] Hilary Bower, Sembia Johnson, Mohamed S Bangura, Alie Joshua Kamara, Osman Kamara, Saidu H Mansaray, Daniel Sesay, Cecilia Turay, Francesco Checchi, and Judith R Glynn. Exposure-specific and age-specific attack rates for ebola virus disease in ebola-affected households, sierra leone. *Emerging infectious diseases*, 22(8):1403, 2016.

[74] Eugene T Richardson, J Daniel Kelly, Mohamed Bailor Barrie, Annelies W Mesman, Sahr Karku, Komba Quiwa, Regan H Marsh, Songor Koedoyoma, Fodei Daboh, Kathryn P Barron, et al. Minimally symptomatic infection in an ebola 'hotspot': a cross-sectional serosurvey. *PLoS neglected tropical diseases*, 10(11):e0005087, 2016.

[75] C. L. Althaus. Estimating the Reproduction Number of Ebola Virus (EBOV) During the 2014 Outbreak in West Africa. *PLoS Currents*, 2014.

[76] M. Barbarossa, A. Dénes, G. Kiss, Y. Nakata, G. Röst, and Z. Vizi. Transmission Dynamics and Final Epidemic Size of Ebola Virus Disease Outbreaks with Varying Interventions. *PLoS ONE*, 10(7):e0131398, July 2015.

[77] C. Browne, H. Gulbudak, and G. Webb. Modeling contact tracing in outbreaks with application to Ebola. *Journal of Theoretical Biology*, 384:33–49, November 2015.

[78] A. Khan, M. Naveed, M. Dur-e Ahmad, and M. Imran. Estimating the basic reproductive ratio for the Ebola outbreak in Liberia and Sierra Leone. *Infectious Diseases of Poverty*, 4, February 2015.

[79] J. Legrand, R. F. Grais, P. Y. Boelle, A. J. Valleron, and A. Flahault. Understanding the dynamics of Ebola epidemics. *Epidemiology & Infection*, 135(4):610–621, May 2007.

[80] J. A. Lewnard, M. L. Ndeffo Mbah, J. A. Alfaro-Murillo, F. L. Altice, L. Bawo, T. G. Nyenswah, and A. P. Galvani. Dynamics and control of Ebola virus transmission in Montserrado, Liberia: a mathematical modelling analysis. *The Lancet Infectious Diseases*, 14(12):1189–1195, December 2014.

[81] C. M. Rivers, E. T. Lofgren, M. Marathe, S. Eubank, and B. L. Lewis. Modeling the Impact of Interventions on an Epidemic of Ebola in Sierra Leone and Liberia. *PLoS Currents*, 6, November 2014.

[82] G. Webb, C. Browne, X. Huo, O. Seydi, M. Seydi, and P. Magal. A Model of the 2014 Ebola Epidemic in West Africa with Contact Tracing. *PLoS Currents*, 2015.

[83] S. E. Bellan, J. R. C. Pulliam, J. Dushoff, and L. A. Meyers. Ebola control: effect of asymptomatic infection and acquired immunity. *The Lancet*, 384(9953):1499–1500, October 2014.

[84] A. Pandey, K. E. Atkins, J. Medlock, N. Wenzel, J. P. Townsend, J. E. Childs, T. G. Nyenswah, M. L. Ndeffo-Mbah, and A. P. Galvani. Strategies for containing Ebola in West Africa. *Science*, 346(6212):991–995, November 2014.

[85] Zhilan Feng, Yiqiang Zheng, Nancy Hernandez-Ceron, Henry Zhao, John W Glasser, and Andrew N Hill. Mathematical models of ebola,consequences of underlying assumptions. *Mathematical Biosciences*, 277:89–107, 2016.

[86] G. Chowell and H. Nishiura. Transmission dynamics and control of Ebola virus disease (EVD): a review. *BMC medicine*, 12(1):196, 2014.

[87] M. D. Van Kerkhove, A. I. Bento, H. L. Mills, N. M. Ferguson, and C. A. Donnelly. A review of epidemiological parameters from Ebola outbreaks to inform early public health decision-making. *Scientific Data*, 2:150019, May 2015.

[88] T. H. Roels, A. S. Bloom, J. Buffington, G. L. Muhungu, W. R. Mac Kenzie, A. S. Khan, R. Ndambi, D. L. Noah, H. R. Rolka, C. J. Peters, and T. G. Ksiazek. Ebola Hemorrhagic Fever, Kikwit, Democratic Republic of the Congo, 1995: Risk Factors for Patients without a Reported Exposure. *The Journal of infectious diseases*, 179(Supplement 1):S92–S97, February 1999.

[89] Ebola Situation Reports.

[90] 2014 Ebola Outbreak in West Africa - Reported Cases Graphs Ebola Hemorrhagic Fever, CDC.

[91] Liberia Ebola Situation Report no. 58, October 2014.

[92] Gordon L Swartzman and Stephen P Kaluzny. *Ecological simulation primer.* Biological Resource Management, 1987.

[93] J. S. Weitz and J. Dushoff. Modeling Post-death Transmission of Ebola: Challenges for Inference and Opportunities for Control. *Scientific Reports*, 5:8751, March 2015.

A. CHAPTER 2 SUPPLEMENTARY MATERIAL

A.1 Basic reproduction number

A.1.1 Basic reproduction number for isolated age groups

The reproduction number of the each age group in (2.1) was obtained using the next generation matrix operator. The infected compartments of the $i-th$ model are E_i, J_i, I_i for $i = 1, \ldots, 4$, therefore the matrix $\mathscr{F}$ describes the new infections and $\mathscr{V}$, the rates out of each compartment considered. For demonstration purposes, we obtain the basic reproduction number for the first age group:

$$\mathscr{F}_1(U) = \begin{pmatrix} \beta_1 S_1 \left(A_{1,1} \frac{(I_1+\varepsilon J_1)}{N_1} + A_{1,2} \frac{(I_2+\varepsilon J_2)}{N_2} + A_{1,3} \frac{(I_3+\varepsilon J_3)}{N_3} + A_{1,4} \frac{(I_4+\varepsilon J_4)}{N_4} \right) \\ 0 \\ 0 \end{pmatrix},$$

$$\mathscr{V}_1(U) = \begin{pmatrix} \alpha E_1 \\ -(1-\delta_1)\alpha E_1 + \gamma_a J_1 \\ -\delta_1 \alpha E_1 + (\mu_1 + \eta_1 + \gamma) I_1 \end{pmatrix}.$$

Let $U^* = (S_i = 1, E_i = I_i = J_i = D_i = H_i = R_i = 0)$ for $i = 1, \ldots, 4$, be the disease-free equilibrium and define $F_1 = D\mathscr{F}_1(U^*)$ and $V_1 = D\mathscr{V}_1(U^*)$.

$$F_1 = \begin{pmatrix} 0 & A_{1,1}\beta_1\varepsilon_1 & A_{1,1}\beta_1 \\ 0 & 0 & 0 \\ 0 & 0 & 0 \end{pmatrix}, \quad V_1 = \begin{pmatrix} \alpha & 0 & 0 \\ -\alpha(1-\delta_1) & \gamma_a & 0 \\ -\alpha\delta_1 & 0 & \gamma + \eta_1 + \mu_1 \end{pmatrix}.$$

Therefore, the basic reproduction number for each group is $\mathcal{R}_{0_i} = \rho(F_1 V_1^{-1})$, where $\rho(F_1 V_1^{-1})$ denotes the spectral radius of the matrix $F_1 V_1^{-1}$, is the following

$$F_1 V_1^{-1} = \begin{pmatrix} A_{1,1}\beta_1 \left(\frac{\delta_1}{\gamma+\eta_1+\mu_1} + \frac{\varepsilon_1(1-\delta_1)}{\gamma_a}\right) & \frac{A_{1,1}\beta_1\varepsilon_1}{\gamma_a} & \frac{A_{1,1}\beta_1}{\gamma+\eta_1+\mu_1} \\ 0 & 0 & 0 \\ 0 & 0 & 0 \end{pmatrix}.$$

The largest eigenvalue corresponds to the $\mathcal{R}_{0_1}$ value:

$$\mathcal{R}_{0_1} = \beta_1 A_{1,1}\left(\frac{\delta_1}{\gamma+\mu_1} + \frac{\varepsilon_1(1-\delta_1)}{\gamma_a}\right).$$

Therefore, the basic reproduction number for each group is

$$\mathcal{R}_{0_i} = \beta_i A_{i,i}\left(\frac{\delta_i}{\gamma+\mu_i} + \frac{\varepsilon_1(1-\delta_i)}{\gamma_a}\right), \quad i = 1, \ldots, 4.$$

A.1.2 Basic reproduction number for multiple interacting age groups

The reproduction number of all the age groups in (2.1) is obtained using the next generation matrix operator. The infected compartments of the model are E_i, J_i, I_i for $i = 1, \ldots, 4$, therefore the matrix $\mathscr{F}$ describes the new infections in the total population and $\mathscr{V}$, the rates out of each compartment considered.

$$\mathscr{F}(U) = \begin{pmatrix} \beta_1 S_1 \left(A_{1,1}\frac{(I_1+\varepsilon J_1)}{N_1} + A_{1,2}\frac{(I_2+\varepsilon J_2)}{N_2} + A_{1,3}\frac{(I_3+\varepsilon J_3)}{N_3} + A_{1,4}\frac{(I_4+\varepsilon J_4)}{N_4}\right) \\ 0 \\ 0 \\ \beta_2 S_2 \left(A_{2,1}\frac{(I_1+\varepsilon J_1)}{N_1} + A_{2,2}\frac{(I_2+\varepsilon J_2)}{N_2} + A_{2,3}\frac{(I_3+\varepsilon J_3)}{N_3} + A_{2,4}\frac{(I_4+\varepsilon J_4)}{N_4}\right) \\ 0 \\ 0 \\ \beta_3 S_3 \left(A_{3,1}\frac{(I_1+\varepsilon J_1)}{N_1} + A_{3,2}\frac{(I_2+\varepsilon J_2)}{N_2} + A_{3,3}\frac{(I_3+\varepsilon J_3)}{N_3} + A_{3,4}\frac{(I_4+\varepsilon J_4)}{N_4}\right) \\ 0 \\ 0 \\ \beta_4 S_4 \left(A_{4,1}\frac{(I_1+\varepsilon J_1)}{N_1} + A_{4,2}\frac{(I_2+\varepsilon J_2)}{N_2} + A_{4,3}\frac{(I_3+\varepsilon J_3)}{N_3} + A_{4,4}\frac{(I_4+\varepsilon J_4)}{N_4}\right) \\ 0 \\ 0 \end{pmatrix},$$

$$\mathscr{V}(U) = \begin{pmatrix} \alpha E_1 \\ -(1-\delta_1)\alpha E_1 + \gamma_a J_1 \\ -\delta_1 \alpha E_1 + (\mu_1 + \eta_1 + \gamma) I_1 \\ \vdots \\ \alpha E_4 \\ -(1-\delta_4)\alpha E_4 + \gamma_a J_4 \\ -\delta_4 \alpha E_4 + (\mu_4 + \eta_4 + \gamma) I_4 \end{pmatrix}.$$

Let $U^* = (S_i = 1, E_i = I_i = J_i = D_i = H_i = R_i = 0)$ for $i = 1, \ldots, 4$, be the disease-free equilibrium and define $F = D\mathscr{F}(U^*)$ and $V = D\mathscr{V}(U^*)$:

$$F = \begin{pmatrix}
0 & A_{1,1}\beta_1\varepsilon_1 & A_{1,1}\beta_1 & 0 & A_{1,2}\beta_1\varepsilon_1 & A_{1,2}\beta_1 & 0 & A_{1,3}\beta_1\varepsilon_1 & A_{1,3}\beta_1 & 0 & A_{1,4}\beta_1\varepsilon_1 & A_{1,4}\beta_1 \\
0 & 0 & 0 & 0 & 0 & 0 & 0 & 0 & 0 & 0 & 0 & 0 \\
0 & 0 & 0 & 0 & 0 & 0 & 0 & 0 & 0 & 0 & 0 & 0 \\
0 & A_{2,1}\beta_2\varepsilon_1 & A_{2,1}\beta_2 & 0 & A_{2,2}\beta_2\varepsilon_1 & A_{2,2}\beta_2 & 0 & A_{2,3}\beta_2\varepsilon_1 & A_{2,3}\beta_2 & 0 & A_{2,4}\beta_2\varepsilon_1 & A_{2,4}\beta_2 \\
0 & 0 & 0 & 0 & 0 & 0 & 0 & 0 & 0 & 0 & 0 & 0 \\
0 & 0 & 0 & 0 & 0 & 0 & 0 & 0 & 0 & 0 & 0 & 0 \\
0 & A_{3,1}\beta_3\varepsilon_1 & A_{3,1}\beta_3 & 0 & A_{3,2}\beta_3\varepsilon_1 & A_{3,2}\beta_3 & 0 & A_{3,3}\beta_3\varepsilon_1 & A_{3,3}\beta_3 & 0 & A_{3,4}\beta_3\varepsilon_1 & A_{3,4}\beta_3 \\
0 & 0 & 0 & 0 & 0 & 0 & 0 & 0 & 0 & 0 & 0 & 0 \\
0 & 0 & 0 & 0 & 0 & 0 & 0 & 0 & 0 & 0 & 0 & 0 \\
0 & A_{4,1}\beta_4\varepsilon_1 & A_{4,1}\beta_4 & 0 & A_{4,2}\beta_4\varepsilon_1 & A_{4,2}\beta_4 & 0 & A_{4,3}\beta_4\varepsilon_1 & A_{4,3}\beta_4 & 0 & A_{4,4}\beta_4\varepsilon_1 & A_{4,4}\beta_4 \\
0 & 0 & 0 & 0 & 0 & 0 & 0 & 0 & 0 & 0 & 0 & 0 \\
0 & 0 & 0 & 0 & 0 & 0 & 0 & 0 & 0 & 0 & 0 & 0
\end{pmatrix},$$

V =

$$\begin{pmatrix}
\alpha & 0 & 0 & 0 & 0 & 0 & 0 & 0 & 0 & 0 & 0 & 0 \\
\alpha(\delta_1 - 1) & \gamma_a & 0 & 0 & 0 & 0 & 0 & 0 & 0 & 0 & 0 & 0 \\
-\alpha\delta_1 & 0 & \gamma + \eta_1 + \mu_1 & 0 & 0 & 0 & 0 & 0 & 0 & 0 & 0 & 0 \\
0 & 0 & 0 & \alpha & 0 & 0 & 0 & 0 & 0 & 0 & 0 & 0 \\
0 & 0 & 0 & \alpha(\delta_2 - 1) & \gamma_a & 0 & 0 & 0 & 0 & 0 & 0 & 0 \\
0 & 0 & 0 & -\alpha\delta_2 & 0 & \gamma + \eta_2 + \mu_2 & 0 & 0 & 0 & 0 & 0 & 0 \\
0 & 0 & 0 & 0 & 0 & 0 & \alpha & 0 & 0 & 0 & 0 & 0 \\
0 & 0 & 0 & 0 & 0 & 0 & \alpha(\delta_3 - 1) & \gamma_a & 0 & 0 & 0 & 0 \\
0 & 0 & 0 & 0 & 0 & 0 & -\alpha\delta_3 & 0 & V_{9,9} & 0 & 0 & 0 \\
0 & 0 & 0 & 0 & 0 & 0 & 0 & 0 & 0 & \alpha & 0 & 0 \\
0 & 0 & 0 & 0 & 0 & 0 & 0 & 0 & 0 & \alpha(\delta_4 - 1) & \gamma_a & 0 \\
0 & 0 & 0 & 0 & 0 & 0 & 0 & 0 & 0 & -\alpha\delta_4 & 0 & V_{12\times 12}
\end{pmatrix},$$

where $V_{12\times 12} = \gamma + \eta_4 + \mu_4, V_{9,9} = \gamma + \eta_3 + \mu_3$.

The basic reproduction number for each group is $\mathcal{R}_0 = \rho(FV^{-1})$, where $\rho(FV^{-1})$ denotes the spectral radius of the block matrix FV^{-1} we can write in the following way:

$$FV^{-1} = \begin{pmatrix} K_{1,1} & K_{1,2} & K_{1,3} & K_{1,4} \\ K_{2,1} & K_{2,2} & K_{2,3} & K_{2,4} \\ K_{3,1} & K_{3,2} & K_{3,3} & K_{3,4} \\ K_{4,1} & K_{4,2} & K_{4,3} & K_{4,4} \end{pmatrix},$$

$$K_{i,j} = \begin{pmatrix} \beta_i A_{i,j} \left(\frac{(1-\delta_j)\varepsilon_1}{\gamma_a} + \frac{\delta_j}{\gamma+\eta_j+\mu_j} \right) & \beta_i A_{i,j} \frac{\varepsilon_1}{\gamma_a} & \beta_i A_{i,j} \frac{1}{\gamma+\eta_j+\mu_j} \\ 0 & 0 & 0 \\ 0 & 0 & 0 \end{pmatrix}, \text{ for } i,j = 1,\ldots,4.$$

Since we do not consider hospitalization we set $\eta_i = 0$. The non-zero eigenvalues of FV^{-1} are given by the following matrix:

$$H = \begin{pmatrix} h_{1,1} & h_{1,2} & h_{1,3} & h_{1,4} \\ h_{2,1} & h_{2,2} & h_{2,3} & h_{2,4} \\ h_{3,1} & h_{3,2} & h_{3,3} & h_{3,4} \\ h_{4,1} & h_{4,2} & h_{4,3} & h_{4,4} \end{pmatrix}, \quad h_{i,j}=\beta_i A_{i,j}\left(\frac{(1-\delta_j)\varepsilon_1}{\gamma_a}+\frac{\delta_j}{\gamma+\mu_j}\right), \quad i,j = 1,\ldots,4.$$

Define $\rho(H)$ as the dominant eigenvalue of H, then the basic reproduction number for the whole population is given by $\mathcal{R}_0 = \rho(H)$.

A.1.3 Group plots of staggered-release scenarios

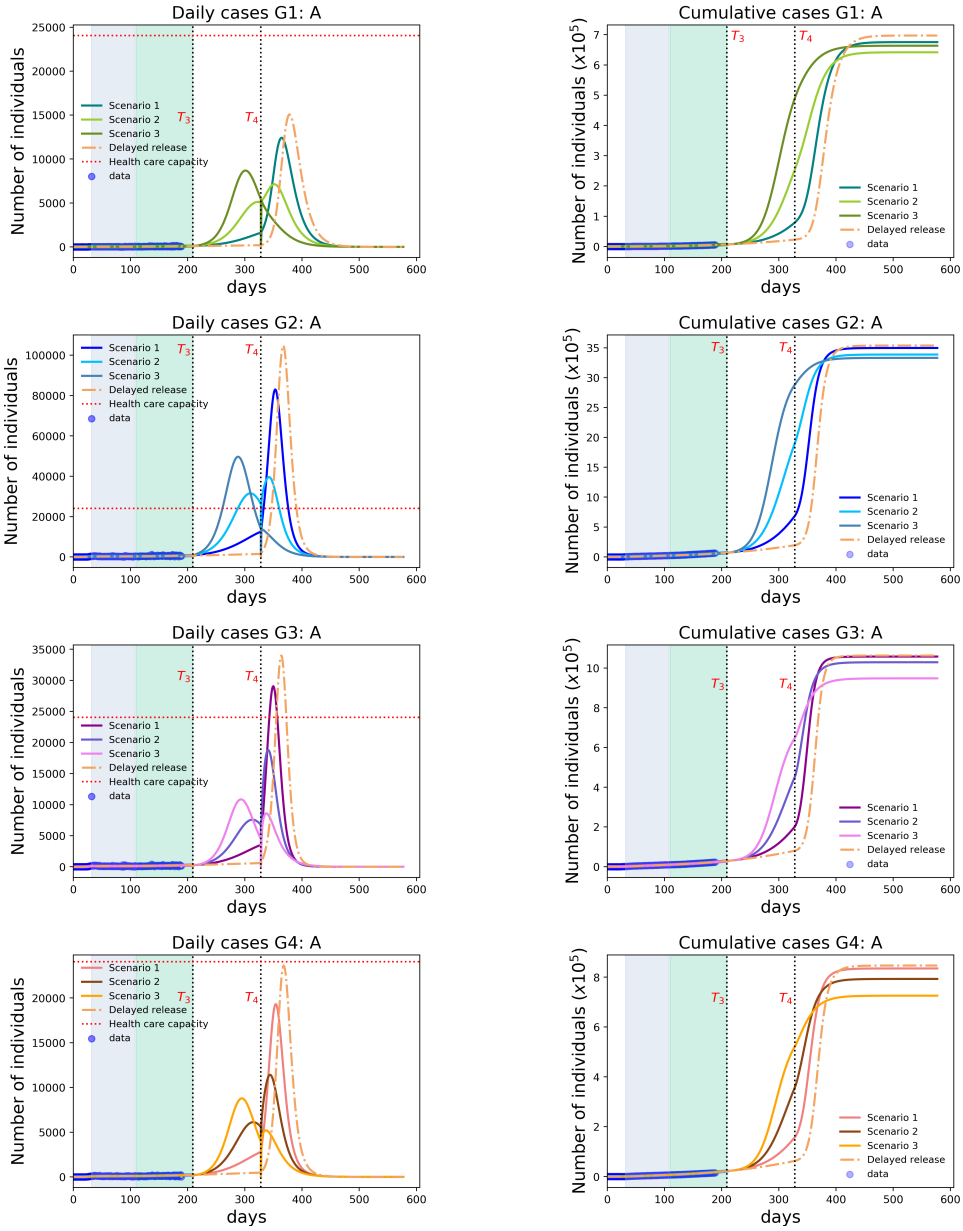

Figure A.1.: Daily and cumulative cases when we use staggered-release strategy A in reopening phase 2 ($T_3 - T_4$).

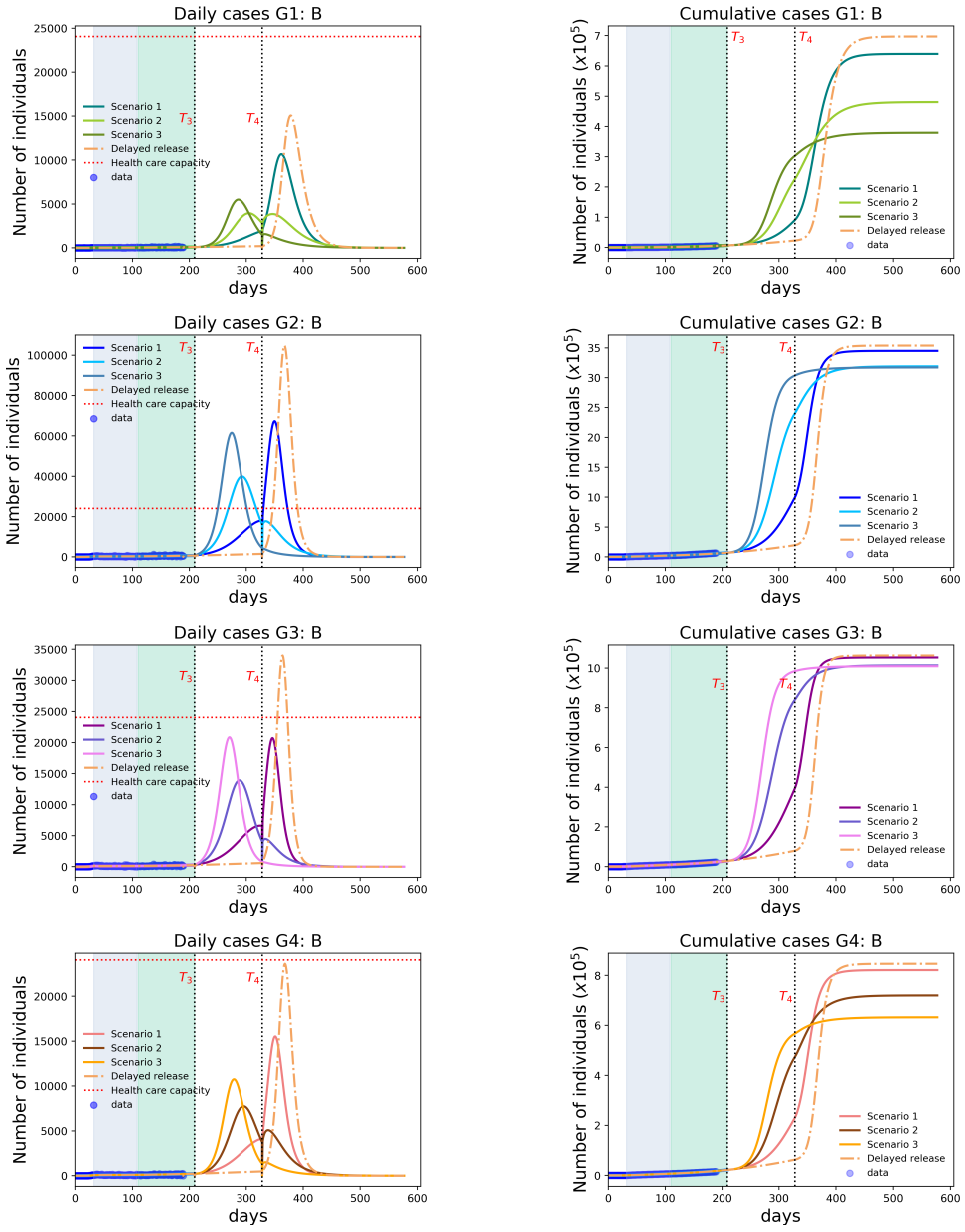

Figure A.2.: Daily and cumulative cases when we use staggered-release strategy B in reopening phase 2 ($T_3 - T_4$).

B. CHAPTER 3 SUPPLEMENTARY MATERIAL

B.1 Derivation of $\mathcal{R}_0$

The reproduction number of the original system (3.11) was obtained using the next generation matrix operator described in [5]. The infected compartments of the model (3.11) are I_j for $j = 1, 2$, therefore the matrix $\mathscr{F}$ describes the new infections and $\mathscr{V}$, the rates out of each compartment considered.

$$\mathscr{F}(U) = \begin{pmatrix} \frac{\beta(I_1+I_2)}{A(t)}S(t) \\ 0 \end{pmatrix} \quad \text{and} \quad \mathscr{V}(U) = \begin{pmatrix} (\mu + n\gamma)I_1 \\ -n\gamma I_1 + (\mu + n\gamma)I_2 \end{pmatrix}.$$

Let U_0 be the disease-free equilibrium and define $F = D\mathscr{F}(U_0)$ and $V = D\mathscr{V}(U_0)$. Then

$$F = \begin{pmatrix} \beta & \beta \\ 0 & 0 \end{pmatrix}, \quad V = \begin{pmatrix} 2\gamma + \mu & 0 \\ -2\gamma & 2\gamma + \mu \end{pmatrix}.$$

Therefore, following the definition of the basic reproduction number by Diekmann [5] is $\mathcal{R}_0 = \rho(FV^{-1})$ where $\rho(M)$ denotes the spectral radius of the matrix M and the matrix FV^{-1} is the following

$$FV^{-1} = \begin{pmatrix} \frac{\beta(4\gamma+\mu)}{(2\gamma+\mu)^2} & \frac{\beta}{2\gamma+\mu} \\ 0 & 0 \end{pmatrix}.$$

$\mathcal{R}_0$ is given by the largest eigenvalue of FV^{-1}, i.e.,

$$\mathcal{R}_e = \frac{\beta(4\gamma + \mu)}{(2\gamma + \mu)^2} = \frac{2\Gamma + \nu}{(\Gamma + \nu)^2}.$$

B.2 Endemic equilibrium computation

System (3.14) always has the disease-free equilibrium (DFE) denoted by U_0:

$$s = 1,\ i_1 = i_2 = q_1 = q_2 = r = 0.$$

Let $U^* = (i_1^*, i_2^*, q_1^*, q_2^*, r^*)$ denote a positive or endemic equilibrium (EE) of (3.14). Then U^* satisfies the following equations:

$$\begin{aligned}
0 &= (i_1^* + i_2^*)(1 - i_1^* - i_2^* - r^*) - (\Gamma + \nu) i_1^* + i_1^* \left[\Gamma i_2^* - (\nu + \Omega)(q_1^* + q_2^*) + \Omega q_1^*\right], \\
0 &= \Gamma i_1^* - (\Gamma + \nu) i_2^* + i_2^* \left[\Gamma i_2^* - (\nu + \Omega)(q_1^* + q_2^*) + \Omega q_1^*\right], \\
0 &= \Gamma i_2^* - (\nu + \Omega) q_1^* + q_1^* \left[\Gamma i_2^* - (\nu + \Omega)(q_1^* + q_2^*) + \Omega q_1^*\right], \\
0 &= \Omega q_1^* - (\nu + \Omega) q_2^* + q_2^* \left[\Gamma i_2^* - (\nu + \Omega)(q_1^* + q_2^*) + \Omega q_1^*\right], \\
0 &= \Omega q_2^* - \nu r^* + r^* \left[\Gamma i_2^* - (\nu + \Omega)(q_1^* + q_2^*) + \Omega q_1^*\right].
\end{aligned} \tag{B.1}$$

From adding the third and fourth equations above at the non-trivial equilibrium, we get the following equivalence:

$$(1 + q_1^* + q_2^*)\left[\Gamma i_2^* - (\nu + \Omega)(q_1^* + q_2^*) + \Omega q_1^*\right] = 0.$$

Because at the nontrivial equilibrium, $(1 + q_1^* + q_2^*) > 0$, we can conclude that

$$\Gamma i_2^* - (\nu + \Omega)(q_1^* + q_2^*) + \Omega q_1^* = \Gamma i_2^* - \nu(q_1^* + q_2^*) - \Omega q_2^* = 0. \tag{B.2}$$

The solution to the system of equations (B.1) and (B.2) satisfies:

$$\begin{aligned}
&i_1^* = \nu(\Gamma + \nu)(\Omega + \nu)^2 k, \quad i_2^* = \Gamma\nu(\Omega + \nu)^2 k, \\
&q_1^* = \Gamma^2\nu(\Omega + \nu)k, \qquad q_2^* = \Gamma^2\nu\Omega k, \qquad r^* = \Gamma^2\Omega^2 k,
\end{aligned} \tag{B.3}$$

where

$$k = \frac{(1 - \nu)(2\Gamma + \nu) - \Gamma^2}{(2\Gamma + \nu)(\Gamma^2\Omega^2 + (\nu + \Omega)^2(2\Gamma\nu + \nu^2))}. \tag{B.4}$$

B.3 Coefficients of the characteristic polynomial

Recall that the endemic equilibrium U^* is given in (B.3). The characteristic polynomial at U^* has the following form:

$$|yI - DF(U^*)| = y^5 + ay^4 + by^3 + cy^2 + dy + e, \tag{B.5}$$

where the coefficient are:

$$\begin{aligned}
a &= \frac{1}{(2\Gamma+\nu)\left(\Gamma^2\Omega^2 + 2\Gamma\nu(\nu+\Omega)^2 + \nu^2(\nu+\Omega)^2\right)}\Big[3\Gamma^4\Omega^2 + 2\Gamma^3\left(2\nu^3 + 4\nu^2\Omega + 7\nu\Omega^2 + 2\Omega^3\right) \\
&\quad + 2\Gamma^2\nu\left(9\nu^3 + \nu^2(22\Omega+2) + \nu\Omega(19\Omega+4) + \Omega^2(5\Omega+2)\right) + 2\Gamma\nu^2(\nu+\Omega)^2(7\nu+4\Omega+2) \\
&\quad + \nu^3(\nu+\Omega)^2(3\nu+2\Omega+1)\Big], \\
b &= \frac{1}{(2\Gamma+\nu)\left(\Gamma^2\Omega^2 + 2\Gamma\nu(\nu+\Omega)^2 + \nu^2(\nu+\Omega)^2\right)}\Big[\Gamma^4\left(-4\nu^3 - 8\nu^2\Omega + 5\nu\Omega^2 + 6\Omega^3\right) \\
&\quad + 2\Gamma^3\left(4\nu^3(\Omega+1) + \nu^2(17\Omega+8)\Omega + 4\nu(3\Omega+1)\Omega^2 + \Omega^4\right) \\
&\quad + \Gamma^2\nu\left(17\nu^4 + \nu^3(62\Omega+24) + \nu^2\Omega(83\Omega+56) + 2\nu\Omega^2(21\Omega+20) + \Omega^3(5\Omega+8)\right) \\
&\quad + 2\Gamma\nu^2(\nu+\Omega)^2\left(6\nu^2 + \nu(10\Omega+9) + 2\Omega(\Omega+2)\right) + \nu^3(\nu+\Omega)^2\left(2\nu^2 + 4\nu(\Omega+1) + \Omega(\Omega+2)\right)\Big], \\
c &= \frac{1}{(2\Gamma+\nu)\left(\Gamma^2\Omega^2 + 2\Gamma\nu(\nu+\Omega)^2 + \nu^2(\nu+\Omega)^2\right)}\Big[\Gamma^6\nu(\nu+\Omega)^2 + 4\Gamma^5(\nu-1)\nu(\nu+\Omega)^2 \\
&\quad + \Gamma^4\big(6\nu^5 + 2\nu^4(6\Omega-11) + \nu^3\left(6\Omega^2 - 52\Omega + 4\right) + \nu^2(8-29\Omega)\Omega + 4\nu\Omega^2(\Omega+1) + 3\Omega^4\big) \\
&\quad + 2\Gamma^3\nu\big(2\nu^5 + 4\nu^4(\Omega-4) + 2\nu^3\left(\Omega^2 - 18\Omega + 7\right) + 3\nu^2(12-5\Omega)\Omega + 10\nu\Omega^2(\Omega+3) \\
&\quad + \Omega^3(5\Omega+8)\big) + \Gamma^2\nu\big(\nu^6 + \nu^5(2\Omega-19) + \nu^4\left(\Omega^2 - 32\Omega + 49\right) + \nu^3\Omega(7\Omega+138) \\
&\quad + \nu^2\Omega^2(32\Omega+133) + 12\nu\Omega^3(\Omega+4) + 4\Omega^4\big) - 2\Gamma\nu^2(\nu+\Omega)^2\left(4\nu^3 - \nu^2(2\Omega+15) - \nu\Omega(3\Omega+14) - 2\Omega^2\right) \\
&\quad - \nu^3(\nu+\Omega)^2\left(2\nu^3 - 6\nu^2 - \nu\Omega(\Omega+6) - \Omega^2\right)\Big], \\
d &= \frac{\nu(\Gamma+\nu)(\nu+\Omega)^2}{(2\Gamma+\nu)\left(\Gamma^2\Omega^2 + 2\Gamma\nu(\nu+\Omega)^2 + \nu^2(\nu+\Omega)^2\right)}\Big[2\Gamma^5(\nu+\Omega) \\
&\quad + 2\Gamma^4(3\nu-4)(\nu+\Omega) + \Gamma^3\left(6\nu^3 + 6\nu^2(\Omega-4) + \nu(8-28\Omega) - (\Omega-8)\Omega\right) \\
&\quad + \Gamma^2\left(2\nu^4 + 2\nu^3(\Omega-12) - 4\nu^2(7\Omega-6) + \nu(32-3\Omega)\Omega + 8\Omega^2\right) \\
&\quad + \Gamma\nu\left(-13\nu^3 - 2\nu^2(8\Omega-9) + \nu(26-3\Omega)\Omega + 8\Omega^2\right) + \nu^2\left(-3\nu^3 - 4\nu^2(\Omega-1) - \nu(\Omega-6)\Omega + 2\Omega^2\right)\Big], \\
e &= -\frac{\nu(\Gamma+\nu)^2\left(\Gamma^2 + 2\Gamma(\nu-1) + (\nu-1)\nu\right)(\nu+\Omega)^2\left(\Gamma^2(-\nu)(\nu+2\Omega) + 2\Gamma(\nu+\Omega)^2 + \nu(\nu+\Omega)^2\right)}{(2\Gamma+\nu)\left(\Gamma^2\Omega^2 + 2\Gamma\nu(\nu+\Omega)^2 + \nu^2(\nu+\Omega)^2\right)}.
\end{aligned}$$

B.4 Computations to obtain the complex conjugate eigenvalues

We will look for eigenvalues of $DF(U^*)(\nu)$ of the form $y = \epsilon\tilde{y}$, where $\epsilon = \nu^{1/2}$. Substituting the coefficients in the characteristic polynomial,

$$(\epsilon\tilde{y})^5 + a(\epsilon\tilde{y})^4 + b(\epsilon\tilde{y})^3 + c(\epsilon\tilde{y})^2 + d(\epsilon\tilde{y}) + (e_1(\Omega)\epsilon^2 + e_2(\Omega,\epsilon^2)\epsilon^4) = 0.$$

Dividing by ϵ^2 and letting $\epsilon \to 0$ implies

$$\begin{aligned} c(\Omega,0)\tilde{y}^2 &= -e_1(\Omega), \text{ so we obtain} \\ \mathcal{Y}_1 &= \pm i\sqrt{\frac{e_1(\Omega)}{c(\Omega,0)}}, \\ &= \pm i\sqrt{\frac{2(2-\Gamma)}{3}}, \end{aligned}$$

substitute $\tilde{y} = \mathcal{Y}_1 + \epsilon\mathcal{Y}$, divide by ϵ and letting $\epsilon \to 0$, we can define:

$$G(\mathcal{Y},\Omega,\epsilon) = \mathcal{Y}_1^3 b(0,\Omega) + c(0,\Omega)\mathcal{Y}\mathcal{Y}_1 + d_1(\Omega)\mathcal{Y}_1.$$

By (B.6), we have that

$$\mathcal{Y}_2 = \frac{\frac{6\Gamma^2(2-\Gamma)}{\Gamma+16} - \Omega}{3\Gamma\Omega}.$$

We denote the first term of the Taylor series expansion of Ω_0 by $\Omega^* = \frac{6\Gamma^2(2-\Gamma)}{\Gamma+16}$, so

$$G(0,\Omega_0,0) = 0,$$

and

$$G_{\mathcal{Y}}(0,\Omega_0,0) = 3\Gamma\Omega^2\mathcal{Y}_1 \neq 0.$$

By the implicit function theorem, we know there is a function $\mathcal{Y}(\Omega,\epsilon)$, which is analytic in Ω and ϵ in a neighborhood of $(\Omega^*,0)$ with $\mathcal{Y}(\Omega^*,0) = 0$ and $G(\mathcal{Y},\Omega,\epsilon) = 0$ if and only if $\mathcal{Y} = \mathcal{Y}(\Omega,\epsilon)$. Hence, we can write

$$\mathcal{Y}(\Omega,\epsilon) = \mathcal{Y}_2(\Omega) + \epsilon\mathcal{Y}_3(\Omega,\epsilon),$$

where $\mathcal{Y}_2(\Omega^*) = 0$ and $\mathcal{Y}_3$ is an analytic function of Ω and ϵ in a neighborhood of $(\Omega^*, 0)$. We can then write the other eigenvalues, besides $y_{3,4,5}$, in the following form:

$$y_\pm(\Omega,\epsilon) = \epsilon\tilde{y}_\pm(\Omega,\epsilon) = \epsilon(\mathcal{Y}_1 + \epsilon\mathcal{Y}_2 + \epsilon^2\mathcal{Y}_3) = \pm i\epsilon\sqrt{\frac{2(2-\Gamma)}{3}} + \epsilon^2\frac{\frac{6\Gamma^2(2-\Gamma)}{\Gamma+16} - \Omega}{3\Gamma\Omega} + \epsilon^3\mathcal{Y}_3.$$

B.5 Calculation of the Center Manifold and Stability of Periodic Solutions

B.5.1 Stability of periodic solutions

To prove the stability of the Hopf bifurcation in 3 we use the following result from [8], Chapter 3, Section 1B. Consider the system

$$\dot{y} = F(y,\mu), y \in \mathbb{R}^5, \ \ \mu \in \mathbb{R},$$

where F is $C^r(r \geq 5)$ on a sufficiently large open set containing $(0,0)$, and $F(0,0) = 0$. Suppose that $D_yF(0,0)$ has two purely imaginary conjugate eigenvalues and three strictly negative eigenvalues. Then by the center manifold theorem ([8], Chapter 2, Section 1B), near $(y,\mu) = (0,0)$, the system (3.14) can be reduced to a two dimensional system with the parameter μ. Assume that at the bifurcation point, which means $\mu = 0$, the reduction of the system to the center manifold will take the following form

$$\begin{pmatrix}\dot{x}\\ \dot{y}\end{pmatrix} = \begin{pmatrix}0 & \Im y(\Omega_0)\\ -\Im y(\Omega_0) & 0\end{pmatrix}\begin{pmatrix}x\\ y\end{pmatrix} + \begin{pmatrix}G^1(x,y,0)\\ G^2(x,y,0)\end{pmatrix},$$

where $\Im y(\Omega_0)$ is the imaginary part of the eigenvalues of $D_yF(0,0)$, $(x,y) \in \mathbb{R}^2$, and $G^i(x,y,\mu)(i = 1,2)$ are real-values functions of x, y, μ which are of order higher than 1 in x and y. The stability of the bifurcating periodic solution is given by the sign of the following expression

$$\begin{aligned}\alpha = &\frac{1}{16}\Big(G^{(1)}_{xxx} + G^{(1)}_{xyy} + G^{(2)}_{xxy} + G^{(2)}_{yyy}\Big)\\ &-\frac{1}{16\Im y_+(\Omega_0(0))}\Big[G^{(1)}_{xy}\Big(G^{(1)}_{xx} + G^{(1)}_{yy}\Big) - G^{(2)}_{xy}\Big(G^{(2)}_{xx} + G^{(2)}_{yy}\Big) - G^{(1)}_{xx}G^{(2)}_{xx} + G^{(1)}_{yy}G^{(2)}_{yy}\Big],\end{aligned}$$

where all partial derivatives are evaluated at the bifurcation point $(x_1, x_2, \mu) = (0,0,0)$.

Lemma 1 *The bifurcating periodic solution is locally asymptotically stable if $\alpha < 0$ (supercritical case); it is unstable if $\alpha > 0$.*

B.5.2 Shifting the system to the endemic equilibrium

Therefore, to begin the center manifold reduction we use the simplified system (3.14) and we transform the endemic equilibrium in (3.14) to the origin by letting

$$I_1 = i_1 - i_1^*,\ I_2 = i_2 - i_2^*,\ Q_1 = q_1 - q_1^*,\ Q_2 = q_2 - q_2^* \text{ and } R = r - r^*.$$

The transformed system is

$$\begin{aligned}
I_1' &= i_1^*\Big[-2I_1 + (\Gamma-2)I_2 - \nu Q_1 - (\nu+\Omega)Q_2 - R\Big] - i_2^*\big(2I_1 + 2I_2 + R\big) - r^*\big(I_1 + I_2\big) \\
&\quad + I_1\Big[-\Gamma + (\Gamma-2)I_2 - \nu - \nu Q_1 + Q_2(-\nu-\Omega) - R + 1\Big] + I_2(1-R) - I_1^2 - I_2^2, \\
I_2' &= i_2^*\Big[-\nu Q_1 - (\nu+\Omega)Q_2\Big] + \nu I_2 q_1^* + (\nu+\Omega)I_2 q_2^* + \Gamma I_1 + \Gamma I_2^2 \\
&\quad - I_2\Big[(\Gamma+\nu) + \nu Q_1 + (\nu+\Omega)Q_2\Big], \\
Q_1' &= \Gamma I_2 q_1^* - Q_1 q_1^* - (\nu+\Omega)Q_2 q_1^* + \Gamma I_2 + \Gamma I_2 Q_1 - (\nu+\Omega)Q_1 \\
&\quad - (\nu+\Omega)Q_1 Q_2 - Q_1^2\nu, \qquad \text{(B.6)} \\
Q_2' &= -\Omega Q_1 q_1^* - \Omega Q_2 q_1^* + \Gamma I_2 q_2^* + \Omega Q_1 q_2^* + I_2 Q_2 \Gamma + \Omega Q_1 - \nu Q_1 Q_2 \\
&\quad - (\nu+\Omega)Q_2 - (\nu+\Omega)Q_2^2, \\
R' &= -\Omega Q_1 q_2^* - \Omega Q_2 q_2^* + \Gamma I_2 r * - \Omega Q_2 r^* + I_2 R\Gamma - \nu Q_1 R - \Omega Q_2 \\
&\quad - (\nu+\Omega)Q_2 R - \nu R.
\end{aligned}$$

By (3.20) the system (B.6) has two complex conjugate eigenvalues given by

$$\begin{aligned}
y_{\pm}(\Omega,\epsilon) &= \epsilon\mathcal{Y}_1 + \epsilon^2\mathcal{Y}_2 + \epsilon^3\mathcal{Y}_3(\Omega,\epsilon), \\
&= \pm i\epsilon\sqrt{\frac{2(2-\Gamma)}{3}} + \epsilon^2\frac{\frac{6\Gamma^2(2-\Gamma)}{\Gamma+16} - \Omega}{3\Gamma\Omega} + \epsilon^3\mathcal{Y}_3(\Omega,\epsilon).
\end{aligned}$$

Note that the leading real part ($\mathcal{Y}_2$) of $y_\pm$ is zero at Ω^*. To calculate the real part of the eigenvector, we need to calculate $y_\pm$ to the third order of ϵ. Let

$$y_\pm(\Omega,\epsilon) = \epsilon\mathcal{Y}_1(\Omega) + \epsilon^2\mathcal{Y}_2(\Omega) + \epsilon^3\mathcal{Y}_3(\Omega) + \epsilon^4\mathcal{Y}_4(\Omega,\epsilon).$$

Using (3.19) and (3.21) we have the following expansions for the coefficients of the characteristic polynomial (B.5) around ϵ:

$$\begin{aligned}
a &= a(\Omega,\epsilon^2) = \tfrac{3\Gamma}{2} + 2\Omega + a_1(\Omega,\epsilon^2)\epsilon^2,\\
b &= b(\Omega,\epsilon^2) = \Omega(3\Gamma+\Omega) + b_1(\Omega,\epsilon^2)\epsilon^2,\\
c &= c(\Omega,\epsilon^2) = \tfrac{3\Gamma\Omega^2}{2} + c_1(\Omega,\epsilon^2)\epsilon^2,\\
d &= d(\Omega,\epsilon^2) = d_1(\Omega)\epsilon^2 + d_2(\Omega,\epsilon^2)\epsilon^4,\\
e &= e(\Omega,\epsilon^2) = e_1(\Omega)\epsilon^2 + e_2(\Omega,\epsilon^2)\epsilon^4,
\end{aligned} \tag{B.7}$$

where

$$\begin{aligned}
a_1 &= \frac{2}{\Gamma} + \frac{13}{4},\\
b_1 &= \frac{4\Omega}{\Gamma} + \frac{5\Gamma}{2} + \frac{9\Omega}{2} + 4,\\
c_1 &= \frac{1}{4}\left(2\Gamma^3 - 8\Gamma^2 + \frac{8\Omega^2}{\Gamma} + 8\Gamma(\Omega+1) + \Omega(5\Omega+32)\right),\\
d_1 &= \frac{1}{2}\Omega\left(2\Gamma^3 - 8\Gamma^2 - \Gamma(\Omega-8) + 8\Omega\right),\\
d_2 &= \frac{1}{4}\left(12\Gamma^3 + 6\Gamma^2(\Omega-8) - \frac{8\Omega^2}{\Gamma} + \Gamma(48-36\Omega) - 3(\Omega-24)\Omega\right),\\
e_1 &= -(\Gamma-2)\Gamma\Omega^2,\\
e_2 &= \Omega\left(\Gamma^3 - 6\Gamma^2 - 2\Gamma(\Omega-4) + \Omega\right).
\end{aligned}$$

Substitution of the expansion of each coefficient around ϵ and the expression for y into the characteristic equation leads to the following equation:

$$\begin{aligned}
&\left(\epsilon\mathcal{Y}_1 + \epsilon^2\mathcal{Y}_2 + \epsilon^3\mathcal{Y}_3\right)^5 + a(\epsilon)\left(\epsilon\mathcal{Y}_1 + \epsilon^2\mathcal{Y}_2 + \epsilon^3\mathcal{Y}_3\right)^4 + b(\epsilon)\left(\epsilon\mathcal{Y}_1 + \epsilon^2\mathcal{Y}_2 + \epsilon^3\mathcal{Y}_3\right)^3\\
&+c(\epsilon)\left(\epsilon\mathcal{Y}_1 + \epsilon^2\mathcal{Y}_2 + \epsilon^3\mathcal{Y}_3\right)^2 + d(\epsilon)\left(\epsilon\mathcal{Y}_1 + \epsilon^2\mathcal{Y}_2 + \epsilon^3\mathcal{Y}_3\right) + e(\epsilon) = 0.
\end{aligned}$$

Substituting the Taylor expansions in (B.7) up to ϵ^4 and ignoring higher order terms, we obtain

$$\begin{aligned}
O(\epsilon^5) &= \frac{\epsilon^2}{4\Gamma}\left(-4\Gamma^3\Omega^2+8\Gamma^2\Omega^2+6\Gamma^2\Omega^2\mathcal{Y}_1^2\right)\\
&\quad+\frac{\epsilon^3}{4\Gamma}\left(4\Gamma^4\Omega\mathcal{Y}_1-16\Gamma^3\Omega\mathcal{Y}_1-2\Gamma^2\Omega^2\mathcal{Y}_1+12\Gamma^2\Omega^2\mathcal{Y}_1\mathcal{Y}_2+16\Gamma^2\Omega\mathcal{Y}_1+16\Gamma\Omega^2\mathcal{Y}_1+4\Gamma\Omega\mathcal{Y}_1^3(3\Gamma+\Omega)\right)\\
&\quad+\frac{\epsilon^4}{4\Gamma}\Big[4\Gamma^4\Omega-24\Gamma^3\Omega-8\Gamma^2(\Omega-4)\Omega+4\Gamma\Omega^2+2\Gamma^4\mathcal{Y}_1^2-8\Gamma^3\mathcal{Y}_1^2+6\Gamma^2\Omega^2\mathcal{Y}_2^2+12\Gamma^2\Omega^2\mathcal{Y}_1\mathcal{Y}_3\\
&\quad+8\Gamma^2(\Omega+1)\mathcal{Y}_1^2+2\Gamma\Omega\mathcal{Y}_2\left(2\Gamma^3-8\Gamma^2-\Gamma(\Omega-8)+8\Omega\right)+2\Gamma\mathcal{Y}_1^4(3\Gamma+4\Omega)+\Gamma\Omega(5\Omega+32)\mathcal{Y}_1^2\\
&\quad+12\Gamma\Omega\mathcal{Y}_1^2\mathcal{Y}_2(3\Gamma+\Omega)+8\Omega^2\mathcal{Y}_1^2\Big].
\end{aligned}$$

Dividing by ϵ^2 we get

$$\begin{aligned}
O(\epsilon^3) &= \tfrac{1}{2}\Gamma\Omega^2\left(-2\Gamma+3\mathcal{Y}_1^2+4\right)\\
&\quad+\tfrac{1}{2}\Omega\mathcal{Y}_1\epsilon\left(2\Gamma^3-8\Gamma^2-\Gamma\Omega+8\Gamma+6\Gamma\Omega\mathcal{Y}_2+2\mathcal{Y}_1^2(3\Gamma+\Omega)+8\Omega\right)\\
&\quad+\tfrac{1}{4}\epsilon^2\Big[\mathcal{Y}_1^2\left(2\Gamma^3-8\Gamma^2+\tfrac{8\Omega^2}{\Gamma}+8\Gamma(\Omega+1)+12\Omega\mathcal{Y}_2(3\Gamma+\Omega)+\Omega(5\Omega+32)\right)\\
&\quad+2\Omega\Big(2\left(\Gamma^3-6\Gamma^2-2\Gamma(\Omega-4)+\Omega\right)+\mathcal{Y}_2\left(2\Gamma^3-8\Gamma^2-\Gamma(\Omega-8)+8\Omega\right)\\
&\quad+3\Gamma\Omega\mathcal{Y}_2^2\Big)+12\Gamma\Omega^2\mathcal{Y}_3\mathcal{Y}_1+\mathcal{Y}_1^4(6\Gamma+8\Omega)\Big].
\end{aligned}\tag{B.8}$$

Note that, previously we already computed

$$\mathcal{Y}_1=\pm i\sqrt{2/3(2-\Gamma)},\quad \mathcal{Y}_2=\frac{\frac{6\Gamma^2(2-\Gamma)}{\Gamma+16}-\Omega}{3\Gamma\Omega}.$$

From the coefficient of ϵ^2 in (B.8) we get $\mathcal{Y}_3$:

$$\begin{aligned}
\mathcal{Y}_3(\Omega) &= -\frac{1}{3\Gamma\Omega^2\mathcal{Y}_1}\left[\frac{1}{4}\mathcal{Y}_1^2\left(2\Gamma^3-8\Gamma^2+\frac{8\Omega^2}{\Gamma}+8\Gamma(\Omega+1)+12\Omega\mathcal{Y}_2(3\Gamma+\Omega)+\Omega(5\Omega+32)\right)\right.\\
&\quad+\frac{1}{2}\Omega\left(2\left(\Gamma^3-6\Gamma^2-2\Gamma(\Omega-4)+\Omega\right)+\mathcal{Y}_2\left(2\Gamma^3-8\Gamma^2-\Gamma(\Omega-8)+8\Omega\right)+3\Gamma\Omega\mathcal{Y}_2^2\right)\\
&\quad\left.+\frac{1}{4}\mathcal{Y}_1^4(6\Gamma+8\Omega)\right].
\end{aligned}$$

Note that at the bifurcation point $\Omega_0(0)=\Omega^*$ given in Theorem (3.3.1) we have that $\mathcal{Y}_2(\Omega^*)=0$ and $\mathcal{Y}_1(\Omega^*)=\pm i\sqrt{2/3(2-\Gamma)}$. It follows that

$$\begin{aligned}
\mathcal{Y}_3(\Omega^*) &= i\frac{6\Gamma^5+6\Gamma^4(3\Omega^*-4)+\Gamma^3(24-68\Omega^*)+\Gamma^2(128-21\Omega^*)\Omega^*+4\Gamma\Omega^*(3\Omega^*-32)-48(\Omega^*)^2}{18\sqrt{6}\sqrt{2-\Gamma}\Gamma^2(\Omega^*)^2},\\
&=: \mp i\rho,
\end{aligned}$$

where

$$\rho = \frac{6\Gamma^5 + 6\Gamma^4(3\Omega^* - 4) + \Gamma^3(24 - 68\Omega^*) + \Gamma^2(128 - 21\Omega^*)\Omega^* + 4\Gamma\Omega^*(3\Omega^* - 32) - 48(\Omega^*)^2}{18\sqrt{6}\sqrt{2-\Gamma}\Gamma^2(\Omega^*)^2}. \tag{B.9}$$

Therefore, the two complex eigenvalues at the bifurcation point $\Omega = \Omega_0$ (where the real part is zero) can be written as

$$y_{\pm}(\Omega_0, \epsilon) \quad = \quad \pm i\left(\sqrt{2/3(2-\Gamma)}\epsilon - \rho\epsilon^3\right) + O(\epsilon^5).$$

Recall that the system (B.6) has three real eigenvalues given by (3.20):

$$y_{3,4}(\Omega, \nu) = -\Omega + O(\nu), \qquad y_5(\Omega, \nu) = -\frac{3\Gamma}{2}. \tag{B.10}$$

To derive the center manifold reduction of the system (B.6), we first calculate eigenvectors of the Jacobian matrix corresponding to $y_{\pm}(\Omega_0)$ and $y_{3,4,5}(\Omega_0)$. Introduce new parameters:

$$\lambda = \Omega - \Omega_0, \quad \beta = \frac{(\Gamma + \nu)\left(\Gamma\left(\frac{1}{\Gamma+\nu} - 1\right) - \nu + 1\right)}{(2\Gamma + \nu)\left(\Gamma^2\Omega_0^2 + 2\Gamma\nu\left(\nu + \Omega_0\right)^2 + \nu^2\left(\nu + \Omega_0\right)^2\right)}. \tag{B.11}$$

The equilibrium in terms of the new parameters λ and β in (B.11) can be written as:

$$\begin{aligned}
i_1^* &= \beta\nu(\Gamma + \nu)\left(\nu + \Omega_0\right)^2 + O(\lambda), \\
i_2^* &= \beta\Gamma\nu\left(\nu + \Omega_0\right)^2 + O(\lambda), \\
q_1^* &= \beta\Gamma^2\nu\left(\nu + \Omega_0\right) + O(\lambda), \\
q_2^* &= \beta\Gamma^2\nu\Omega_0 + O(\lambda), \\
r^* &= \beta\Gamma^2\Omega_0^2 + O(\lambda).
\end{aligned} \tag{B.12}$$

Then, System (B.6) shifted to the endemic equilibrium given in (B.12) can be written as

$$\begin{pmatrix} I_1' \\ I_2' \\ Q_1' \\ Q_2' \\ R' \end{pmatrix} = C \begin{pmatrix} I_1 \\ I_2 \\ Q_1 \\ Q_2 \\ R \end{pmatrix} + \begin{pmatrix} F_1(I_1, I_2, Q_1, Q_2, R, \lambda) \\ F_2(I_1, I_2, Q_1, Q_2, R, \lambda) \\ F_3(I_1, I_2, Q_1, Q_2, R, \lambda) \\ F_4(I_1, I_2, Q_1, Q_2, R, \lambda) \\ F_5(I_1, I_2, Q_1, Q_2, R, \lambda) \end{pmatrix},$$

where, the matrix C for the linear part is given by

$$C = \begin{pmatrix} C_{1,1} & C_{1,2} & -\beta\nu^2(\Gamma+\nu)(\nu+\Omega_0)^2 & -\beta\nu(\Gamma+\nu)(\nu+\Omega_0)^3 & -\beta\nu(2\Gamma+\nu)(\nu+\Omega_0)^2 \\ \Gamma & \beta\Gamma^2\nu(\nu+\Omega_0)^2-\Gamma-\nu & \beta\Gamma\nu^2(\nu+\Omega_0)^2 & -\beta\Gamma\nu(\nu+\Omega_0)^3 & 0 \\ 0 & \beta\nu(\nu+\Omega_0)\Gamma^3+\Gamma & \left(-\beta\Gamma^2\nu^2-1\right)(\nu+\Omega_0) & -\beta\Gamma^2\nu(\nu+\Omega_0)^2 & 0 \\ 0 & \beta\Gamma^3\nu\Omega_0 & \left(1-\beta\Gamma^2\nu^2\right)\Omega_0 & (-\nu-\Omega_0)\left(\beta\nu\Omega_0\Gamma^2+1\right) & 0 \\ 0 & \beta\Gamma^3\Omega_0^2 & -\beta\Gamma^2\nu\Omega_0^2 & -\Omega_0\left(\beta\Omega_0^2\Gamma^2+\beta\nu\Omega_0\Gamma^2-1\right) & -\nu \end{pmatrix}, \tag{B.13}$$

with

$$\begin{aligned} C_{1,1} &= -\beta\Gamma^2\Omega_0^2 - 2\beta\nu(2\Gamma+\nu)(\nu+\Omega_0)^2 - \Gamma - \nu + 1, \\ C_{1,2} &= -\beta\Gamma^2\Omega_0^2 + \beta\nu((\Gamma-2)(\Gamma+\nu)-2\Gamma)(\nu+\Omega_0)^2 + 1. \end{aligned}$$

B.5.3 Computation of eigenvectors for the matrix C in (B.9) for the linearized system

The nonlinear functions in System (B.13) are:

$$\begin{aligned} F_1 &= -I_1^2 + I_1((\Gamma-2)I_2 - \nu Q_1 - Q_2(\nu+\Omega_0) - R) - I_2^2 - I_2 R + O(\lambda), \\ F_2 &= I_2^2 - I_2(\nu Q_1 + Q_2(\nu+\Omega_0)) + O(\lambda), \\ F_3 &= \Gamma I_2 Q_1 - \nu Q_1^2 - Q_1 Q_2(\nu+\Omega_0) + O(\lambda), \\ F_4 &= \Gamma I_2 Q_2 - \nu Q_1 Q_2 + Q_2^2(-(\nu+\Omega_0)) + O(\lambda), \\ F_5 &= \Gamma I_2 R - \nu Q_1 R - Q_2 R(\nu+\Omega_0) + O(\lambda). \end{aligned} \tag{B.14}$$

Note that

$$F_i(0,0,0,0,0,0,0) = \frac{\partial F_i}{\partial j}(0,0,0,0,0,0,0) = 0, \text{ for } i = 1,\ldots,5 \text{ and } j = I_1, I_2, Q_1, Q_2, R.$$

The matrix C has two imaginary and three negative eigenvalues. Let $\vec{\phi} = (\phi_1, \phi_2, \phi_3, \phi_4, \phi_5)^T$ be an eigenvector of C corresponding to the eigenvalue $y_+(\Omega_0) = i\left(\sqrt{2/3(2-\Gamma)}\epsilon - \rho\epsilon^3\right) + O(\epsilon^5)$. Then

$$\left(C - y_+(\Omega_0)I\right)\vec{\phi} = 0.$$

Rewrite the expression of β in (B.11) as

$$\beta = -\frac{\Gamma-2}{2\left(\Gamma^2\Omega_0^2\right)} + \frac{(\Gamma-8)\epsilon^2}{4\Gamma^3\Omega_0^2} + \frac{\epsilon^4\left(16(\Gamma-2)\Gamma-(\Gamma-24)\Omega_0\right)}{8\Gamma^4\Omega_0^3} + O\left(\epsilon^5\right).$$

Then,

$$C = \begin{pmatrix} C[1,1] & C[1,2] & O(\epsilon^4) & \frac{(\Gamma-2)\Omega_0\epsilon^2}{2\Gamma}+O(\epsilon^4) & \frac{(\Gamma-2)\epsilon^2}{\Gamma}+O(\epsilon^4) \\ \Gamma & -\Gamma-\frac{\Gamma\epsilon^2}{2}+O(\epsilon^4) & O(\epsilon^4) & \frac{(\Gamma-2)\Omega_0\epsilon^2}{2\Gamma}+O(\epsilon^4) & 0 \\ 0 & \Gamma-\frac{((\Gamma-2)\Gamma)\epsilon^2}{2\Omega_0}+O(\epsilon^4) & -\Omega_0-\epsilon^2+O(\epsilon^4) & \left(\frac{\Gamma}{2}-1\right)\epsilon^2+O(\epsilon^4) & 0 \\ 0 & -\frac{((\Gamma-2)\Gamma)\epsilon^2}{2\Omega_0}+O(\epsilon^4) & \Omega_0+O(\epsilon^4) & -\Omega_0+\left(\frac{\Gamma}{2}-2\right)\epsilon^2+O(\epsilon^4) & 0 \\ 0 & C[5,2] & \left(\frac{\Gamma}{2}-1\right)\epsilon^2+O(\epsilon^4) & C[5,4] & -\epsilon^2+O(\epsilon^4), \end{pmatrix},$$

where

$$\begin{aligned} C[1,1] &= -\frac{\Gamma}{2}+\left(\frac{3}{4}-\frac{2}{\Gamma}\right)\epsilon^2+O(\epsilon^4), \\ C[1,2] &= \frac{\Gamma}{2}+\left(-\frac{\Gamma}{2}+\frac{11}{4}-\frac{2}{\Gamma}\right)\epsilon^2+O\left(\epsilon^4\right), \\ C[5,4] &= \frac{\Gamma\Omega_0}{2}+\left(\frac{\Gamma-2}{2}+\left(\frac{2}{\Gamma}-\frac{1}{4}\right)\Omega_0\right)\epsilon^2+O\left(\epsilon^4\right), \\ C[5,2] &= \left(\Gamma-\frac{\Gamma^2}{2}\right)+\left(\frac{\Gamma}{4}-2\right)\epsilon^2+O\left(\epsilon^4\right). \end{aligned}$$

From the equation (B.5.3) we obtain the following equation:

$$\begin{pmatrix} (1,1) & \frac{\Gamma}{2}+\left(-\frac{\Gamma}{2}+\frac{11}{4}-\frac{2}{\Gamma}\right)\epsilon^2+O\left(\epsilon^4\right) & O\left(\epsilon^4\right) & \frac{(\Gamma-2)\Omega_0\epsilon^2}{2\Gamma}+O\left(\epsilon^4\right) & \frac{(\Gamma-2)\epsilon^2}{\Gamma}+O\left(\epsilon^4\right) \\ \Gamma & (2,2) & O\left(\epsilon^4\right) & \frac{(\Gamma-2)\Omega_0\epsilon^2}{2\Gamma}+O\left(\epsilon^4\right) & 0 \\ 0 & \Gamma-\frac{((\Gamma-2)\Gamma)\epsilon^2}{2\Omega_0}+O\left(\epsilon^4\right) & (3,3) & \left(\frac{\Gamma}{2}-1\right)\epsilon^2+O\left(\epsilon^4\right) & 0 \\ 0 & -\frac{((\Gamma-2)\Gamma)\epsilon^2}{2\Omega_0}+O\left(\epsilon^4\right) & \Omega_0+O\left(\epsilon^4\right) & (4,4) & 0 \\ 0 & \left(\Gamma-\frac{\Gamma^2}{2}\right)+\left(\frac{\Gamma}{4}-2\right)\epsilon^2+O\left(\epsilon^4\right) & \left(\frac{\Gamma}{2}-1\right)\epsilon^2+O\left(\epsilon^4\right) & (5,4) & (5,5) \end{pmatrix}\begin{pmatrix}\phi_1\\ \phi_2\\ \phi_3\\ \phi_4\\ \phi_5\end{pmatrix}=0,$$

where

$$\begin{aligned}
(1,1) &= -\frac{\Gamma}{2} - i\sqrt{\frac{2}{3}}\sqrt{2-\Gamma}\epsilon + \left(\frac{3}{4} - \frac{2}{\Gamma}\right)\epsilon^2 + i\rho\epsilon^3 + O\left(\epsilon^4\right), \\
(2,2) &= -\Gamma - i\sqrt{\frac{2}{3}}\sqrt{2-\Gamma}\epsilon - \frac{\Gamma\epsilon^2}{2} + i\rho\epsilon^3 + O\left(\epsilon^4\right), \\
(3,3) &= -\Omega_0 - i\sqrt{\frac{2}{3}}\sqrt{2-\Gamma}\epsilon - \epsilon^2 + i\rho\epsilon^3 + O\left(\epsilon^4\right), \\
(4,4) &= -\Omega_0 - i\sqrt{\frac{2}{3}}\sqrt{2-\Gamma}\epsilon + \left(\frac{\Gamma}{2} - 2\right)\epsilon^2 + i\rho\epsilon^3 + O\left(\epsilon^4\right), \\
(5,4) &= \frac{\Gamma\Omega_0}{2} + \left(\frac{\Gamma-2}{2} + \left(\frac{2}{\Gamma} - \frac{1}{4}\right)\Omega_0\right)\epsilon^2 + O\left(\epsilon^4\right), \\
(5,5) &= -i\sqrt{\frac{2}{3}}\sqrt{2-\Gamma}\epsilon - \epsilon^2 + i\rho\epsilon^3 + O\left(\epsilon^4\right).
\end{aligned}$$

If we ignore the $O\left(\epsilon^4\right)$ terms, we obtain the following set of equations:

$$\begin{aligned}
0 &= \phi_1\left(-\frac{2\epsilon^2}{\Gamma} - i\sqrt{\frac{2}{3}}\sqrt{2-\Gamma}\epsilon - \frac{\Gamma}{2} + i\rho\epsilon^3 + \frac{3\epsilon^2}{4}\right) \\
&\quad + \frac{1}{4}\phi_2\left(-\frac{8\epsilon^2}{\Gamma} - 2\Gamma\left(\epsilon^2 - 1\right) + 11\epsilon^2\right) + \frac{(\Gamma-2)\Omega_0\epsilon^2\phi_4}{2\Gamma} + \frac{(\Gamma-2)\epsilon^2\phi_5}{\Gamma}, \\
0 &= \Gamma\phi_1 + \frac{1}{6}\phi_2\left(-3\Gamma\left(\epsilon^2+2\right) + 2i\epsilon\left(3\rho\epsilon^2 - \sqrt{6}\sqrt{2-\Gamma}\right)\right) + \frac{(\Gamma-2)\Omega_0\epsilon^2\phi_4}{2\Gamma}, \\
0 &= \phi_2\left(\Gamma - \frac{(\Gamma-2)\Gamma\epsilon^2}{2\Omega_0}\right) + \phi_3\left(-\Omega_0 + \frac{1}{3}i\epsilon\left(-\sqrt{6}\sqrt{2-\Gamma} + 3\rho\epsilon^2 + 3i\epsilon\right)\right) \\
&\quad + \frac{1}{2}(\Gamma-2)\epsilon^2\phi_4, \\
0 &= -\frac{(\Gamma-2)\Gamma\epsilon^2\phi_2}{2\Omega_0} + \Omega_0\phi_3 + \phi_4\left(-\Omega_0 + \frac{1}{6}\epsilon\left(3(\Gamma-4)\epsilon - 2i\sqrt{6}\sqrt{2-\Gamma} + 6i\rho\epsilon^2\right)\right), \\
0 &= \phi_2\left(-\frac{\Gamma^2}{2} + \frac{\Gamma\epsilon^2}{4} + \Gamma - 2\epsilon^2\right) + \frac{1}{2}(\Gamma-2)\epsilon^2\phi_3 \\
&\quad + \frac{\phi_4\left(\Omega_0\left(2\Gamma^2 - \Gamma\epsilon^2 + 8\epsilon^2\right) + 2(\Gamma-2)\Gamma\epsilon^2\right)}{4\Gamma} + \frac{1}{3}i\epsilon\phi_5\left(-\sqrt{6}\sqrt{2-\Gamma} + 3\rho\epsilon^2 + 3i\epsilon\right).
\end{aligned}$$

Thus, we obtain the following expressions for ϕ_i up to $O\left(\epsilon^4\right)$ with ϕ_5 being arbitrary:

$$
\begin{aligned}
\phi_1 &= \left(i\left[\frac{\epsilon^3\left(\sqrt{6}\sqrt{2-\Gamma}\left(2\Gamma^2-7\Gamma+6\right)\Gamma^2+\Omega_0^2\left(6\sqrt{6}\sqrt{2-\Gamma}-9\Gamma\rho\right)+\sqrt{6}\sqrt{2-\Gamma}(5\Gamma+2)\Gamma\Omega_0\right)}{9\Gamma^2\Omega_0^2} \right.\right. \\
&+ \left.\left. \frac{\sqrt{\frac{2}{3}}\sqrt{2-\Gamma}\epsilon}{\Gamma} \right] \right. \\
&+ \frac{\epsilon^4\left(\Omega_0^2\left(9\Gamma^2\delta_1+6\sqrt{6}\sqrt{2-\Gamma}\rho+9\right)+18\Gamma(\Gamma-2)\Omega_0+2\Gamma(2\Gamma-3)(\Gamma-2)^2\right)}{9\Gamma^2\Omega_0^2} \\
&- \left. \frac{\epsilon^2\left(-\frac{2(\Gamma-2)\Gamma}{\Omega_0}+\frac{4}{\Gamma}-5\right)}{3\Gamma} \right)\phi_5, \\
\phi_2 &= \phi_5\left(\left[\frac{i\epsilon^3\left(\sqrt{6}\sqrt{2-\Gamma}\Gamma\left(2\Gamma^2-7\Gamma+6\right)+3\sqrt{6}\sqrt{2-\Gamma}(\Gamma+2)\Omega_0-9\rho\Omega_0^2\right)}{9\Gamma\Omega_0^2} + \frac{i\sqrt{\frac{2}{3}}\sqrt{2-\Gamma}\epsilon}{\Gamma} \right] \right. \\
&+ \left. \epsilon^4\delta_1+\epsilon^2\left(\frac{2(\Gamma-2)}{3\Omega_0}+\frac{1}{\Gamma}\right) \right), \\
\phi_3 &= \phi_5\left(\frac{\epsilon^2\left(2\Gamma^2-6\Gamma+3\Omega_0+4\right)}{3\Omega_0^2}+\epsilon_4\delta_2 \right. \\
&+ \left. \left[\frac{i\epsilon^3\left(3\sqrt{6}\Gamma\sqrt{2-\Gamma}\Omega_0+\sqrt{6}(2\Gamma-1)(2-\Gamma)^{5/2}-9\rho\Omega_0^2\right)}{9\Omega_0^3} + \frac{i\sqrt{\frac{2}{3}}\sqrt{2-\Gamma}\epsilon}{\Omega_0} \right] \right), \\
\phi_4 &= \phi_5\left(-\frac{\epsilon^4\left(\sqrt{6}(2-\Gamma)^{3/2}\rho\Omega_0+\sqrt{6}\sqrt{2-\Gamma}\rho 2\Omega_0^3-(\Gamma-2)^2(2\Gamma-3)\right)}{3\Omega_0^3} \right. \\
&+ \left. \frac{\epsilon^2\left(2(\Gamma-2)^2+3\Omega_0\right)}{3\Omega_0^2} \right) + \left[\frac{i\epsilon^3\left(-3\sqrt{6}(2-\Gamma)^{3/2}\Omega_0+\sqrt{6}(2\Gamma-3)(2-\Gamma)^{5/2}-9\rho\Omega_0^2\right)}{9\Omega_0^3} \right. \\
&+ \left. \frac{i\sqrt{\frac{2}{3}}\sqrt{2-\Gamma}\epsilon}{\Omega_0} \right],
\end{aligned}
$$

with

$$
\begin{aligned}
\delta_1 &= \frac{1}{9\Gamma\Omega_0^3}\left(3\left(2\Gamma^3+\Gamma^2-22\Gamma+24\right)\Omega_0+3\Omega_0^2\left(\sqrt{6}\sqrt{2-\Gamma}(\Gamma+2)\rho+6\right) \right. \\
&\left. -3\sqrt{6}\sqrt{2-\Gamma}\rho 2\Omega_0^4+8(\Gamma-2)^3(\Gamma-1) \right),
\end{aligned}
$$

$$
\delta_2 = \frac{\left(3\Omega_0^2\left(\sqrt{6}\sqrt{2-\Gamma}\Gamma\rho+3\right)-3\sqrt{6}\sqrt{2-\Gamma}\rho 2\Omega_0^4+3(\Gamma-2)^2(2\Gamma+3)\Omega_0+2(\Gamma-2)^3(2\Gamma-3)\right)}{9\Omega_0^4}.
$$

If we choose $\phi_5 = 1$, an eigenvectors is given by

$$\begin{aligned}\vec{\phi} &= \begin{pmatrix}\phi_1\\ \phi_2\\ \phi_3\\ \phi_4\\ \phi_5\end{pmatrix} = \begin{pmatrix} i\left[\epsilon^3\gamma_0 + \epsilon\frac{\sqrt{\frac{2}{3}}\sqrt{2-\Gamma}}{\Gamma}\right] + \epsilon^4\delta_0 - \frac{\epsilon^2\left(-\frac{2(\Gamma-2)\Gamma}{\Omega_0}+\frac{4}{\Gamma}-5\right)}{3\Gamma} \\ i\left[\epsilon^3\gamma_1 + \epsilon\frac{\sqrt{\frac{2}{3}}\sqrt{2-\Gamma}}{\Gamma}\right] + \epsilon^4\delta_1 + \epsilon^2\left(\frac{2(\Gamma-2)}{3\Omega_0}+\frac{1}{\Gamma}\right) \\ i\left[\epsilon^3\gamma_2 + \epsilon\frac{\sqrt{\frac{2}{3}}\sqrt{2-\Gamma}}{\Omega_0}\right] + \frac{\epsilon^2\left(2\Gamma^2-6\Gamma+3\Omega_0+4\right)}{3\Omega_0^2} + \epsilon^4\delta_2 \\ i\left[\epsilon^3\gamma_3 + \epsilon\frac{\sqrt{\frac{2}{3}}\sqrt{2-\Gamma}}{\Omega_0}\right] + \epsilon^4\delta_3 + \frac{\epsilon^2\left(2(\Gamma-2)^2+3\Omega_0\right)}{3\Omega_0^2} \\ 1 \end{pmatrix} + O(\epsilon^5), \\ &= \vec{\phi}_{re} + i\vec{\phi}_{im},\end{aligned}$$

where the real and imaginary parts of $\vec{\phi}$ are

$$\vec{\phi}_{re} = \begin{pmatrix} \epsilon^4\delta_0 - \frac{\epsilon^2\left(-\frac{2(\Gamma-2)\Gamma}{\Omega_0}+\frac{4}{\Gamma}-5\right)}{3\Gamma} \\ \epsilon^4\delta_1 + \epsilon^2\left(\frac{2(\Gamma-2)}{3\Omega_0}+\frac{1}{\Gamma}\right) \\ \epsilon^4\delta_2 + \frac{\epsilon^2\left(2\Gamma^2-6\Gamma+3\Omega_0+4\right)}{3\Omega_0^2} \\ \epsilon^4\delta_3 + \frac{\epsilon^2\left(2(\Gamma-2)^2+3\Omega_0\right)}{3\Omega_0^2} \\ 1 \end{pmatrix} + O(\epsilon^5) \quad \text{and} \quad \vec{\phi}_{im} = \begin{pmatrix} \epsilon^3\gamma_0 + \epsilon\frac{\sqrt{\frac{2}{3}}\sqrt{2-\Gamma}}{\Gamma} \\ \epsilon^3\gamma_1 + \epsilon\frac{\sqrt{\frac{2}{3}}\sqrt{2-\Gamma}}{\Gamma} \\ \epsilon^3\gamma_2 + \epsilon\frac{\sqrt{\frac{2}{3}}\sqrt{2-\Gamma}}{\Omega_0} \\ \epsilon^3\gamma_3 + \epsilon\frac{\sqrt{\frac{2}{3}}\sqrt{2-\Gamma}}{\Omega_0} \\ 0 \end{pmatrix} + O(\epsilon^4),$$

respectively. At $\Omega_0(0) = \frac{6(2-\Gamma)\Gamma^2}{\Gamma+16}$, then we obtain

$$\vec{\phi}_{re} = \begin{pmatrix} \epsilon^2\frac{14(\Gamma-2)}{9\Gamma^2} + \epsilon^4\delta_0 \\ \epsilon^2\frac{8(\Gamma-2)}{9\Gamma^2} + \epsilon^4\delta_1 \\ -\epsilon^2\frac{(\Gamma+16)\left(8\Gamma^2-15\Gamma+16\right)}{54(\Gamma-2)\Gamma^4} + \epsilon^4\delta_2 \\ -\epsilon^2\frac{(\Gamma+16)\left(4\Gamma^2-7\Gamma+16\right)}{27(\Gamma-2)\Gamma^4} + \epsilon^4\delta_3 \\ 1 \end{pmatrix} + O(\epsilon^5), \quad \vec{\phi}_{im} = \begin{pmatrix} \epsilon\frac{\sqrt{\frac{2}{3}}\sqrt{2-\Gamma}}{\Gamma} + \epsilon^3\gamma_0 \\ \epsilon\frac{\sqrt{\frac{2}{3}}\sqrt{2-\Gamma}}{\Gamma} + \epsilon^3\gamma_1 \\ \epsilon\frac{\Gamma+16}{3\sqrt{6}\sqrt{2-\Gamma}\Gamma^2} + \epsilon^3\gamma_2 \\ \epsilon\frac{\Gamma+16}{3\sqrt{6}\sqrt{2-\Gamma}\Gamma^2} + \epsilon^3\gamma_3 \\ 0 \end{pmatrix} + O(\epsilon^4). \quad \text{(B.15)}$$

By the implicit function theorem, we know that the solution for the eigenvector $\vec{\phi}$ exists in a neighborhood of $\epsilon = 0$.

Let $\vec{\xi} = (\xi_1, \xi_2, \xi_3, \xi_4, \xi_5)^T$ be an eigenvector corresponding to the eigenvalue $y_5 = \dfrac{-3\Gamma}{2}$. To obtain the first order term of $y_5(\nu)$, let

$$y_5(\nu) = \frac{-3\Gamma}{2} + \alpha_1\nu + O(\nu^4).$$

By matching coefficients from the ν coefficient, we can obtain α_1 as

$$\alpha_1 = \frac{-72\Gamma^4 + 3\Gamma^3(32\Omega - 75) + 12\Gamma^2(25\Omega - 6) + 4\Gamma(24 - 41\Omega)\Omega - 32\Omega^2}{36\Gamma(3\Gamma - 2\Omega)^2}.$$

Following the same procedure as above, and assuming $\xi_5 = 1 + O(\nu^2)$ with $\Omega_0(0) = \frac{6(2-\Gamma)\Gamma^2}{\Gamma+16}$, we obtain

$$\begin{aligned}
\xi_1 &= \frac{3\left(4\Gamma^2 - 7\Gamma + 16\right)^2}{2\left(24\Gamma^4 - 225\Gamma^3 + 578\Gamma^2 - 704\Gamma + 512\right)} + \Delta_1, \\
\xi_2 &= -\frac{3\left(4\Gamma^2 - 7\Gamma + 16\right)^2}{24\Gamma^4 - 225\Gamma^3 + 578\Gamma^2 - 704\Gamma + 512} + \Delta_2, \\
\xi_3 &= \frac{2(\Gamma + 16)\left(4\Gamma^2 - 7\Gamma + 16\right)}{(\Gamma - 2)\left(24\Gamma^3 - 177\Gamma^2 + 224\Gamma - 256\right)} + \Delta_3, \\
\xi_4 &= \frac{8\Gamma(\Gamma + 16)}{24\Gamma^3 - 177\Gamma^2 + 224\Gamma - 256} + \Delta_4,
\end{aligned}$$

where

$$\begin{aligned}
\Delta_1 &= \frac{\left(18432\Gamma^{11} - 340032\Gamma^{10} + 4597120\Gamma^9 - 28052424\Gamma^8 + 107724121\Gamma^7 - 275189568\Gamma^6 + 518814528\Gamma^5\right)\nu}{36\Gamma^2\left(24\Gamma^4 - 225\Gamma^3 + 578\Gamma^2 - 704\Gamma + 512\right)^2\left(4\Gamma^2 - 7\Gamma + 16\right)} \\
&+ \frac{\left(-702376960\Gamma^4 + 693731328\Gamma^3 - 404226048\Gamma^2 + 104857600\Gamma + 67108864\right)\nu}{36\Gamma^2\left(24\Gamma^4 - 225\Gamma^3 + 578\Gamma^2 - 704\Gamma + 512\right)^2\left(4\Gamma^2 - 7\Gamma + 16\right)}, \\
\Delta_2 &= \frac{\left(-9216\Gamma^{11} + 8448\Gamma^{10} + 209812\Gamma^9 - 2042091\Gamma^8 + 6841816\Gamma^7 - 17479089\Gamma^6 + 17802600\Gamma^5\right)\nu}{9\Gamma^2\left(4\Gamma^2 - 7\Gamma + 16\right)\left(24\Gamma^4 - 225\Gamma^3 + 578\Gamma^2 - 704\Gamma + 512\right)^2} \\
&+ \frac{\left(4129664\Gamma^4 - 55996416\Gamma^3 + 66453504\Gamma^2 - 41418752\Gamma - 8388608\right)\nu}{9\Gamma^2\left(4\Gamma^2 - 7\Gamma + 16\right)\left(24\Gamma^4 - 225\Gamma^3 + 578\Gamma^2 - 704\Gamma + 512\right)^2}, \\
\Delta_3 &= \frac{(\Gamma + 16)\left(36864\Gamma^{11} - 33792\Gamma^{10} - 783664\Gamma^9 + 8351688\Gamma^8 - 34925455\Gamma^7 + 116460034\Gamma^6\right)\nu}{54(\Gamma - 2)^2\Gamma^2\left(-24\Gamma^3 + 177\Gamma^2 - 224\Gamma + 256\right)^2\left(4\Gamma^2 - 7\Gamma + 16\right)^2} \\
&+ \frac{(\Gamma + 16)\left(-251227200\Gamma^5 + 445918720\Gamma^4 - 571113472\Gamma^3 + 662568960\Gamma^2 - 507510784\Gamma + 301989888\right)\nu}{54(\Gamma - 2)^2\Gamma^2\left(-24\Gamma^3 + 177\Gamma^2 - 224\Gamma + 256\right)^2\left(4\Gamma^2 - 7\Gamma + 16\right)^2}, \\
\Delta_4 &= \frac{\left(36864\Gamma^{10} + 30720\Gamma^9 - 820048\Gamma^8 + 7040984\Gamma^7 - 26388649\Gamma^6 + 84686624\Gamma^5\right)(\Gamma + 16)\nu}{54(\Gamma - 2)\Gamma^2\left(4\Gamma^2 - 7\Gamma + 16\right)^2\left(-24\Gamma^3 + 177\Gamma^2 - 224\Gamma + 256\right)^2} \\
&+ \frac{\left(-205072128\Gamma^4 + 384548864\Gamma^3 - 486998016\Gamma^2 + 387973120\Gamma - 150994944\right)(\Gamma + 16)\nu}{54(\Gamma - 2)\Gamma^2\left(4\Gamma^2 - 7\Gamma + 16\right)^2\left(-24\Gamma^3 + 177\Gamma^2 - 224\Gamma + 256\right)^2}.
\end{aligned}$$

If we substitute $\nu = \epsilon^2$, then we obtain the eigenvector:

$$\vec{\xi} = \begin{pmatrix} \xi_1 \\ \xi_2 \\ \xi_3 \\ \xi_4 \\ \xi_5 \end{pmatrix} = \begin{pmatrix} \frac{3\left(4\Gamma^2-7\Gamma+16\right)^2}{2(24\Gamma^4-225\Gamma^3+578\Gamma^2-704\Gamma+512)} + \Delta_1(\epsilon^2) \\ -\frac{3\left(4\Gamma^2-7\Gamma+16\right)^2}{24\Gamma^4-225\Gamma^3+578\Gamma^2-704\Gamma+512} + \Delta_2(\epsilon^2) \\ \frac{2(\Gamma+16)\left(4\Gamma^2-7\Gamma+16\right)}{(\Gamma-2)(24\Gamma^3-177\Gamma^2+224\Gamma-256)} + \Delta_3(\epsilon^2) \\ \frac{8\Gamma(\Gamma+16)}{24\Gamma^3-177\Gamma^2+224\Gamma-256} + \Delta_4(\epsilon^2) \\ 1 \end{pmatrix} + O(\epsilon^4). \tag{B.16}$$

Let $\vec{\Psi} = (\Psi_1, \Psi_2, \Psi_3, \Psi_4, \Psi_5)^T$ and $\vec{\tau} = (\tau_1, \tau_2, \tau_3, \tau_4, \tau_5)^T$ be the eigenvectors corresponding to $y_{3,4} = -\Omega + \lambda_1\epsilon$, where $\lambda_1 = \pm\frac{i\sqrt{\Gamma-2\Gamma}}{\sqrt{2\Omega-3\Gamma}}$ is the linear term of the Taylor expansion of the eigenvalue around ϵ. Two eigenvectors corresponding to these two eigenvalues are given by

$$\vec{\Psi} = \begin{pmatrix} \Psi_1 \\ \Psi_2 \\ \Psi_3 \\ \Psi_4 \\ \Psi_5 \end{pmatrix} = \begin{pmatrix} \frac{\left(36\Gamma^4-129\Gamma^3+355\Gamma^2-448\Gamma+256\right)\epsilon^2}{9\Gamma^3(4\Gamma^2-7\Gamma+16)} + \psi_1 \\ \frac{\left(36\Gamma^4-135\Gamma^3+271\Gamma^2-256\Gamma+256\right)\epsilon^2}{9\Gamma^3(4\Gamma^2-7\Gamma+16)} + \psi_2 \\ -\frac{(\Gamma+16)\epsilon}{3\sqrt{2-\Gamma}\Gamma^2\sqrt{\frac{12(2-\Gamma)\Gamma^2}{\Gamma+16}-3\Gamma}} - \frac{(\Gamma+16)\left(36\Gamma^4-207\Gamma^3+395\Gamma^2-608\Gamma-256\right)\epsilon^2}{54(\Gamma-2)\Gamma^4(4\Gamma^2-7\Gamma+16)} + \psi_3 \\ -\frac{2}{\Gamma} + \frac{(\Gamma+16)\epsilon}{3\sqrt{6-3\Gamma}\Gamma^2\sqrt{-\frac{\Gamma\left(4\Gamma^2-7\Gamma+16\right)}{\Gamma+16}}} + \psi_4 \\ 1 \end{pmatrix} + O(\epsilon^4), \tag{B.17}$$

where

$$\begin{aligned}
\psi_1 &= -\frac{\left(-864\Gamma^5+3084\Gamma^4-8893\Gamma^3+8016\Gamma^2-3840\Gamma-4096\right)\epsilon^3}{54\sqrt{6-3\Gamma}\Gamma^3(\Gamma+16)\left(-\frac{\Gamma\left(4\Gamma^2-7\Gamma+16\right)}{\Gamma+16}\right)^{3/2}}, \\
\psi_2 &= \frac{\left(144\Gamma^3-251\Gamma^2+608\Gamma+256\right)\epsilon^3}{54\sqrt{6-3\Gamma}\Gamma^3\left(-\frac{\Gamma\left(4\Gamma^2-7\Gamma+16\right)}{\Gamma+16}\right)^{3/2}}, \\
\psi_3 &= \frac{\left(216\Gamma^6-2394\Gamma^5+10153\Gamma^4-18098\Gamma^3+23712\Gamma^2+2560\Gamma-8192\right)\epsilon^3}{324\sqrt{6-3\Gamma}(\Gamma-2)\Gamma^5\left(-\frac{\Gamma\left(4\Gamma^2-7\Gamma+16\right)}{\Gamma+16}\right)^{3/2}}, \\
\psi_4 &= \frac{\left(-252\Gamma^6+2025\Gamma^5-7237\Gamma^4+12338\Gamma^3-14496\Gamma^2-2560\Gamma+8192\right)\epsilon^2}{54(\Gamma-2)\Gamma^5\left(4\Gamma^2-7\Gamma+16\right)} \\
&- \frac{\left(216\Gamma^5-1962\Gamma^4+5941\Gamma^3-10320\Gamma^2+9984\Gamma+4096\right)\epsilon^3}{324\sqrt{6-3\Gamma}\Gamma^5\left(-\frac{\Gamma\left(4\Gamma^2-7\Gamma+16\right)}{\Gamma+16}\right)^{3/2}},
\end{aligned}$$

and

$$\vec{\tau} = \begin{pmatrix} \tau_1 \\ \tau_2 \\ \tau_3 \\ \tau_4 \\ \tau_5 \end{pmatrix} = \begin{pmatrix} \frac{\left(-36\Gamma^4+129\Gamma^3-355\Gamma^2+448\Gamma-256\right)\epsilon^2}{9\Gamma^3(4\Gamma^2-7\Gamma+16)} + \kappa_1 \\ \frac{\left(36\Gamma^4-135\Gamma^3+271\Gamma^2-256\Gamma+256\right)\epsilon^2}{9\Gamma^3(4\Gamma^2-7\Gamma+16)} + \kappa_2 \\ \frac{(\Gamma+16)\epsilon}{3\sqrt{6-3\Gamma}\Gamma^2\sqrt{-\frac{\Gamma(4\Gamma^2-7\Gamma+16)}{\Gamma+16}}} - \frac{(\Gamma+16)\left(36\Gamma^4-207\Gamma^3+395\Gamma^2-608\Gamma-256\right)\epsilon^2}{54(\Gamma-2)\Gamma^4(4\Gamma^2-7\Gamma+16)} + \kappa_3 \\ -\frac{2}{\Gamma} - \frac{(\Gamma+16)\epsilon}{3\sqrt{6-3\Gamma}\Gamma^2\sqrt{-\frac{\Gamma(4\Gamma^2-7\Gamma+16)}{\Gamma+16}}} + \kappa_4 \\ 1 \end{pmatrix} + O(\epsilon^4), \tag{B.18}$$

where

$$\begin{aligned}
\kappa_1 &= \frac{\left(864\Gamma^5 - 3084\Gamma^4 + 8893\Gamma^3 - 8016\Gamma^2 + 3840\Gamma + 4096\right)\epsilon^3}{54\sqrt{6-3\Gamma}\Gamma^3(\Gamma+16)\left(-\frac{\Gamma(4\Gamma^2-7\Gamma+16)}{\Gamma+16}\right)^{3/2}}, \\
\kappa_2 &= -\frac{\left(144\Gamma^3 - 251\Gamma^2 + 608\Gamma + 256\right)\epsilon^3}{54\sqrt{6-3\Gamma}\Gamma^3\left(-\frac{\Gamma(4\Gamma^2-7\Gamma+16)}{\Gamma+16}\right)^{3/2}}, \\
\kappa_3 &= -\frac{\left(216\Gamma^6 - 2394\Gamma^5 + 10153\Gamma^4 - 18098\Gamma^3 + 23712\Gamma^2 + 2560\Gamma - 8192\right)\epsilon^3}{324\sqrt{6-3\Gamma}(\Gamma-2)\Gamma^5\left(-\frac{\Gamma(4\Gamma^2-7\Gamma+16)}{\Gamma+16}\right)^{3/2}}, \\
\kappa_4 &= \frac{\left(-252\Gamma^6 + 2025\Gamma^5 - 7237\Gamma^4 + 12338\Gamma^3 - 14496\Gamma^2 - 2560\Gamma + 8192\right)\epsilon^2}{54(\Gamma-2)\Gamma^5\left(4\Gamma^2 - 7\Gamma + 16\right)}, \\
&+ \frac{\left(216\Gamma^5 - 1962\Gamma^4 + 5941\Gamma^3 - 10320\Gamma^2 + 9984\Gamma + 4096\right)\epsilon^3}{324\sqrt{6-3\Gamma}\Gamma^5\left(-\frac{\Gamma(4\Gamma^2-7\Gamma+16)}{\Gamma+16}\right)^{3/2}}.
\end{aligned}$$

Let $P = (\vec{\phi}_{re}, \vec{\phi}_{im}, \vec{\Psi}, \vec{\tau}, \vec{\xi})$ be the matrix formed by the eigenvectors. Then,

$$P^{-1}CP = \begin{pmatrix} 0 & \Im y_+(\Omega_0) & 0 & 0 & 0 \\ \Im y_-(\Omega_0) & 0 & 0 & 0 & 0 \\ 0 & 0 & y_3(\Omega_0) & 0 & 0 \\ 0 & 0 & 0 & y_4(\Omega_0) & 0 \\ 0 & 0 & 0 & 0 & y_5(\Omega_0) \end{pmatrix}.$$

B.5.4 Center Manifold reduction

We now compute P^{-1} from the matrix P that we obtain from replacing $\Omega_0(0) = \frac{6(2-\Gamma)\Gamma^2}{\Gamma+16}$ in the eigenvectors we obtained previously in Equations (B.15, B.17, B.18, B.16),

$$P = \begin{pmatrix} \phi_{re\,1} & \phi_{im\,1} & \Psi_1 & \tau_1 & \xi_1 \\ \phi_{re\,2} & \phi_{im\,2} & \Psi_2 & \tau_2 & \xi_2 \\ \phi_{re\,3} & \phi_{im\,3} & \Psi_3 & \tau_3 & \xi_3 \\ \phi_{re\,4} & \phi_{im\,4} & \Psi_4 & \tau_4 & \xi_4 \\ \phi_{re\,5} & \phi_{im\,5} & \Psi_5 & \tau_5 & \xi_5 \end{pmatrix}.$$

Consider the change of variables: $(r,s,t,u,v)^T = P^{-1}(I_1, I_2, Q_1, Q_2, R)^T$. We can obtain the expressions for $I_1, \ldots, R$ in terms of (r,s,t,u,v) since $P(r,s,t,u,v)^T = (I_1, I_2, Q_1, Q_2, R)^T$.

$$\begin{aligned}
I_1 &= I_1(r,s,t,u,v) = \frac{14(\Gamma-2)r\epsilon^2}{9\Gamma^2} + \frac{\sqrt{\frac{2}{3}}\sqrt{2-\Gamma}s\epsilon}{\Gamma} + \frac{\left(36\Gamma^4 - 129\Gamma^3 + 355\Gamma^2 - 448\Gamma + 256\right)t\epsilon^2}{9\Gamma^3\left(4\Gamma^2 - 7\Gamma + 16\right)} \\
&\quad - \frac{\left(36\Gamma^4 - 129\Gamma^3 + 355\Gamma^2 - 448\Gamma + 256\right)u\epsilon^2}{9\Gamma^3\left(4\Gamma^2 - 7\Gamma + 16\right)} + vc_1, \\
I_2 &= I_2(r,s,t,u,v) = \frac{8(\Gamma-2)r\epsilon^2}{9\Gamma^2} + \frac{\sqrt{\frac{2}{3}}\sqrt{2-\Gamma}s\epsilon}{\Gamma} \\
&\quad + \frac{\left(36\Gamma^4 - 135\Gamma^3 + 271\Gamma^2 - 256\Gamma + 256\right)t\epsilon^2}{9\Gamma^3\left(4\Gamma^2 - 7\Gamma + 16\right)} + \frac{\left(36\Gamma^4 - 135\Gamma^3 + 271\Gamma^2 - 256\Gamma + 256\right)u\epsilon^2}{9\Gamma^3\left(4\Gamma^2 - 7\Gamma + 16\right)} + vc_2, \\
Q_1 &= Q_1(r,s,t,u,v) = -\frac{(\Gamma+16)\left(8\Gamma^2 - 15\Gamma + 16\right)r\epsilon^2}{54(\Gamma-2)\Gamma^4} + \frac{(\Gamma+16)s\epsilon}{3\sqrt{6}\sqrt{2-\Gamma}\Gamma^2} \\
&\quad + t\left(-\frac{(\Gamma+16)\epsilon}{3\sqrt{6-3\Gamma}\Gamma^2\sqrt{-\frac{\Gamma\left(4\Gamma^2-7\Gamma+16\right)}{\Gamma+16}}} - \frac{(\Gamma+16)\left(36\Gamma^4 - 207\Gamma^3 + 395\Gamma^2 - 608\Gamma - 256\right)\epsilon^2}{54(\Gamma-2)\Gamma^4\left(4\Gamma^2 - 7\Gamma + 16\right)}\right) \\
&\quad + u\left(\frac{(\Gamma+16)\epsilon}{3\sqrt{6-3\Gamma}\Gamma^2\sqrt{-\frac{\Gamma\left(4\Gamma^2-7\Gamma+16\right)}{\Gamma+16}}} - \frac{(\Gamma+16)\left(36\Gamma^4 - 207\Gamma^3 + 395\Gamma^2 - 608\Gamma - 256\right)\epsilon^2}{54(\Gamma-2)\Gamma^4\left(4\Gamma^2 - 7\Gamma + 16\right)}\right) \\
&\quad + vc_3,
\end{aligned}$$

$$
\begin{aligned}
Q_2 &= Q_2(r,s,t,u,v) = -\frac{(\Gamma+16)\left(4\Gamma^2-7\Gamma+16\right)r\epsilon^2}{27(\Gamma-2)\Gamma^4}+\frac{(\Gamma+16)s\epsilon}{3\sqrt{6}\sqrt{2-\Gamma}\Gamma^2}\\
&\quad +t\Bigg(\frac{(\Gamma+16)\epsilon}{3\sqrt{6-3\Gamma}\Gamma^2\sqrt{-\frac{\Gamma\left(4\Gamma^2-7\Gamma+16\right)}{\Gamma+16}}}\\
&\qquad +\frac{\left(-252\Gamma^6+2025\Gamma^5-7237\Gamma^4+12338\Gamma^3-14496\Gamma^2-2560\Gamma+8192\right)\epsilon^2}{54(\Gamma-2)\Gamma^5\left(4\Gamma^2-7\Gamma+16\right)}-\frac{2}{\Gamma}\Bigg)\\
&\quad +u\Big(-\frac{(\Gamma+16)\epsilon}{3\sqrt{6-3\Gamma}\Gamma^2\sqrt{-\frac{\Gamma\left(4\Gamma^2-7\Gamma+16\right)}{\Gamma+16}}}\\
&\quad +\frac{\left(-252\Gamma^6+2025\Gamma^5-7237\Gamma^4+12338\Gamma^3-14496\Gamma^2-2560\Gamma+8192\right)\epsilon^2}{54(\Gamma-2)\Gamma^5\left(4\Gamma^2-7\Gamma+16\right)}-\frac{2}{\Gamma}\Big)+vc_4,\\
R &= R(r,s,t,u,v) = r+t+u+v+O(\epsilon^4)(r+s+t+u+v),
\end{aligned}
$$

where,

$$
\begin{aligned}
c_1 &= v\Big(\left(54\Gamma^2\left(-16\Gamma^5+120\Gamma^4-417\Gamma^3+706\Gamma^2-704\Gamma+512\right)\left(4\Gamma^2-7\Gamma+16\right)^3\right.\\
&\quad +\left(55296\Gamma^{13}-990720\Gamma^{12}+8595456\Gamma^{11}-46743488\Gamma^{10}+178857944\Gamma^9\right.\\
&\quad -508011990\Gamma^8+1109812017\Gamma^7-1892799736\Gamma^6+2551247424\Gamma^5-2668182528\Gamma^4\\
&\quad \left.+2090696704\Gamma^3-1053818880\Gamma^2+255852544\Gamma+67108864\right)\epsilon^2\Big)\Big/\\
&\quad \Big(36\Gamma^2\left(4\Gamma^2-7\Gamma+16\right)\left(-16\Gamma^5+120\Gamma^4-417\Gamma^3+706\Gamma^2-704\Gamma+512\right)^2\Big),\\
c_2 &= \frac{3\left(4\Gamma^2-7\Gamma+16\right)^2}{16\Gamma^5-120\Gamma^4+417\Gamma^3-706\Gamma^2+704\Gamma-512}\\
&\quad +\Big(\Big(18432\Gamma^{12}-286464\Gamma^{11}+2016064\Gamma^{10}-9745264\Gamma^9+34694316\Gamma^8-97805364\Gamma^7\\
&\quad +217236971\Gamma^6-390283800\Gamma^5+532818816\Gamma^4-536637440\Gamma^3+340918272\Gamma^2\\
&\quad -116916224\Gamma-8388608\Big)\epsilon^2\Big)\Big/\Big(9\Gamma^2\left(-16\Gamma^5+120\Gamma^4-417\Gamma^3+706\Gamma^2-704\Gamma+512\right)^2\\
&\quad \left(4\Gamma^2-7\Gamma+16\right)\Big),\\
c_3 &= -\frac{2(\Gamma+16)\left(4\Gamma^2-7\Gamma+16\right)}{(\Gamma-2)\left(16\Gamma^4-88\Gamma^3+241\Gamma^2-224\Gamma+256\right)}\\
&\quad -\Big(\left(\Gamma+16\right)\left(82944\Gamma^{12}-1138944\Gamma^{11}+6872704\Gamma^{10}-27056096\Gamma^9+75436916\Gamma^8\right.\\
&\quad -167690721\Gamma^7+299243246\Gamma^6-460974272\Gamma^5+511160832\Gamma^4-345473024\Gamma^3\\
&\quad \left.-122552320\Gamma^2+356515840\Gamma-301989888\right)\epsilon^2\Big)\Big/\Big(54(\Gamma-2)^2\Gamma^2\left(4\Gamma^2-7\Gamma+16\right)^2\\
&\quad \left(16\Gamma^4-88\Gamma^3+241\Gamma^2-224\Gamma+256\right)^2\Big),\\
c_4 &= -\frac{16(\Gamma+16)}{16\Gamma^4-88\Gamma^3+241\Gamma^2-224\Gamma+256}\\
&\quad -\Big(\left(\Gamma+16\right)\left(73728\Gamma^{11}-1016832\Gamma^{10}+6065152\Gamma^9-23871536\Gamma^8+65002792\Gamma^7\right.\\
&\quad -125948247\Gamma^6+143738080\Gamma^5-26974464\Gamma^4-242728960\Gamma^3\\
&\quad \left.+449249280\Gamma^2-387973120\Gamma+150994944\right)\epsilon^2\Big)\Big/\Big(27(\Gamma-2)\Gamma^3\left(4\Gamma^2-7\Gamma+16\right)^2\\
&\quad \left(16\Gamma^4-88\Gamma^3+241\Gamma^2-224\Gamma+256\right)^2\Big).
\end{aligned}
$$

Let

$$\begin{pmatrix} f_1(r,s,t,u,v,\lambda) \\ f_2(r,s,t,u,v,\lambda) \\ f_3(r,s,t,u,v,\lambda) \\ f_4(r,s,t,u,v,\lambda) \\ f_5(r,s,t,u,v,\lambda) \end{pmatrix} = P^{-1} \begin{pmatrix} F_1(I_1(r,s,t,u,v), I_2(r,s,t,u,v), Q_1(r,s,t,u,v), Q_2(r,s,t,u,v), R(r,s,t,u,v), \lambda) \\ F_2(I_1(r,s,t,u,v), I_2(r,s,t,u,v), Q_1(r,s,t,u,v), Q_2(r,s,t,u,v), R(r,s,t,u,v), \lambda) \\ F_3(I_1(r,s,t,u,v), I_2(r,s,t,u,v), Q_1(r,s,t,u,v), Q_2(r,s,t,u,v), R(r,s,t,u,v), \lambda) \\ F_4(I_1(r,s,t,u,v), I_2(r,s,t,u,v), Q_1(r,s,t,u,v), Q_2(r,s,t,u,v), R(r,s,t,u,v), \lambda) \\ F_5(I_1(r,s,t,u,v), I_2(r,s,t,u,v), Q_1(r,s,t,u,v), Q_2(r,s,t,u,v), R(r,s,t,u,v), \lambda) \end{pmatrix}. \tag{B.19}$$

. From B.14 we obtain the expressions for $f_i(r,s,t,u,v,\lambda)$ when we substitute the expressions for $I_1,\ldots,R$ with $I_1(r,s,t,u,v),\ldots,R(r,s,t,u,v)$ in $F_i(I_1,\ldots,R)$ to obtain $F_1\Big(I_1(r,s,t,u,v), I_2(r,s,t,u,v), Q_1(r,s,t,u,v), Q_2(r,s,t,u,v), R(r,s,t,u,v), \lambda\Big)$, for $i = 1,\ldots,5$. The expressions for $f_i(r,s,t,u,v,\lambda)$ have the following shape; however, the coefficient values $a_i,\ldots,e_i$ are omitted due to size constraints.

$$\begin{aligned} f_1(r,s,t,u,v,\lambda) &= a_1rs + a_2rt + a_3ru + a_4rv + a_5r^2 + a_6s^2 + a_7t^2 + a_8u^2 + a_9v^2, \\ f_2(r,s,t,u,v,\lambda) &= b_1rs + b_2rt + b_3ru + b_4rv + b_5r^2 + b_6s^2 + b_7t^2 + b_8u^2 + b_9v^2, \\ f_3(r,s,t,u,v,\lambda) &= c_1rs + c_2rt + c_3ru + c_4rv + c_5r^2 + c_6s^2 + c_7t^2 + c_8u^2 + c_9v^2, \\ f_4(r,s,t,u,v,\lambda) &= d_1rs + d_2rt + d_3ru + d_4rv + d_5r^2 + d_6s^2 + d_7t^2 + d_8u^2 + d_9v^2, \\ f_5(r,s,t,u,v,\lambda) &= e_1rs + e_2rt + e_3ru + e_4rv + e_5r^2 + e_6s^2 + e_7t^2 + e_8u^2 + e_9v^2. \end{aligned}$$

Then, we obtain the following new systems:

$$\begin{pmatrix} r' \\ s' \end{pmatrix} = \begin{pmatrix} 0 & \Im y_+(\Omega_0) \\ \Im y_-(\Omega_0) & 0 \end{pmatrix} \begin{pmatrix} r \\ s \end{pmatrix} + \begin{pmatrix} f_1(r,s,t,u,v,\lambda) \\ f_2(r,s,t,u,v,\lambda) \end{pmatrix}, \tag{B.20}$$

and

$$\begin{pmatrix} t' \\ u' \\ v' \end{pmatrix} = \begin{pmatrix} y_3(\Omega_0) & 0 & 0 \\ 0 & y_4(\Omega_0) & 0 \\ 0 & 0 & y_5(\Omega_0) \end{pmatrix} \begin{pmatrix} t \\ u \\ v \end{pmatrix} + \begin{pmatrix} f_3(r,s,t,u,v,\lambda) \\ f_4(r,s,t,u,v,\lambda) \\ f_5(r,s,t,u,v,\lambda) \end{pmatrix}. \tag{B.21}$$

Note that $y_3(\Omega_0),\ y_4(\Omega_0),\ y_5(\Omega_0) < 0$. Now consider the following functions $t = h_3(r,s)$, $u = h_4(r,s)$ and $v = h_5(r,s)$ such that

$$h_j(0,0) = \frac{\partial h_j}{\partial r}(0,0) = \frac{\partial h_j}{\partial s}(0,0) = 0, \quad j = 3,4,5. \tag{B.22}$$

By the center manifold theorem [8], the functions $t = h_3(r,s)$, $u = h_4(r,s)$ and $v = h_5(r,s)$ can be used to restrict the system (B.20, B.21) to a two dimensional system in r and s with the parameter λ. We compute these functions using the following equation:

$$\begin{pmatrix} \frac{\partial h_3}{\partial r} & \frac{\partial h_3}{\partial s} \\ \frac{\partial h_4}{\partial r} & \frac{\partial h_4}{\partial s} \\ \frac{\partial h_5}{\partial r} & \frac{\partial h_5}{\partial s} \end{pmatrix} \left\{ \begin{pmatrix} 0 & \Im y_+(\Omega_0) \\ \Im y_-(\Omega_0) & 0 \end{pmatrix} \begin{pmatrix} r \\ s \end{pmatrix} + \begin{pmatrix} f_1(r,s,h_3,h_4,h_5) \\ f_2(r,s,h_3,h_4,h_5) \end{pmatrix} \right\} \\ - \begin{pmatrix} y_3(\Omega_0) & 0 & 0 \\ 0 & y_4(\Omega_0) & 0 \\ 0 & 0 & y_5(\Omega_0) \end{pmatrix} \begin{pmatrix} h_3(r,s) \\ h_4(r,s) \\ h_5(r,s) \end{pmatrix} - \begin{pmatrix} f_3(r,s,t,u,v) \\ f_4(r,s,t,u,v) \\ f_5(r,s,t,u,v) \end{pmatrix} = 0. \tag{B.23}$$

We compute the functions $h_i(r,s,\lambda)$ for $i = 3,4,5$ from (B.23) up to the second order. Also, since the formula for α includes derivatives evaluated at $(r,s,\lambda) = (0,0,0)$, thus we can neglect the second order terms that have λ as a factor. Assume,

$$h_j(r,s,\lambda) = \kappa_{j1} r^2 + \kappa_{j2} rs + \kappa_{j3} s^2 + O(\lambda) + O([r,s|^3). \tag{B.24}$$

where $O(|r,s|^3)$ contains terms of order higher than 2 in r,s. If we substitute B.24 into B.23 we obtain a system of equations so we can solve for κ_{ji} for $j = 3,4,5$ and $i = 1,2,3$. We can solve for κ_{ji} by looking at the coefficients of the three second order terms r^2, rs, s^2 and treating λ as a variable. Thus, for h_3 we have the following,

$$\begin{aligned} r^2 \quad : \quad & \frac{11(\Gamma-2)\epsilon}{9\sqrt{6-3\Gamma}\sqrt{-\frac{\Gamma(4\Gamma^2-7\Gamma+16)}{\Gamma+16}}} + \frac{11\left(144\Gamma^6 - 744\Gamma^5 + 3157\Gamma^4 - 7814\Gamma^3 + 17856\Gamma^2 - 18944\Gamma + 16384\right)\epsilon^2}{243\left(4\Gamma^2 - 7\Gamma + 16\right)^2\Gamma^2} \\ & + \frac{6(2-\Gamma)\Gamma^2\kappa_{31}}{\Gamma+16} - \sqrt{\frac{2}{3}}\sqrt{2-\Gamma}\kappa_{32}\epsilon = O(\epsilon^3), \\ rs \quad : \quad & \left(\frac{486\Gamma^4}{\sqrt{-\frac{\Gamma(4\Gamma^2-7\Gamma+16)}{\Gamma+16}}} - \frac{18\sqrt{3}\left(144\Gamma^6 - 744\Gamma^5 + 3157\Gamma^4 - 7814\Gamma^3 + 17856\Gamma^2 - 18944\Gamma + 16384\right)\Gamma^2\epsilon}{\sqrt{2-\Gamma}\left(4\Gamma^2 - 7\Gamma + 16\right)^2} \right. \\ & - \frac{\sqrt{-\frac{\Gamma(4\Gamma^2-7\Gamma+16)}{\Gamma+16}}}{(\Gamma-2)\left(4\Gamma^2-7\Gamma+16\right)^4}\Big(41472\Gamma^{12} - 435456\Gamma^{11} + 2923776\Gamma^{10} - 13068576\Gamma^9 + 43404398\Gamma^8 \\ & -105474479\Gamma^7 + 201874781\Gamma^6 - 280752752\Gamma^5 + 364375808\Gamma^4 - 399220736\Gamma^3 + 600768512\Gamma^2 \\ & \left. -527433728\Gamma + 486539264\Big)\right)\frac{1}{729\sqrt{2}\Gamma^3} + 2\sqrt{\frac{2}{3}}\sqrt{2-\Gamma}\kappa_{31}\epsilon - \frac{6(\Gamma-2)\Gamma^2\kappa_{32}}{\Gamma+16} - \frac{2}{3}\sqrt{2}\sqrt{6-3\Gamma}\kappa_{33}\epsilon = O(\epsilon^3), \end{aligned}$$

$$
\begin{aligned}
s^2 \quad : \quad & -\frac{\left(12\Gamma^4-59\Gamma^3+117\Gamma^2+18\Gamma-224\right)\epsilon}{6\sqrt{6-3\Gamma}(\Gamma+16)\sqrt{-\frac{\Gamma\left(4\Gamma^2-7\Gamma+16\right)}{\Gamma+16}}} \\
& -\Bigg(\Big(1728\Gamma^9-14256\Gamma^8+68532\Gamma^7-194609\Gamma^6+409587\Gamma^5-469998\Gamma^4+148640\Gamma^3+1227264\Gamma^2 \\
& -1646592\Gamma+1835008\Big)\epsilon^2\Bigg)\frac{1}{162(\Gamma+16)\left(4\Gamma^2-7\Gamma+16\right)^2\Gamma^2}+\sqrt{\frac{2}{3}}\sqrt{2-\Gamma}\kappa_{32}\epsilon+\frac{6(2-\Gamma)\Gamma^2\kappa_{33}}{\Gamma+16}=O(\epsilon^3).
\end{aligned}
$$

Thus, if we solve the system of equations for κ_{3i}, $i=1,2,3$ we obtain the expression for $h_3(r,s,\lambda)$:

$$
\begin{aligned}
h_3(r,s,\lambda) \quad = \quad & \frac{(\Gamma+16)\left(11\Gamma^2-21\Gamma+16\right)}{54\sqrt{6-3\Gamma}(\Gamma-2)\Gamma^3\sqrt{-\frac{\Gamma(4\Gamma^2-7\Gamma+16)}{\Gamma+16}}}r^2\epsilon^2+\frac{(\Gamma+16)}{9\sqrt{2}(\Gamma-2)\Gamma\sqrt{-\frac{\Gamma(4\Gamma^2-7\Gamma+16)}{\Gamma+16}}}rs\epsilon \\
& +\frac{\left(36\Gamma^5-177\Gamma^4+351\Gamma^3+56\Gamma^2-608\Gamma+512\right)}{108\sqrt{3}(2-\Gamma)^{3/2}\Gamma^3\sqrt{-\frac{\Gamma(4\Gamma^2-7\Gamma+16)}{\Gamma+16}}}s^2\epsilon+O(\epsilon^3)+O(|r,s|^3)+O(\lambda).
\end{aligned}
$$

We perform a similar procedure to obtain $h_{4,5}$:

$$
\begin{aligned}
h_4(r,s,\lambda) \quad = \quad & -\frac{(\Gamma+16)\left(11\Gamma^2-21\Gamma+16\right)}{54\sqrt{6-3\Gamma}(\Gamma-2)\Gamma^3\sqrt{-\frac{\Gamma(4\Gamma^2-7\Gamma+16)}{\Gamma+16}}}r^2\epsilon^2-\frac{(\Gamma+16)}{9\sqrt{2}(\Gamma-2)\Gamma\sqrt{-\frac{\Gamma(4\Gamma^2-7\Gamma+16)}{\Gamma+16}}}rs\epsilon \\
& -\frac{\left(36\Gamma^5-177\Gamma^4+351\Gamma^3+56\Gamma^2-608\Gamma+512\right)}{108\sqrt{3}(2-\Gamma)^{3/2}\Gamma^3\sqrt{-\frac{\Gamma(4\Gamma^2-7\Gamma+16)}{\Gamma+16}}}s^2\epsilon+O(\epsilon^3)+O(|r,s|^3)+O(\lambda), \\
h_5(r,s,\lambda) \quad = \quad & -\frac{56\left(16\Gamma^4-88\Gamma^3+241\Gamma^2-224\Gamma+256\right)(\Gamma-2)^2r^2\epsilon^2}{243\Gamma^3\left(4\Gamma^2-7\Gamma+16\right)^2} \\
& +\frac{8\left(16\Gamma^4-88\Gamma^3+241\Gamma^2-224\Gamma+256\right)(\Gamma-2)^2rs\epsilon}{27\sqrt{3-\frac{3\Gamma}{2}}\Gamma^2\left(4\Gamma^2-7\Gamma+16\right)^2} \\
& -\frac{8\left(48\Gamma^5-440\Gamma^4+1691\Gamma^3-3323\Gamma^2+3232\Gamma-2816\right)(\Gamma-2)^2s^2\epsilon^2}{243\Gamma^3\left(4\Gamma^2-7\Gamma+16\right)^2} \\
& +O(\epsilon^3)+O(|r,s|^3)+O(\lambda).
\end{aligned}
$$

By substituting the expressions for h_j with $j=3,4,5$ for t in B.21, we get the vector field reduced to the center manifold point ($\lambda=0$):

$$
\begin{pmatrix} r' \\ s' \end{pmatrix}=\begin{pmatrix} 0 & \Im y_+(\Omega_0) \\ \Im y_-(\Omega_0) & 0 \end{pmatrix}\begin{pmatrix} r \\ s \end{pmatrix}+\begin{pmatrix} g^1(r,s,0) \\ g^2(r,s,0) \end{pmatrix},
$$

where

$$
\begin{aligned}
g^1(r,s,0) &= f_1(r,s,h_3(r,s,0),h_4(r,s,0),h_5(r,s,0),0),\\
&= a_1rs + a_2rh_3 + a_3rh_4 + a_4rh_5 + a_5r^2 + a_6s^2 + a_7h_3^2 + a_8h_4^2 + a_9h_5^2,\\
g^2(r,s,0) &= f_2(r,s,h_3(r,s,0),h_4(r,s,0),h_5(r,s,0),0),\\
&= b_1rs + b_2rh_3 + b_3rh_4 + b_4rh_5 + b_5r^2 + b_6s^2 + b_7h_3^2 + b_8h_4^2 + b_9h_5^2.
\end{aligned}
$$

B.5.5 Computation of the sign of α

We omit the coefficient values a_i, b_i with $i = 1, \ldots, 9$ due to size constraints. Then, we obtain

$$
\begin{aligned}
g^1_{rrr}(0,0,0) &= \frac{56\left(256\Gamma^6 - 1864\Gamma^5 + 7258\Gamma^4 - 13745\Gamma^3 + 10376\Gamma^2 - 2048\Gamma - 6144\right)}{243\Gamma^3\left(4\Gamma^2 - 7\Gamma + 16\right)^2}\epsilon^2 + O(\epsilon^3),\\
g^1_{rss}(0,0,0) &= \frac{2}{729(\Gamma-2)\Gamma^4\left(4\Gamma^2 - 7\Gamma + 16\right)^2}\Big(3072\Gamma^9 - 38480\Gamma^8 + 248472\Gamma^7 - 931785\Gamma^6\\
&\quad +2115827\Gamma^5 - 2643936\Gamma^4 + 1445472\Gamma^3 + 1154560\Gamma^2 - 2383872\Gamma + 1179648\Big)\epsilon^2 + O(\epsilon^3),\\
g^2_{rrs}(0,0,0) &= \frac{4}{6561\sqrt{3}(\Gamma-2)^4\Gamma^4(\Gamma+16)\left(4\Gamma^2 - 7\Gamma + 16\right)^3\left(16\Gamma^4 - 88\Gamma^3 + 241\Gamma^2 - 224\Gamma + 256\right)}\\
&\quad \Bigg(2\sqrt{3}(\Gamma-2)^3\Big(663552\Gamma^{16} - 8368128\Gamma^{15} + 94353408\Gamma^{14} - 867281664\Gamma^{13}\\
&\quad +5878685600\Gamma^{12} - 28924170352\Gamma^{11} + 105641521212\Gamma^{10} - 292808439595\Gamma^9 + 624043036257\Gamma^8\\
&\quad -1029494799504\Gamma^7 + 1301803129344\Gamma^6 - 1242933030912\Gamma^5 + 858486865920\Gamma^4\\
&\quad -393852485632\Gamma^3 + 108749914112\Gamma^2 - 8858370048\Gamma + 21474836480\Big)\Bigg)\epsilon^2 + O(\epsilon^3),\\
g^2_{sss}(0,0,0) &= \frac{1}{6561(2-\Gamma)^{7/2}\Gamma^9\left(4\Gamma^2 - 7\Gamma + 16\right)^2}\sqrt{\frac{2}{3}}\Big(147456\Gamma^{16} - 3228096\Gamma^{15} + 33644656\Gamma^{14}\\
&\quad -217040020\Gamma^{13} + 963855265\Gamma^{12} - 3092085315\Gamma^{11} + 7310636951\Gamma^{10} - 12737306497\Gamma^9\\
&\quad +16035426720\Gamma^8 - 13774008064\Gamma^7 + 6857110016\Gamma^6 - 863544320\Gamma^5 + 325533696\Gamma^4\\
&\quad -3481796608\Gamma^3 + 5209325568\Gamma^2 - 3556769792\Gamma + 1073741824\Big)\epsilon^2 + O(\epsilon^3),\\
g^1_{rs}(0,0,0) &= \frac{2\left(8\Gamma^4 - 60\Gamma^3 + 213\Gamma^2 - 280\Gamma + 384\right)\epsilon}{9\sqrt{3 - \frac{3\Gamma}{2}}\Gamma\left(4\Gamma^2 - 7\Gamma + 16\right)}\\
&\quad + \frac{2\sqrt{2}\left(8\Gamma^4 - 60\Gamma^3 + 213\Gamma^2 - 280\Gamma + 384\right)\left(36\Gamma^4 - 129\Gamma^3 + 355\Gamma^2 - 448\Gamma + 256\right)\epsilon^2}{243(\Gamma-2)\Gamma(\Gamma+16)^2\left(\frac{\Gamma\left(4\Gamma^2-7\Gamma+16\right)}{\Gamma+16}\right)^{3/2}} + O(\epsilon^3),\\
g^1_{rr}(0,0,0) &= -\frac{32\left(11\Gamma^4 - 78\Gamma^3 + 357\Gamma^2 - 493\Gamma + 816\right)\epsilon^2}{81\Gamma^2\left(4\Gamma^2 - 7\Gamma + 16\right)} + O(\epsilon^3),\\
g^1_{ss}(0,0,0) &= \frac{2\left(-16\Gamma^5 + 212\Gamma^4 - 867\Gamma^3 + 2231\Gamma^2 - 2512\Gamma + 3072\right)\epsilon^2}{27\Gamma^2\left(4\Gamma^2 - 7\Gamma + 16\right)} + O(\epsilon^3),
\end{aligned}
$$

$$
\begin{aligned}
g^2_{rs}(0,0,0) &= -\frac{4}{3} - \frac{4\left(36\Gamma^4 - 129\Gamma^3 + 355\Gamma^2 - 448\Gamma + 256\right)\epsilon}{27\sqrt{6-3\Gamma}\Gamma(\Gamma+16)\sqrt{\frac{\Gamma\left(4\Gamma^2-7\Gamma+16\right)}{\Gamma+16}}} - \frac{2}{729(\Gamma-2)\Gamma^3(\Gamma+16)\left(4\Gamma^2-7\Gamma+16\right)^2} \\
&\quad \Big(10368\Gamma^{10} - 89856\Gamma^9 + 523296\Gamma^8 - 2214822\Gamma^7 + 6609656\Gamma^6 - 13388811\Gamma^5 + 16103040\Gamma^4 \\
&\quad -9588992\Gamma^3 + 1044480\Gamma^2 + 4718592\Gamma + 5242880\Big)\epsilon^2 + O(\epsilon^3), \\
g^2_{rr}(0,0,0) &= -\frac{44\sqrt{\frac{2}{3}}\sqrt{2-\Gamma}\epsilon}{9\Gamma} + O(\epsilon^2), \\
g^2_{ss}(0,0,0) &= \frac{2(\Gamma-2)(\Gamma-7)\epsilon}{3\sqrt{3-\frac{3\Gamma}{2}}\Gamma} + O(\epsilon^2).
\end{aligned}
$$

Thus, if we replace the previous expressions in the formula for α we have the following form:

$$
\begin{aligned}
\alpha = \frac{1}{16}&\left(g^{(1)}_{rrr} + g^{(1)}_{rss} + g^{(2)}_{rrs} + g^{(2)}_{sss}\right) \\
&-\frac{1}{16\Im y_+(\Omega_0(0))}\left[g^{(1)}_{rs}\left(g^{(1)}_{rr} + g^{(1)}_{ss}\right) - g^{(2)}_{rs}\left(g^{(2)}_{rr} + g^{(2)}_{ss}\right) - g^{(1)}_{rr}g^{(2)}_{rr} + g^{(1)}_{ss}g^{(2)}_{ss}\right]\Big|_{r=r=\lambda=0}.
\end{aligned}
$$

Let

$$
\begin{aligned}
D_1 &= \frac{1}{\epsilon^2}\left(g^{(1)}_{rrr} + g^{(1)}_{rss} + g^{(2)}_{rrs} + g^{(2)}_{sss}\right)\Big|_{r=r=\lambda=0}, \\
D_2 &= \frac{1}{\sqrt{2/3(2-\Gamma)}\epsilon^3}\left(g^{(1)}_{rs}\left(g^{(1)}_{rr} + g^{(1)}_{ss}\right) - g^{(2)}_{rs}\left(g^{(2)}_{rr} + g^{(2)}_{ss}\right) - g^{(1)}_{rr}g^{(2)}_{rr} + g^{(1)}_{ss}g^{(2)}_{ss}\right)\Big|_{r=r=\lambda=0}.
\end{aligned}
$$

Then, $\alpha = \frac{\epsilon^2}{16}(D_1 - D_2) < 0$ for sufficiently small $\epsilon > 0$. The software Mathematica was used to verify the inequality.

VITA

Joan Ponce was born in 1990 in Gainesville, Florida. She graduated from the University of Florida with a Bachelor of Science Degree in Mathematics in May 2013. In August of 2014, she started her Doctor of Philosophy degree in Mathematical Biology at Purdue University under the supervision of Professor Zhilan Feng.